

1 Influence of basement heterogeneity on the architecture of low subsidence rate Paleozoic  
2 intracratonic basins (Reggane, Ahnet, Mouydir and Illizi basins, Hoggar massif)

3 Paul Perron<sup>1</sup>, Michel Guiraud<sup>1</sup>, Emmanuelle Vennin<sup>1</sup>, Isabelle Moretti<sup>2</sup>, Éric Portier<sup>3</sup>, Laetitia  
4 Le Pourtier<sup>4</sup>, Moussa Konaté<sup>5</sup>

<sup>5</sup> <sup>1</sup>Université de Bourgogne Franche-Comté, Centre des Sciences de la Terre, UMR CNRS  
<sup>6</sup> 6282 Biogéosciences, 6 Bd Gabriel, 21000 Dijon, France.

<sup>7</sup> <sup>2</sup>ENGIE, Département Exploration & Production, 1, place Samuel de Champlain, Faubourg  
<sup>8</sup> de l'Arche, 92930 Paris La Défense, France.

9     <sup>3</sup>NEPTUNE Energy International S.A., 9-11 Allée de l'Arche – Tour EGEE – 92400  
10 Courbevoie, France.

11 <sup>4</sup>Sorbonne Université, CNRS-INSU, Institut des Sciences de la Terre Paris, ISTEPI UMR  
12 7193, F-75005 Paris, France.

13      <sup>5</sup>Département de Géologie, Université Abdou Moumouni de Niamey, BP :10662, Niamey,  
14      Niger.

15 Corresponding author: paul.perron@u-bourgogne.fr, paul.perron@hotmail.fr

16 Abstract

17 The Paleozoic intracratonic North African Platform is characterized by an association of  
18 arches (ridges, domes, swells or paleo-highs) and low subsidence rate syncline basins of  
19 different wavelengths (75–620 km). In the Reggane, Ahnet, ~~and~~ Mouydir and Illizi basins are  
20 successively delimited from east to west by the Amguid El Biod, Arak-Foum Belrem, and  
21 Azzel Matti arches, ~~bounded by inherited Precambrian sub vertical fault systems which were~~  
22 ~~repeatedly reactivated or inverted during the Paleozoic. Major unconformities are related to~~  
23 several tectonic events such as the Cambrian-Ordovician extension, Ordovician-Silurian

24 glacial rebound, Silurian–Devonian “Caledonian” extension/compression, late Devonian  
25 extension/compression, and “Hercynian” compression. Through the analysis of new  
26 unpublished geological data (i.e. satellite images, well-logs, seismic lines), the deposits  
27 associated with these arches and syncline basins exhibit thickness variations and facies  
28 changes ranging from continental to marine environments. The arches are characterized by  
29 thin amalgamated deposits with condensed and erosional surfaces, whereas the syncline  
30 basins exhibit thicker and well-preserved successions. In addition, the vertical facies  
31 succession evolves from thin Silurian to Givetian deposits into thick Upper Devonian  
32 sediments. Synsedimentary structures and major unconformities are related to several tectonic  
33 events such as the Cambrian–Ordovician extension, Ordovician–Silurian glacial rebound,  
34 Silurian–Devonian “Caledonian” extension/compression, late Devonian  
35 extension/compression, and “Hercynian” compression. Synsedimentary deformations are  
36 evidenced by wedges, truncations, and divergent onlaps. Locally, deformation is characterized  
37 by near-vertical planar normal faults responsible for horst and graben structuring associated  
38 with folding during the Cambrian–Ordovician–Silurian period. These structures may have  
39 been inverted or reactivated during the Devonian (i.e. Caledonian, Mid-Late Devonian)  
40 compression and the Carboniferous (i.e. pre-Hercynian to Hercynian).

41 Additionally, basement characterization from geological and geophysics data (aeromagnetic  
42 and gravity maps), shows an interesting age-dependent zonation of the terranes which are  
43 bounded by mega shear zones with the arches-basins framework. The “old” terranes are  
44 situated under arches while the “young” terranes are located under the basins depocenter. This  
45 structural framework results from the accretion of Archean and Proterozoic terranes inherited  
46 from during the Pan-African former orogeny (e.g. Pan-African orogeny (750–580 900–520  
47 Ma).

48 So, the sedimentary infilling pattern and the nature of deformation result from the slow  
49 Paleozoic repeatedly reactivation of Precambrian terranes bounded by sub-vertical  
50 lithospheric fault zones systems. Alternating periods of tectonic quiescence and low-rate  
51 subsidence acceleration associated with extension and local inversion tectonics correspond to  
52 a succession of Paleozoic geodynamic events (i.e. far-field orogenic belt, glaciation).

53 Keywords: intracratonic basin, Paleozoic, arches, low-rate subsidence, tectonic heritage,  
54 terranes, Central Sahara

55

## 56 1 Introduction

57 Paleozoic deposits fill numerous intracratonic basins, which may also be referred to as  
58 “cratonic basins”, “interior cratonic basins”, or “intracontinental sags”. Intracratonic basins  
59 are widespread around the world (see Fig. 6 from Heine et al., 2008) and exploration for non-  
60 conventional petroleum has revived interest in them. They are located in “stable” lithospheric  
61 areas and share several common features (Allen and Armitage, 2011): such as Their  
62 geometries are (i.e. large circular, elliptical, saucer-shaped to oval). Their stratigraphy is (i.e.  
63 filled with continental to shallow-water sediments). Their low subsidence rate of  
64 sedimentation (an average of 7 m/Myr), there is low (5 to 50 m/Ma) and long-term subsidence  
65 (sometimes more than 540 Myr). and Their structural framework shows (reactivation of  
66 structures and emergence of arches also referred to in the literature as “ridges”, “paleo-highs”,  
67 “domes”, and “swells”). Multiple hypotheses and models have been proposed to explain how  
68 these slowly subsiding, long-lived intracratonic basins formed and evolved (see Allen and  
69 Armitage, 2011 and references therein or Hartley and Allen, 1994). However, their tectonic  
70 and sedimentary architectures are often poorly constrained.

71 The main specificities of intracratonic basins are found on the Paleozoic North Saharan  
72 Platform. The sedimentary infilling during c. 250 Myr is relatively thin (i.e. around a few  
73 hundred to a few thousand meters), of great lateral extent (i.e. 46 9 million km<sup>2</sup>), and is  
74 separated by major regional unconformities (Beuf et al., 1968a, 1971; Carr, 2002; Eschard et  
75 al., 2005, 2010; Fabre, 1988, 2005; Fekirine and Abdallah, 1998; Guiraud et al., 2005;  
76 [Kracha, 2011](#); Legrand, 2003a). Depositional environments were mainly continental to  
77 shallow-marine and homogeneous. Very slow and subtle lateral variations occurred over time  
78 (Beuf et al., 1971; Carr, 2002; Fabre, 1988; Guiraud et al., 2005; Legrand, 2003a). The  
79 Paleozoic North Saharan Platform is arranged (Fig. 1) into an association of long-lived broad  
80 synclines (i.e. basins [or sub-basins](#)) and anticlines (i.e. arches ~~swells, domes, highs, or ridges~~)  
81 of different wavelengths ( $\lambda$ : 75–620 km). Burov and Cloetingh (2009) report deformation  
82 wavelengths of the order of 200–600 km when the whole lithosphere is involved and of 50–  
83 100 km when the crust is decoupled from the lithospheric mantle. This insight suggests that  
84 the inherited basement fabric influences [intracratonic](#) basin architecture at a large scale.  
85 [Besides, pre-existing structures, such as shear zones and terrane suture zones, are present](#)  
86 [throughout the lithosphere, affecting the geometry and evolution of upper-crustal structural](#)  
87 [framework forming during later tectonic events \(Peace et al., 2018; Phillips et al., 2018\).](#)  
88 ~~Intracratonic basins are affected by basement involved faults which are often reactivated in~~  
89 ~~response to tectonic pulses (Beuf et al., 1971; Boote et al., 1998; Eschard et al., 2010; Fabre,~~  
90 ~~1988; Frizon de Lamotte et al., 2013; Galeazzi et al., 2010; Guiraud et al., 2005; Wendt et al.,~~  
91 ~~2006).~~

92 In this study of the [Reggane](#), [Ahnet](#), [and](#) [Mouydir](#) [and](#) [Illizi](#) basins, a multidisciplinary  
93 workflow involving various tools (e.g. seismic profiles, satellite images) and techniques (e.g.  
94 photo-geology, seismic interpretation, well correlation, geophysics, geochronology) has  
95 enabled us to (1) make a tectono-sedimentary analysis, (2) determine the spatial arrangement

96 of depositional environments calibrated by biostratigraphic zonation, (3) characterize basin  
97 geometry, and (4) ascertain the inherited architecture of the basement and its tectonic  
98 evolution. We propose a conceptual coupled model explaining the architecture of the  
99 intracratonic basins of the North Saharan Platform. This model highlights the role of  
100 basement heritage heterogeneities in an accreted mobile belt and their influence on the  
101 structure and evolution of intracratonic basins. It is a first step towards a better understanding  
102 of the factors and mechanisms that drive intracratonic basins.

103 **2 Geological setting: The Paleozoic North Saharan Platform and the Reggane, Ahnet,  
104 and Mouydir and Illizi basins**

105 The Reggane, Ahnet, and Mouydir and Illizi basins (Figs 1 and ~~3~~ 2) are located in south-  
106 western Algeria, north-west of the Hoggar massif (Ahaggar). They are ~~N-S-oval~~ depressions  
107 filled by Paleozoic deposits. The basins are bounded to the south by the Hoggar massif  
108 (Tuareg Shield), ~~to the west by the Azzel Matti arch, to the east by the Amguid El Biad arch~~  
109 and they are separated from together by the Azzel Matti, the Arak-Foum Belrem the Amguid  
110 El Biad arches.

111 Figure ~~2~~ 3 synthetizes the lithostratigraphy, the large-scale sequence stratigraphic framework  
112 delimited by ~~five~~ six main regional unconformities (A to F), and the tectonic events proposed  
113 in the literature (cf. references under Fig. ~~2~~ 3) affecting the Paleozoic North Saharan Platform.

114 During the Paleozoic, the Reggane, Ahnet, and Mouydir and Illizi basins were part of a set of  
115 the super-continent Gondwana (Fig. 1). This super-continent resulted from the collision of the  
116 West African Craton (WAC) and the East Saharan Craton (ESC), sandwiching the Tuareg  
117 Shield (TS) mobile belt during the Pan-African orogeny (Craig et al., 2008; Guiraud et al.,  
118 2005; Trompette, 2000). This orogenic cycle followed by the chain's collapse (c. 1000–525  
119 Ma) was also marked by phases of oceanization and continentalization (c. 900–600 Ma)

120 giving rise to the heterogeneous terranes in the accreted mobile belt (Trompette, 2000). The  
121 Hoggar shield massif is composed of several accreted, sutured, and amalgamated terranes of  
122 various ages and compositions resulting from multiple phases of geodynamic events  
123 (Bertrand and Caby, 1978; Black et al., 1994; Caby, 2003; Liégeois et al., 2003). Twenty-  
124 three well preserved terranes in the Hoggar were identified and grouped into Archean,  
125 Paleoproterozoic, and Mesoproterozoic–Neoproterozoic juvenile Pan-African terranes (see  
126 legend in Fig. 1). In the West African Craton, the Reguibat shield is composed of Archean  
127 terrains in the west and of Paleoproterozoic terranes in the east (Peucat et al., 2003, 2005).

128 Then, there is evidence of a complex and polyphased history throughout the Paleozoic (Fig. 2  
129 3), with alternating periods of quiescence and tectonic activity, individualizing and  
130 rejuvenating ancient NS, NE–SW, or NW–SE structures in arch and basin configurations  
131 (Badalini et al., 2002; Bennacef et al., 1971; Beuf et al., 1968b, 1971; Boote et al., 1998;  
132 Boudjema, 1987; Chavand and Claraeq, 1960; Coward and Ries, 2003; Craig et al., 2008;  
133 Eschard et al., 2005, 2010; Fabre, 1988, 2005; Frizon de Lamotte et al., 2013; Guiraud et al.,  
134 2005; Logan and Duddy, 1998; Lüning, 2005; Wendt et al., 2006). The Paleozoic successions  
135 of the North Saharan Platform are predominantly composed of siliciclastic detrital sediments  
136 (Beuf et al., 1971; Eschard et al., 2005). They form the largest area of detrital sediments ever  
137 found on continental crust (Burke et al., 2003), dipping gently NNW (Beuf et al., 1971, 1969;  
138 Fabre, 1988, 2005; Fröhlich et al., 2010; Gariel et al., 1968; Le Heron et al., 2009). Carbonate  
139 deposits are observed from the Mid–Late Devonian to the Carboniferous (Wendt, 1985, 1988,  
140 1995; Wendt et al., 1993, 1997, 2006, 2009a; Wendt and Kaufmann, 1998). From south to  
141 north, the facies progressively evolve from continental fluvial to shallow marine (i.e. upper  
142 to lower shoreface) and then to offshore facies (Beuf et al., 1971; Carr, 2002; Eschard et al.,  
143 2005, 2010; Fabre, 1988, 2005; Fekirine and Abdallah, 1998; Guiraud et al., 2005; Legrand,  
144 1967a).

145 **3 Data and methods**

146 A multidisciplinary approach has been used in this study integrating new data (i.e. satellite  
147 images, seismic lines and well-logs data) in particular from the Reggane, Ahnet, Mouydir,  
148 Illizi basins and Hoggar massif (see supplementary data + Fig. 4):  
149 –Geographic Information System analysis (GIS);  
150 –The basins and the main geological structures were identified from Landsat satellite images;  
151 –Seismic section interpretation;  
152 –Sedimentological and well log analysis;  
153 –Biostratigraphy and sequence stratigraphy;  
154 –Geochronology and geophysical data.

155 The Paleozoic series of the Ahnet and Mouydir basins are well-exposed over an area of  
156 approximately 170,000 km<sup>2</sup> and are well observed in satellite images (Google Earth and  
157 Landsat from USGS). Furthermore, a significant geological database (i.e. wells, seismic  
158 records, field trips, geological reports) has been compiled in the course of petroleum  
159 exploration since the 1950s. The sedimentological dataset is based on the integration and  
160 analysis of cores, outcrops, well-logs, and of lithological and biostratigraphic data. They were  
161 synthetized from internal SONATRACH (Dokka, 1999), IFP-SONATRACH consortium  
162 reports (Eschard et al., 1999), and published articles (Beuf et al., 1971; Biju-Duval et al.,  
163 1968; Wendt et al., 2006). Facies described from cores and outcrops of these studies were  
164 grouped into facies associations corresponding to the main depositional environments  
165 observed on the Saharan Platform (Table 1). Characteristic gamma-ray patterns (electrofacies)  
166 are proposed to illustrate the different facies associations. The gamma-ray (GR) peaks are  
167 commonly interpreted as the maximum flooding surfaces (MFS) (e.g. Catuneanu et al., 2009;

168 Galloway, 1989; Milton et al., 1990; Serra and Serra, 2003). Time calibration of well-logs ~~and~~  
169 ~~outcrops~~ is based on palynomorphs (essentially Chitinozoans and spores) and outcrops on  
170 conodonts, goniatites, and brachiopods (Wendt et al., 2006). Palynological data of wells (W1,  
171 W7, W12, W19 and W20) from internal unpublished data (Abdesselam-Rouighi, 1991;  
172 Azzoune, 1999; Hassan, 1984; Khiar, 1974) are based on biozonations from Magloire, (1967)  
173 and Boumendjel et al., (1988). Well W18 is supported by palynological data and biozonations  
174 from Hassan Kemandji et al., (2008).

175 Synsedimentary extensional and compressional markers are characterized in this structural  
176 framework based on the analyses of satellite images (Figs 4 ~~5~~ and 5 ~~6~~), seismic profiles (Fig.  
177 ~~6~~ ~~7~~), 21 wells (W1 to W21), and 12 outcrop cross-sections (O1 to O12). Wells and outcrop  
178 sections are arranged into three E–W sections (Figs 9 ~~10~~, 10 ~~11~~ and ~~supplementary data 2~~ ~~12~~)  
179 and one N–S section (~~supplementary data 3~~ Fig. 13). Satellite images (Figs 4 ~~5~~ and 5 ~~6~~) and  
180 seismic profiles (Fig. ~~6~~ ~~7~~) are located at key areas (i.e. near arches) illustrating the relevant  
181 structures (Fig. 3 ~~2~~). The calibration of the key stratigraphic horizon on seismic profiles (Figs  
182 ~~7~~ ~~9~~ ~~and 10~~) was settled by sonic well-log data using PETREL and OPENDTECT software.  
183 Nine key horizons easily extendable at the regional scale are identified and essentially  
184 correspond to major depositional unconformities: near top Infra-Cambrian, near top  
185 Ordovician, near top Silurian, near top Pragian, near top Givetian, near top mid-Frasnian, near  
186 top Famennian, top near base Quaternary and top near Hercynian unconformities (Figs ~~7~~ ~~9~~  
187 ~~and~~ ~~10~~). The stratigraphic layers are identified by the integration of satellite images (Google  
188 Earth and Landsat USGS: <https://earthexplorer.usgs.gov/>), digital elevation model (DEM) and  
189 the 1:200,000 geological maps of Algeria (Bennacef et al., 1974; Bensalah et al., 1971).

190 Subsidence analysis characterizes the vertical displacements of a given sedimentary  
191 depositional surface by tracking its subsidence and uplift history (Van Hinte, 1978). The  
192 resulting curve details the total subsidence history for a given stratigraphic column (Allen and

193 Allen, 2005; Van Hinte, 1978). Backstripping is also used to restore the initial thicknesses of  
194 a sedimentary column (Allen and Allen, 2005; Angevine et al., 1990). Lithologies and  
195 paleobathymetries have been defined using facies analysis or literature data. Porosity and the  
196 compaction proxy are based on experimental data from (Slater and Christie, 1980). In this  
197 study, subsidence analyses were performed on sections using OSXBackstrip software  
198 performing 1D Airy backstripping (after Allen and Allen, 2005; Watts, 2001); available at:  
199 <http://www.ux.uis.no/nestor/work/programs.html>.

200 The 800 km<sup>2</sup> outcrop of basement rocks of the Hoggar shield massif provides an exceptional  
201 case study of an exhumed mobile belt composed of accreted terranes of different ages. To  
202 reconstruct the nature of the basement, a terrane map (Fig. 42 15 and 16) was put together by  
203 integrating geophysical data (aeromagnetic anomaly map: <https://www.geomag.us/>, Bouguer  
204 gravity anomaly map: <http://bgi.omp.obs-mip.fr/>), satellite images (7ETM+ from Landsat  
205 USGS: <https://earthexplorer.usgs.gov/>) data, geological maps (Berger et al., 2014; Bertrand  
206 and Caby, 1978; Black et al., 1994; Caby, 2003; Fezaa et al., 2010; Liégeois et al., 1994,  
207 2003, 2005, 2013), and geochronological data (e.g. U-Pb radiochronology, see supplementary  
208 data § 1). Geochronological data from published studies were compiled and georeferenced  
209 (Fig. 1). Thermo-tectonic ages were grouped into eight main thermo-orogenic events (Fig. 1):  
210 The Liberian-Ouzzalian event (Archean, >2500 Ma), (the Archean, Eburnean (i.e.  
211 Paleoproterozoic, 2500-1600 Ma), the Kibarian (i.e. Mesoproterozoic, 1600-1100 Ma), the  
212 Neoproterozoic oceanization-rifting (1100-750 Ma), the Neoproterozoic syn-Pan-African  
213 orogeny (i.e. Neoproterozoic, 750-541 Ma), the post-Pan-African (i.e. Neoproterozoic, 541-  
214 443 Ma), the Caledonian orogeny (i.e. Siluro-Devonian, 443-358 Ma), and the Hercynian  
215 orogeny (i.e. Carbo-Permian, 358-252 Ma).

216 **4 Structural framework and tectono-sedimentary structure analyses**

217 The structural architecture of the North Saharan Platform (Fig. 1) is characterized by an  
218 ~~association of syncline basins and anticlines (i.e. arches, domes, etc.). The basins (or sub-~~  
219 ~~basins)~~ are mostly circular to oval shaped. They are bounded by arches which correspond to  
220 ~~the mainly N-S Azzel Matti, Arak Foum Belrem, Amguid El Biod, and Tihemboka arches,~~  
221 ~~the NE-SW Bou Bernous, Ahara, and Gargaf arches, and the NW-SE Saoura and Azzene~~  
222 ~~arches (Fig. 1).~~ The basins are structured by major faults frequently associated with broad  
223 asymmetrical folds displayed by three main trends (Fig. 1): (1) near-N-S, varying from N0°  
224 to N10° or N160°, (2) from N40° to 60°, and (3) N100° to N140° directions (Figs 1, 3A, and  
225 4). These fault zones are about 100 km (e.g. faults F1 and F2, Fig. 4 5) to tens of kilometers  
226 ~~lengths long~~ (e.g. faults F3 to F8, Fig. 4 5). They correspond to the mainly N-S Azzel-Matti,  
227 Arak-Foum Belrem, Amguid El Biod, and Tihemboka arches, the NE-SW Bou Bernous,  
228 Ahara, and Gargaf arches, and the NW-SE Saoura and Azzene arches (Fig. 1).

#### 229 4.1 Synsedimentary extensional markers

230 Extensional markers are characterized by the settlement of steeply west- or eastward-dipping  
231 basement normal faults associated with colinear syndepositional folds of several kilometers in  
232 length (e.g. Fig. ~~6A to E~~ 5A-A', ~~5B-B'~~, ~~5C-C'~~, ~~5E-E'~~ and ~~6 7A~~), represented by footwall  
233 anticline and hanging wall syncline-shaped forced folds. They are located in the vicinity of  
234 different arches (Fig. 3 2) such as the Tihemboka arch (Figs ~~4~~5B-B', ~~5~~5A-A' and ~~5~~6A-B-B'),  
235 Arak-Foum Belrem arch (Figs ~~4~~5A-A', ~~5~~6C-C' to ~~5~~6F-F' and ~~6~~7A, ~~6~~7C), Azzel Matti arch  
236 (Fig. ~~6~~7B), and Bahar El Hamar area intra-basin arch (Fig. ~~6~~7D). These tectonic structures  
237 can be featured by basement blind faults (e.g. ~~fault F5 in Fig. 5~~ 6C-C', ~~fault F1 in Figs 5D-D'~~,  
238 ~~5F-F', and 6A fault F1 in Fig. 7A~~). The deformation pattern is mainly characterized by brittle  
239 faulting in Cambrian-Ordovician series down to the basement and fault-damping in Silurian  
240 series (e.g. ~~fault F2 in Fig. 5A-A'~~, faults F1 to F6 in Fig. ~~6~~7B). The other terms of the series  
241 (i.e. Silurian to Carboniferous) are usually affected by folding except (see F1 faults in Figs ~~5~~

242 [6F-F'](#), [6 7B](#), [6 7D](#) and [6 7C](#)) where the brittle deformation can be propagated to the Upper  
243 Devonian (due to reactivation and/or inversion as suggested in the next paragraph).

244 In association with the extensional markers, thickness variations and tilted divergent onlaps of  
245 the sedimentary series (i.e. wedge-shaped units, progressive unconformities) in the hanging  
246 wall syncline of the fault escarpments are observed (Figs [5 6](#) and [6 7](#)). These are attested  
247 using photogeological analysis of satellite images (Fig. [5 6](#)) and are marked by a gentler dip  
248 angle of the stratification planes away from the fault plane (i.e. fault core zone). The markers  
249 of syndepositional deformation structures are visible in the hanging-wall synclines of  
250 Precambrian to Upper Devonian series (Figs [5 6](#) and [6 7](#)).

251 The footwall anticline and hanging-wall syncline-shaped forced folds recognized in this study  
252 are very similar to those described in the literature by Grasemann et al., (2005); Khalil and  
253 McClay, (2002); Schlische, (1995); Stearns, (1978); Withjack et al., (1990), (2002); Withjack  
254 and Callaway, (2000). The wedge-shaped units (DO0 to DO3; Figs [4 5](#), [5 6](#) and [6 7](#))  
255 associated with the hanging-wall synclines are interpreted as synsedimentary normal fault-  
256 related folding. The whole tectonic framework forms broad extensional horsts and graben  
257 related to synsedimentary forced folds controlling basin shape and sedimentation ([Figs 4, 5](#)  
258 [and 6](#)).

259 Following Khalil and McClay, (2002); Lewis et al., (2015); Shaw et al., (2005); Withjack et  
260 al., (1990), we use the ages of the growth strata (i.e. wedge-shaped units) to determine the  
261 timing of the deformation. The main four wedge-shaped units identified (DO0 to DO3) are  
262 indicative of the activation and/or reactivation of the normal faults (extensional settings)  
263 during Neoproterozoic ([DO0](#)), Cambrian–Ordovician ([DO1](#)), Early to Mid Silurian ([DO2](#))  
264 and Mid to Late Devonian ([DO3](#)) times.

265 In planar view, straight (F1 in Fig. 4 ~~5A-A'~~) and sinuous faults (F2, F3, F3', F4, F4', and F5  
266 in Fig. 4 ~~5AA'~~) can be identified. The sinuous faults are arranged “en echelon” into several  
267 segments with relay ramps. These faults are 10 to several tens of kilometers long with vertical  
268 throws of hundreds of meters that fade rapidly toward the fault tips. The sinuous geometry of  
269 normal undulated faults as well as the rapid lateral variation in fault throw are controlled by  
270 the propagation and the linkage of growing parent and tip synsedimentary normal faults  
271 (Marchal et al., 2003, 1998; Fig. 4A-A'). We use the stratigraphic age of impacted layers (here  
272 Tamadjert Fm.) to date (re)activation of the faults.

273 According to Holbrook and Schumm, (1999), river patterns are extremely sensitive to tectonic  
274 structure activity. Here we find that the synsedimentary activity of the extensional structures  
275 is also evidenced by the influence of the fault scarp on the distribution and orientation of  
276 sinuous channelized sandstone body systems (dotted red lines in Fig. 4 ~~5B-B'~~). It highlights  
277 the (re)activation of the faults during the deposition of these channels, i.e. late Hirnantian  
278 dated by (Girard et al., 2012).

## 279 4.2 Synsedimentary compressional markers (inversion tectonics)

280 After the development of the extensional tectonism described previously, evidence of  
281 synsedimentary compressional markers can be identified. These markers are located and  
282 preferentially observable near the Arak-Foum Belrem arch (Fig. 5 ~~6F-F'~~, F2 in Fig. 6 ~~7C~~), the  
283 Azzel Matti arch (2 in Figs 6 ~~7B~~), and the Bahar El Hamar area intra-basin arch (2 in Fig. 6  
284 ~~7D~~). The tectonic structures take the form of inverse faulting reactivating former basement  
285 faults (F1' in Fig. 5 ~~6F-F'~~, F1 in Fig. 6 ~~7C~~, F1' in Fig. 6 ~~7D~~, F1 in Fig. 6 ~~7B~~). The  
286 synsedimentary inverse faulting is demonstrated by the characterization of asymmetric  
287 anticlines especially observable in satellite images and restricted to the fault footwalls (Figs 4  
288 ~~5A-A'~~ along F1-F2).

289 Landsat image analysis combined with the line drawing of certain seismic lines reveals  
290 several thickness variations reflecting divergent onlaps (i.e. wedge-shaped units) which are  
291 restricted to the hanging-wall asymmetric anticlines (2 in Figs 5 ~~6F-F'~~, 6 7B, 6 7C and 6 7D).  
292 The compressional synsedimentary markers clearly post-date extensional divergent onlaps at  
293 hanging-wall syncline-shaped forced folds (1 in Figs 6 7B, 6 7C and 6 7D). This architecture  
294 is very similar to classical positive inversion structures of former inherited normal faults  
295 (Bellahsen and Daniel, 2005; Bonini et al., 2012; Buchanan and McClay, 1991; Ustaszewski  
296 et al., 2005). Tectonic transport from the paleo-graben hanging-wall toward the paleo-horst  
297 footwall (F1, F2-F2', F4-F4' in Fig. 6 7B; F1-F1' in Fig. 6 ~~B~~ 7D) is evidenced. Further  
298 positive tectonic inversion architecture is identified by tectonic transport from the paleo-horst  
299 footwall to the paleo-graben hanging wall (F1-F1' in Fig. 5 ~~6F-F'~~; F1, F5, and F6 in Fig. 6  
300 7C). This second type of tectonic inversion is very similar to the transported fault models  
301 defined by (Butler, 1989; Madritsch et al., 2008). The local positive inversions of inherited  
302 normal faults occurred during Silurian–Devonian (F4' Fig. 6 7B) and Mid to Late Devonian  
303 times (Figs 6 7B, 6 7C and 6 7D). A late significant compression event between the end of the  
304 Carboniferous and the Early Mesozoic was responsible for the exhumation and erosion of the  
305 tilted Paleozoic series. This series is related to the Hercynian angular unconformity surface  
306 (Fig. 6 7B).

## 307 5 Stratigraphy and sedimentology

308 The whole sedimentary series described in the literature is composed ~~of fluvatile Cambrian~~  
309 ~~of fluvatile to Braid-deltaic plain Cambrian, not only fluvatile (e.g. Brahmaputra River~~  
310 ~~analogue), with a transitional facies from continental to shallow marine~~ (Beuf et al., 1968b,  
311 1968a, 1971; Eschard et al., 2005, 2010; Sabaou et al., 2009), ~~glacial Ordovician Upper~~  
312 ~~Ordovician glaciogenic deposits~~ (Beuf et al., 1968a, 1968b, 1971; Eschard et al., 2005, 2010),  
313 ~~argillaceous deep marine Silurian argillaceous deep marine Silurian deposits~~ (Djouder et al.,

314 [2018](#); Eschard et al., 2005, 2010; Legrand, 1986, 2003b; Lüning et al., 2000) and offshore to  
315 embayment Carboniferous deposits (Wendt et al., 2009). In this complete sedimentary  
316 succession, we have focused on the Devonian deposits as they are very sensitive to and  
317 representative of basin dynamics. The architecture of the Devonian deposits allows us to  
318 approximate the main forcing factors controlling the sedimentary infilling of the basin and its  
319 synsedimentary deformation. [Nine Eleven](#) facies associations organized into four depositional  
320 environments ([Table 1](#)) are defined to reconstruct the architecture and the lateral and vertical  
321 sedimentary evolution of the basins (Figs [9 10](#), [10 11](#), ~~supplementary data 2 and 3~~ [12 and 13](#)).

## 322 **5.1 Facies association, depositional environments, and erosional unconformities**

323 Based on the compilation and synthesis of internal studies (Eschard et al., 1999), published  
324 papers on the [Algerian platform Saharan platform](#) (Beuf et al., 1971; Eschard et al., 2005,  
325 2010; Henniche, 2002) and on the Ahnet and Mouydir basins (Biju-Duval et al., 1968; Wendt  
326 et al., 2006) ~~plus the present study~~, eleven main facies associations (AF1 to AF5) and four  
327 depositional environments are proposed for the Devonian succession (Table 1). They are  
328 associated with their gamma-ray responses (Figs [7 8](#) and [8 9](#)). They are organized into two  
329 continental/fluvial (AF1 to AF2), four transitional/coastal plain (AF3a to AF3d), three  
330 shoreface (AF4a to AF4c), and two offshore (AF5a to AF5b) sedimentary environments.

### 331 **5.1.1 Continental fluvial environments**

332 This depositional environment features the AF1 (fluvial) and the AF2 (flood plain) facies  
333 association (Table 1). Facies association AF1 is mainly characterized by a thinning-up  
334 sequence with a basal erosional surface and trough cross-bedded intraformational  
335 conglomerates with mud clast lag deposits, quartz pebbles, and imbricated grains (Table 1). It  
336 passes into medium to coarse trough cross-bedded sandstones, planar cross-bedded siltstones,  
337 and laminated shales. These deposits are associated with rare bioturbations (expect at the

338 surface of the sets), ironstones, phosphorites, corroded quartz grains, and phosphatized  
339 pebbles. Laterally, facies association AF2 is characterized by horizontally laminated and very  
340 poorly sorted silt to argillaceous fine sandstones. They contain frequent root traces, plant  
341 debris, well-developed paleosols, bioturbations, nodules, and ferruginous horizons. Current  
342 ripples and climbing ripples are associated in prograding thin sandy layers.

343 In AF1, the basal erosional reworking and high energy processes are characteristic of channel-  
344 filling of fluvial systems (Allen, 1983; Owen, 1995). Eschard et al., (1999) identify three  
345 fluvial systems (see A, B, and C in Fig. 8 9) in the Tassili-N-Ajers outcrops: braided  
346 dominant (AF1a), meandering dominant (AF1b), and straight dominant (AF1c). They  
347 differentiate them by their different sinuosity, directions of accretion (lateral or frontal), the  
348 presence of mud drapes, bioturbations, and giant epsilon cross-bedding. Gamma-ray  
349 signatures of these facies associations (A, B, and C in Fig. 8 9) are cylindrical with an average  
350 value of 20 gAPI. The gamma ray shapes are largely representative of fluvial environments  
351 (Rider, 1996; Serra and Serra, 2003; Wagoner et al., 1990). The bottom is sharp with high  
352 value peaks and the tops are frequently fining-up, which may be associated with high values  
353 caused by argillaceous flood plain deposits and roots (Eschard et al., 1999). AF2 is interpreted  
354 as humid floodplain deposits (Allen, 1983; Owen, 1995) with crevasse splays or preserved  
355 levees of fluvial channels (Eschard et al., 1999). Gamma-ray curves of AF2 (D, Fig. 8 9)  
356 show a rapid succession of low to very high peak values, ranging from 50 to 200 120 gAPI.  
357 AF1 and AF2 are typical of the Pragian “Oued Samene” Formation (Wendt et al., 2006). In  
358 the Illizi basin, these facies are mainly recorded in the Cambrian Ajers Formation (dated  
359 Upper Cambrian? to Ordovician see Fabre, 2005; Vecoli, 2000; Vecoli et al., 1995, 1999,  
360 2008; Vecoli and Playford, 1997) and the Lochkovian to Pragian “Middle Barre” “Barre  
361 Moyenne” and “Upper Barre” “Barre Supérieure” Formations (Beuf et al., 1971; Eschard et  
362 al., 2005).

363 **5.1.2 Transitional coastal plain environments**

364 This depositional environment comprises facies associations AF3a (delta/estuarine), AF3b  
365 (fluvial/tidal distributary channels), AF3c (tidal sand flat), AF3d (lagoon/mudflat) (table 1).  
366 AF3a is mainly dominated by sigmoidal cross-bedded heterolithic rocks with mud drapes. It is  
367 also characterized by fine to coarse, poorly sorted sandstones and siltstones often structured  
368 by combined flow ripples, flaser bedding, wavy bedding, and some rare planar bedding. Mud  
369 clasts, root traces, desiccation cracks, water escape features, and shale pebbles are common.  
370 The presence of epsilon bedding is attested, which is formed by lateral accretion of a river  
371 point bar (Allen, 1983). The bed surface sets are intensively bioturbated (*Skolithos* and  
372 *Planolites*) indicating a shallow marine subtidal setting (Pemberton and Frey, 1982). Faunas  
373 such as brachiopods, trilobites, tentaculites, and graptolites are present. AF3b exhibits a  
374 fining-up sequence featured by a sharp erosional surface, trough cross-bedded, very coarse-  
375 grained, poorly sorted sandstone at the base and sigmoidal cross-bedding at the top (Figs 7 8  
376 and 8 9). AF3c is formed by fine-grained to very coarse-grained sigmoidal cross-bedded  
377 heterolithic sandstones with multidirectional tidal bundles. They are also structured by  
378 lenticular, flaser bedding and occasional current and oscillation ripples with mud cracks. They  
379 reveal intense bioturbation composed of *Skolithos* (Sk), *Thalassinoides* (Th), and *Planolites*  
380 (Pl) ichnofacies indicating a shallow marine subtidal setting (Frey et al., 1990; Pemberton and  
381 Frey, 1982). AF4d is characterized by horizontally laminated mudstones associated with  
382 varicolored shales and fine-grained sandstones. They exhibit mud cracks, occasional wave  
383 ripples, and rare multidirectional current ripples. These sedimentary structures are poorly  
384 preserved because of intense bioturbation composed of *Skolithos* (Sk), *Thalassinoides* (Th),  
385 and *Planolites* (Pl). Fauna includes ammonoids (rare), goniatites, calymenids, pelecypod  
386 molds, and brachiopod coquinas.

387 In AF3a, both tidal and fluvial systems in the same facies association can be interpreted as an  
388 estuarine system (Dalrymple et al., 1992; Dalrymple and Choi, 2007). The gamma-ray  
389 signature is characterized by a convex bell shape with rapidly alternating low to ~~high~~ mid  
390 values (30 to 60 gAPI) due to the mud draping of the sets (see E Fig. 8 9). These forms of  
391 gamma ray are typical of fluvial-tidal influenced environments with upward-fining  
392 parasequences (Rider, 1996; Serra and Serra, 2003; Wagoner et al., 1990). AF3a is identified  
393 at the top of the Pragian “Oued Samene” Formation and in Famennian “Khenig” Formation  
394 (Wendt et al., 2006) in the Ahnet and Mouydir basins. In the Illizi basin, AF3a is mostly  
395 recorded at the top Cambrian of the Ajgers Formation, in the Lochkovian ~~“Middle bar”~~ “Barre  
396 Moyenne”, and at the top Pragian of the ~~“Upper bar”~~ “Barre Supérieure” Formation (Beuf et  
397 al., 1971; Eschard et al., 2005). The AF3b association can be characterized by a mixed fluvial  
398 and tidal dynamic based on criteria such as erosional basal contacts, fining-upward trends or  
399 heterolythic facies (Dalrymple et al., 1992; Dalrymple and Choi, 2007). They are associated  
400 with abundant mud clasts, mud drapes, and bioturbation indicating tidal influences  
401 (Dalrymple et al., 1992, 2012; Dalrymple and Choi, 2007). The major difference with the  
402 estuarine facies association (AF3a) is the slight lateral extent of the channels which are only  
403 visible in outcrops (Eschard et al., 1999). The gamma-ray pattern is very similar to the  
404 estuarine electrofacies (see F Fig. 8 9). AF3c is interpreted as a tidal sandflat laterally present  
405 near a delta (Lessa and Masselink, 1995) and associated with an estuarine environment  
406 (Leuven et al., 2016). The gamma-ray signature (see G Fig. 8 9) is distinguishable by its  
407 concave funnel shape with alternating low and ~~high~~ mid peaks (25 to 60 gAPI) due to the  
408 heterogeneity of the deposits and rapid variations in the sand/shale ratio. These facies are  
409 observed in the ~~“Tigillites Talus”~~ “Talus à Tigillites” Formation of the Illizi basin (Eschard et  
410 al., 2005). In AF4d, both ichnofacies and facies are indicative of tidal mudflat/lagoonal  
411 depositional environments (Dalrymple et al., 1992; Dalrymple and Choi, 2007; Frey et al.,

412 1990). The gamma-ray signature has a distinctively high value (80 to 130 gAPI) and an erratic  
413 shape (see H Fig. 8 9). AF4d is observed in the “Atafaitafa” Formation and in the Emsian  
414 prograding shoreface sequence of the Illizi basin (Eschard et al., 2005). It is also recorded in  
415 the Lochkovian “Oued Samene” Formation and the Famennian “Khenig” Sandstones (Wendt  
416 et al., 2006).

#### 417 5.1.3 Shoreface environments

418 This depositional environment is composed of AF4a (subtidal), AF4b (upper shoreface), and  
419 AF4c (lower shoreface) facies associations (Table 1). AF4a is characterized by the presence  
420 of brachiopods, crinoids, and diversified bioturbations, by the absence of emersion, and by the  
421 greater amplitude of the sets in a dominant mud lithology (Eschard et al., 1999). AF4b is  
422 heterolithic and composed of fine to medium-grained sandstones (brownish) interbedded with  
423 argillaceous siltstones and bioclastic carbonated sandstones. Sedimentary structures include  
424 oscillation ripples, swaley cross-bedding, flaser bedding, cross-bedding, convolute bedding,  
425 wavy bedding, and low-angle planar cross-stratification. Sediments were affected by  
426 moderate to highly diversified bioturbation by *Skolithos* (Sk), *Cruziana*, *Planolites*, (Pl)  
427 *Chondrites* (Ch), *Teichichnus* (Te), *Spirophyton* (Sp) and are composed of ooids, crinoids,  
428 bryozoans, stromatoporoids, tabulate and rugose corals, pelagic stylolinids, neritic  
429 tentaculitids, and brachiopods. AF4c can be distinguished by a low sand/shale ratio, thick  
430 interbeds, abundant HCS, deep groove marks, slumping, and intense bioturbation (Table 1).

431 AF4a is interpreted as a lagoonal shoreface. The gamma-ray pattern (see I Fig. 8 9) is  
432 characterized by a concave bell shape influenced by a low sand/shale ratio with values  
433 fluctuating between 100 and 200 gAPI. AF4a is identified in the “Tigillites Talus” “Talus à  
434 Tigillites” Formation and the Emsian sequence of the Illizi basin (Eschard et al., 2005) and in  
435 the Lochkovian “Oued Samene” Formation (Wendt et al., 2006). AF4b is interpreted as a

436 shoreface environment. The presence of swaley cross-bedding produced by the amalgamation  
437 of storm beds (Dumas and Arnott, 2006) and other cross-stratified beds is indicative of upper  
438 shoreface environments (Loi et al., 2010). The gamma-ray pattern (see J and K Fig. 8 9)  
439 displays concave erratic egg shapes with a very regularly decreasing-upward trend and  
440 ranging from offshore shale with **high mid** values (80 to 60 gAPI) to clean sandstone with  
441 **lower** values at the top (40 to 60 gAPI). AF4b is observed in the “Atafaitafa” Formation  
442 corresponding to the “**Passage zone**” “**Zone de passage**” Formation of the Illizi basin (Eschard  
443 et al., 2005). AF4c is interpreted as a lower shoreface environment (Dumas and Arnott, 2006;  
444 Suter, 2006). The gamma-ray pattern displays the same features as the upper shoreface  
445 deposits with **lower higher** values (i.e. muddier facies) ranging from 100 to 80 gAPI (see J  
446 and K Fig. 8 9).

#### 447 **5.1.4 Offshore marine environments**

448 This depositional environment is composed of AF5a and AF5b facies associations (Table 1).  
449 AF5a is mainly defined by wavy to planar-bedded heterolithic silty-shales interlayered with  
450 fine-grained sandstones. It also contains bundles of skeletal wackestones and calcareous  
451 mudstones. The main sedimentary structures are lenticular sandstones, rare hummocky cross-  
452 bedding (**HCS**), mud mounds, low-angle cross-bedding, tempestite bedding, slumping, and  
453 deep groove marks. Sediments can present rare horizontal bioturbation such as *Zoophycos*  
454 (*Z*), *Teichichnus* (*Te*), and *Planolites* (*Pl*). AF5b is characterized by an association of black  
455 silty shales with occasional bituminous wackestones and packstones. It is composed of  
456 graptolites, goniatites, orthoconic nautiloids, pelagic pelecypods, limestone nodules,  
457 tentaculitids, ostracods, and rare fish remains. Rare bioturbation such as *Zoophycos* (*Z*) is  
458 visible.

459 In AF5a, the occurrence of HCS, the decrease in sand thickness and grain size together with  
460 the ~~fossil traces~~ bioturbation and the floro-faunal associations indicate a deeper marine  
461 environment under the influence of storms (Aigner, 1985; Dott and Bourgeois, 1982; Reading  
462 and Collinson, 2009). AF5a is interpreted as upper offshore deposits (i.e. offshore  
463 transitional). The gamma-ray pattern is serrated and erratic with values well grouped around  
464 high values from 120 to 140 gAPI (see L Fig. 8 9). Positive peaks may indicate siltstone to  
465 sandstone ripple beds. AF5b is interpreted as lower offshore deposits (Aigner, 1985; Stow et  
466 al., 2001; Stow and Piper, 1984). Here again the gamma-ray signature is serrated and erratic  
467 with values well grouped around 140 gAPI (see L Fig. 8 9). Hot shales with anoxic conditions  
468 are characterized by gamma-ray peaks (>140 gAPI). These gamma-ray patterns are typical of  
469 offshore environments dominated by shales (Rider, 1996; Serra and Serra, 2003; Wagoner et  
470 al., 1990). AF5a and AF5b are observed in the Silurian “~~Graptolites~~-shales” “Argiles à  
471 Graptolites” Formation and the Emsian “Orsine” Formation of the Illizi basin (Beuf et al.,  
472 1971; Eschard et al., 2005; Legrand, 1986, 2003b). The “Argiles de Mehden Yahia” and  
473 “~~Termatasset~~” “Argiles de Temertasset” shales have the same facies (Wendt et al., 2006).

## 474 5.2 Sequential framework and unconformities

475 The high-resolution facies analysis, depositional environments, stacking patterns, and surface  
476 geometries observed in the ~~Paleozoic Devonian~~ succession reveal at least two different orders  
477 of depositional sequences (large and medium scale, Fig. 7 8) considered as  
478 transgressive/regressive T/R (Catuneanu et al., 2009). The sequential framework proposed in  
479 Fig. 7 8B result from the integration of the vertical evolution the main surfaces (Fig. 7 8A)  
480 and the gamma-ray pattern (Fig. 8 9). The Devonian series under focus exhibits nine medium-  
481 scale sequences (D1 to D9, Fig. 7 8; Figs 9 10, 10 11, ~~supplementary data 2 and 3~~ 12 and 13)  
482 bounded by 10 major sequence boundaries (HD0 to HD9), and nine major flooding surfaces  
483 (MFS1 to MFS9). The correlation of the different sequences at the scale of the different

484 basins and arches is used to build two E–W (Figs 9–10, 10–11, ~~supplementary data 2~~ and 12)  
485 and one N–S (~~supplementary data 3~~ Fig. 13) cross-sections.

486 The result of the analysis of the general pattern displayed by the successive sequences reveal  
487 two major patterns (Figs 9–10, 12 and 10–13) limited by a major flooding surface MFS5. The  
488 first pattern extends from the Oued Samene to Adrar Morrat Formations and is dated from the  
489 Lochkovian to Givetian. D1 to D5 medium-scale sequences indicate a general proximal  
490 clastic depositional environment (dominated by fluvial to transitional and shoreface facies)  
491 with intensive lateral facies evolution. This first pattern is thin (from 500 m in the basin  
492 depocenter to 200 m around the basin rim) and with successive amalgamated surfaces on the  
493 edge of the arches between the “~~Passage zone~~” “Zone de passage” and “Oued Samene”  
494 Formations (e.g. Figs 5–C–C’, 6A, 6C, 6D, 10 and 9–13). It is delimited at the bottom by the  
495 HD0 surface corresponding to the Silurian/Devonian boundary. D1 to D3 are composed of T–  
496 R sequences with a first deepening transgressive trend indicative of a transition from  
497 continental to marine deposits bounded by a major MFS and evolving into a second  
498 shallowing trend from deep marine to shallow marine depositional environments. D1 to D3  
499 thin progressively toward the edge and the continental deposits, in the central part of the  
500 basin, pass laterally into a major unconformity. The amalgamation of the surfaces and ~~rapid~~  
501 lateral variations of facies between the Ahnet basin and Azzel Matti and Arak-Foum Belrem  
502 arches demonstrate a tectonic control related to the presence of subsiding basins and paleo-  
503 highs (i.e. arches).

504 D4 and D5 display the same T–R pattern with a reduced continental influence and upward  
505 decrease in lateral facies variations and thicknesses where the MFS4 marks the beginning of a  
506 marine-dominated regime in the entire area. It is identified as the early Eifelian transgression  
507 defined by Wendt et al., (2006). The D5 sequence is mainly composed of shoreface  
508 carbonates. Evidence of mud mounds preferentially located along faults are well-documented

509 in the area for that time (Wendt et al., 1993, 1997, 2006; Wendt and Kaufmann, 1998). This  
510 change in the general pattern indicates reduced tectonic influence.

511 MFS5, at the transition between the two main patterns, represents a major flooding surface on  
512 the platform and is featured worldwide by deposition of “hot shales” during the early Frasnian  
513 (Lüning et al., 2003, 2004; Wendt et al., 2006).

514 The second pattern extends from the “Mehden Yahia”, “Temertasset” to “Khenig” Formations  
515 dated Frasnian to Lower Tournaisian. This pattern is composed of part of D5 to D9 medium-  
516 scale sequences. It corresponds to homogenous offshore depositional environments with no  
517 lateral facies variations. However, local deltaic (fluvio-marine) conditions are observed  
518 during the Frasnian at the Arak Foum Belrem arch ([“Grès de Mehden Yahia” in Fig. 10](#) [12](#)).  
519 A successive alternation of shoreface and offshore deposits is organized into five medium-  
520 scale sequences (part of D5, and D6 to D9; Figs [9](#) [10](#), [11](#) and [10](#) [12](#)). [They in particular show](#)  
521 [some regressive phases with the deposition of both “Grès de Mehden Yahia” and “Grès du](#)  
522 [Khnig” sandstones \(bounded by HD6 and HD9\)](#). This pattern [\(i.e. part of D5 to D9 \)](#)  
523 corresponds to the general maximum flooding (Lüning et al., 2003, 2004; Wendt et al., 2006)  
524 under eustatic control with no tectonic influences.

525 **6 Subsidence and tectonic history: An association of low rate extensional subsidence  
526 and positive inversion pulses**

527 The backstripping approach (Fig. [14](#) [14](#)) was applied to five wells (W1, W5, W7, W17, and  
528 W21). The morphology of the backstripped curve and subsidence rates can provide clues as to  
529 the nature of the sedimentary basin (Xie and Heller, 2006). In intracratonic basins,  
530 reconstructed tectonic subsidence curves are almost linear to gently exponential in shape,  
531 similar to those of passive margins and rifts (Xie and Heller, 2006). The compilation of  
532 tectonic backstripped curves from several wells in peri-Hoggar basins (Fig. [14](#) [14](#)A, see Fig. 1

533 for location) and from wells in the study area (Fig. 44 14B) display low rates of subsidence  
534 (from 5 to 50 m/Myr) organized in subsidence patterns of: Inversion of the Low Rate  
535 Subsidence (ILRS type c, red line, Fig. 44 14C), Deceleration of the Low Rate Subsidence  
536 (DLRS type b, black line), and Acceleration of the Low Rate Subsidence (ALRS type a, blue  
537 line).

538 Each period of ILRS, DLRS, and ALRS may be synchronous among the different wells  
539 studied (see B1 to J, Fig. 44 14B) and some wells of published data (see D to J Fig. 44 14A).

540 The Saharan Platform is marked by a rejuvenation of basement structures, around arches (Figs  
541 1, 2, 3, and 4 3), linked to regional geodynamic pulses during Neoproterozoic to Paleozoic  
542 times (Fig. 44 14). A compilation of the literature shows that the main geodynamic events are  
543 associated with discriminant association of subsidence patterns:

544 (A) Late Pan-African compression and collapse (patterns a, b, and c, A Fig. 44 14A). The  
545 Infra-Cambrian (i.e. top Neoproterozoic) is characterized by horst and graben architecture  
546 associated with wedge-shaped unit DO0 in the basement (Fig. 9 and 10 Fig. 7). This  
547 structuring probably related to Pan-African post-orogenic collapse is illustrated by  
548 intracratonic basins infilled with volcano-sedimentary molasses series (Ahmed and Moussine-  
549 Pouchkine, 1987; Coward and Ries, 2003; Fabre et al., 1988; Oudra et al., 2005).

550 (B) Cambrian-Ordovician geodynamic pulse (Fig. 44A-B 14). Highlighted by the wedge-  
551 shaped units DO1 (Figs 5 6A-A' and 6 7), the horst-graben system is correlated with  
552 deceleration (DLRS pattern a, B1) and with local acceleration of the subsidence (ALRS  
553 pattern b, B2). The Cambrian-Ordovician extension is documented on arches (Arak-Foum  
554 Belrem, Azzel Matti, Amguid El Biod, Tihemboka, Gargaf, Murizidié, Dor El Gussa, etc.) of  
555 the Saharan Platform by synsedimentary normal faults, reduced sedimentary successions  
556 (Bennacef et al., 1971; Beuf et al., 1968b, 1968a, 1971; Beuf and Montadert, 1962; Borocco

557 and Nyssen, 1959; Claracq et al., 1958; Echikh, 1998; Eschard et al., 2010; Fabre, 1988;  
558 Ghienne et al., 2003, 2013; Zazoun and Mahdjoub, 2011) and by stratigraphic hiatuses  
559 (Mélou et al., 1999; Oulebsir and Paris, 1995; Paris et al., 2000; Vecoli et al., 1995, 1999).

560 (C) Late Ordovician geodynamic pulse (i.e. Hirnantian glacial and isostatic rebound; Fig.  
561 ~~11A-B~~ 14). Late Ordovician incisions mainly situated at the hanging walls of normal faults  
562 (Fig. ~~6~~ 7C and ~~6~~ 7D) are interpreted as ~~Hirnantian glacial valleys~~ Hirnantian glacial-  
563 Palaeovalleys (Le Heron, 2010; Smart, 2000) and followed by local inversion of low rate  
564 subsidence (ILRS of type c, C in Fig. ~~11A~~ 14).

565 (D) Silurian extensional geodynamic pulse (D, Figs ~~11A~~ 14). The Silurian post-glaciation  
566 period is featured by the reactivation and sealing of the inherited horst and graben fault  
567 system (i.e. wedge-shaped unit DO2; Figs ~~5~~ 6B-B', ~~5~~ 6C-C', ~~6~~ 7A and ~~6~~ 7B). It is linked to an  
568 acceleration of the subsidence (ALRS of pattern b in Fig. ~~11A~~ 14). This tectonic extension is  
569 documented in seismic (Najem et al., 2015) and is associated to the Silurian major  
570 transgression on the Saharan platform (e.g. Eschard et al., 2005; Lüning et al., 2000).

571 (E) Late Silurian to -Early Devonian geodynamic pulse (Caledonian compression; E Fig. ~~11A~~  
572 14). Late Silurian times are marked by reactivation and local positive inversion of the former  
573 structures (Figs ~~5~~ 6C-C' and ~~6~~ 7B); by truncations located at fold hinges (Figs ~~5~~ 6C-C' and ~~6~~  
574 7); and by a major shift from marine to fluvial/transitional environments (e.g. Figs 10 9,  
575 supplementary data 2 and 3). Backstripped curves register an inversion of the subsidence  
576 (ILRS of pattern c, in Fig. ~~11A~~ 14). The Caledonian event is mentioned as related to large-  
577 scale folding or uplifted arches (e.g. the Gargaff, Tihemboka, Ahara, Murizidé-Dor el Gussa  
578 and Amguid El Biod arches) and it is associated with breaks in the series and with angular  
579 unconformities (Beuf et al., 1971; Bijou-Duval et al., 1968; Boote et al., 1998; Boudjema,  
580 1987; Boumendjel et al., 1988; Carruba et al., 2014; Chavand and Claracq, 1960; Coward and

581 Ries, 2003; Dubois and Mazelet, 1964; Echikh, 1998; Eschard et al., 2010; Fekirine and  
582 Abdallah, 1998; Follot, 1950; Frizon de Lamotte et al., 2013; Ghienne et al., 2013; Gindre et  
583 al., 2012; Legrand, 1967b, 1967a; Magloire, 1967).

584 (F) Early Devonian tectonic quiescence (F Figs 41A 14). This is characterized by a  
585 deceleration of the low rate subsidence (DLRS of pattern a, F in Figs 41A 14). During this  
586 period, we have detected Emsian truncation from satellite images (Figs. 6D and 6E) and  
587 erosion and pinch out of upper Emsian to Eifelian series from well cross sections (Figs. 10, 12  
588 and 13). In previous works, these hiatuses/gaps (i.e. Upper Lochkovian, Lower Pragian,  
589 Upper Pragian, Upper Emsian, Lower Eifelian) are observed in the Ahnet basin (Kermandji,  
590 2007; Kermandji et al., 2003, 2008, 2009; Wendt et al., 2006), in the Illizi (Boudjema, 1987)  
591 and in the Reggane (Jäger et al., 2009).

592 (G and H) Middle to late Devonian geodynamic pulse (extension and local inversions, G and  
593 H Fig. 41A 14). The Mid to Late Devonian period is characterized by large wedge hiatuses  
594 and truncations associated with the reactivation of horst and graben structures and local  
595 positive inversion (OD3 in Figs 5 6D-D', 6E, 6F, 6 7 and 10 to 13 9, 10 ~~supplementary data 2~~  
596 ~~and 3~~). This period is characterized by inversion and acceleration of low rate subsidence  
597 (patterns c and b: ILRS - ALRS, Fig. 41A 14). Some of the Middle to Late Devonian syn-  
598 tectonic structures and hiatuses (Early Eifelian e.g. Givetian/Frasnian) are noticed in the  
599 Ahnet basin (Wendt et al., 2006), ~~in the Reggane (Jäger et al., 2009)~~, on the Amguid Ridge  
600 ~~(Wendt et al., 2006)~~ (Wendt et al., 2009b), in the Illizi basin (Boudjema, 1987; Chaumeau et  
601 al., 1961; Eschard et al., 2010; Fabre, 2005; Legrand, 1967a), on the Gargaf (Carruba et al.,  
602 2014; Collomb, 1962; Fabre, 2005; Massa, 1988) and elsewhere on the platform (Frizon de  
603 Lamotte et al., 2013).

604 (H to K I and J) Pre-Hercynian to Hercynian geodynamic pulses (I and J Fig. 11A 14). This  
605 period is organized in Early Carboniferous pre-Hercynian (H I, Fig. 11A 14) to Late  
606 Carboniferous-Early Permian Hercynian (K, Fig. 11A B) compressions limited by Mid  
607 Carboniferous tectonic quiescence/extension (J, Fig. 11A 14). The Carboniferous period is  
608 characterized by a normal reactivation and local positive inversion of the previous structural  
609 patterns involving reverse faults, overturned folds, transpressional flower structures along  
610 strike-slip fault zones (Figs 3, 5 6F-F', 6 7B, 6 7C and 6 7D). The major Carboniferous  
611 tectonic event on the Saharan Platform impacted all arches and it is mainly controlled by  
612 near-vertical basement faults with a strike-slip component (Boote et al., 1998; Caby, 2003;  
613 Carruba et al., 2014; Haddoum et al., 2001, 2013; Liégeois et al., 2003; Wendt et al., 2009a;  
614 Zazoun, 2001, 2008). According these authors basement fabric features exerted a very strong  
615 control on the structural evolution during the Hercynian deformation. Two major hiatuses (i.e.  
616 Mid Tournaisian to Mid Visean– Serpukhovian) are recognized (Wendt et al., 2009a).

617 The geodynamic pulses attest to the reactivation of the terranes and associated lithospheric  
618 fault zones. This observation questions the nature of the Precambrian basement and associated  
619 structural heritage.

620 **7 Basement characterization: Precambrian structural heritage: ~~accreted lithospheric~~**  
621 ~~terrane~~ ~~limited by vertical strike-slip mega shear zones~~

622 ~~The 800 km<sup>2</sup> outcrop of basement rocks of the Hoggar shield massif provides an exceptional~~  
623 ~~ease of an exhumed mobile belt composed of accreted terranes of different ages. The Hoggar~~  
624 ~~shield massif is composed of several accreted, sutured, and amalgamated terranes of various~~  
625 ~~ages and compositions resulting from multiple phases of geodynamic events (Bertrand and~~  
626 ~~Caby, 1978; Black et al., 1994; Caby, 2003; Liégeois et al., 2003).~~

627 To reconstruct the nature of the basement, a terrane map (Fig. 12–15) was put together by  
628 integrating geophysical data (aeromagnetic anomaly map: <https://www.geomag.us/>, Bouguer  
629 gravity anomaly map: <http://bgi.omp.obs-mip.fr/>), satellite images (7ETM+ from Landsat  
630 USGS: <https://earthexplorer.usgs.gov/>) data, geological maps (Berger et al., 2014; Bertrand  
631 and Caby, 1978; Black et al., 1994; Caby, 2003; Fezaa et al., 2010; Liégeois et al., 1994,  
632 2003, 2005, 2013), and geochronological data (e.g. U-Pb radiochronology, see supplementary  
633 data S1). Geochronological data from published studies were compiled and georeferenced  
634 (Fig. 1). Thermo-tectonic ages were grouped into eight main thermo-orogenic events (Fig. 1):  
635 The Liberian-Ouzzalian event (Archean, >2500 Ma), (the Archean, Eburnean (i.e.  
636 Paleoproterozoic, 2500–1600 Ma), the Kibarian (i.e. Mesoproterozoic, 1600–1100 Ma), the  
637 Neoproterozoic oceanization rifting (1100–750 Ma), the Neoproterozoic syn-Pan-African  
638 orogeny (i.e. Neoproterozoic, 750–541 Ma), the post Pan-African (i.e. Neoproterozoic, 541–  
639 443 Ma), the Caledonian orogeny (i.e. Siluro-Devonian, 443–358 Ma), and the Hercynian  
640 orogeny (i.e. Carbo-Permian, 358–252 Ma). Geochronological data show that the different  
641 terranes were reworked during several main thermo-orogenic events. Twenty-three well  
642 preserved terranes in the Hoggar were identified and grouped into Archean, Paleoproterozoic,  
643 and Mesoproterozoic Neoproterozoic juvenile Pan-African terranes (see legend in Fig. 1). In  
644 the West African Craton, the Reguibat shield is composed of Archean terrains in the west and  
645 of Paleoproterozoic terranes in the east (Peucat et al., 2003, 2005). The two main events  
646 deduced from geochronological data are the Neoproterozoic (i.e. Pan-African) and  
647 Paleoproterozoic (i.e. Eburnean) episodes (Bertrand and Caby, 1978). Aeromagnetic anomaly  
648 surveys are commonly used to analyze geological features such as rock types and fault zones  
649 (e.g. Turner et al., 2007). A similar study was led in the meantime showing similar  
650 interpretations (Bournas et al., 2003; Brahimi et al., 2018). In this study, these data highlight  
651 the geometries and the extension of the different terranes under the sedimentary cover. Four

652 main domains can be identified from the aeromagnetic anomaly map, delimited by contrasted  
653 magnetic signatures and interpreted as suture zones (thick black lines, Fig. 42 15A). The  
654 study area is bounded to the south by the Tuareg Shield (TS), to the north, by the south  
655 Atasic Range, to the west by the West African Craton (WAC) and at the east by the East  
656 Saharan Craton (ESC) or Saharan Metacraton (Abdelsalam et al., 2002).

657 The magnetic disturbance features (Fig. 42 15A) show three main magnetic trends. A major  
658 NS sinuous fabric and two minor sinuous 130–140°E and N45°E trends. The major NS  
659 lineaments coincide with terrane boundaries and mega-shear zones (e.g. 4°50', 4°10', WOSZ,  
660 EOSZ, 8°30', RSZ shear zones; Fig. 1). Sigmoidal-shaped terranes 200 to 500 km long and  
661 100 km wide are characterized (red lines in Fig. 42 15A). The whole assemblage forms a  
662 typical SC-shaped shear fabric (Choukroune et al., 1987) associated with vertical mega-shear  
663 zones and suture zones (e.g. WOSZ, EOSZ, 4°10', 4°50' or 8°30' Hoggar shear zones in Fig.  
664 1). The SC fabrics combined with subvertical lithospheric shear zones ([Fig. 16B and C](#)) are  
665 typical features of the Paleoproterozoic accretionary orogens (Cagnard et al., 2011; Chardon  
666 et al., 2009). This architecture is concordant with the Neoproterozoic collage of the Tuareg  
667 Shield (i.e. mobile belt) between the West African Craton and the East Saharan Craton (i.e.  
668 cratonic blocks) described by (Coward and Ries, 2003; Craig et al., 2008).

669 The gravimetric anomaly map (Fig. 42 15B) shows a correlation between gravimetric  
670 anomalies and tectonic architecture (intracratonic syncline-shaped basin and neighboring  
671 arches). Positive anomalies (> 66 mGal) are mainly associated with arches whereas negative  
672 anomalies are related to intracratonic basins (< 66 mGal). Nevertheless, negative anomaly  
673 disturbance is found in the Hoggar massif probably due to Cenozoic volcanism and the  
674 Hoggar swell (Liégeois et al., 2005) or to Eocene Alpine intraplate lithospheric buckling  
675 (Rougier et al., 2013).

676 The Precambrian structural heritage is characterized by accreted lithospheric terranes limited  
677 by vertical strike-slip mega shear zones (Fig. 16B and C). A zonation is observed between the  
678 Paleozoic basins and arches configurations and the different terranes (thermo-tectonic age).

679 Arches are linked to Archean to Paleoproterozoic continental terranes in contrast to syncline-  
680 shaped basins which are associated with Meso-Neoproterozoic terranes (Figs 1, 2 and 12A-B-  
681 16A-E).

682 **8 Low subsidence rate intracratonic Paleozoic basins of the Central Sahara provide a**  
683 **basis for an integrated modeling study**

684 Paleozoic intracratonic basins with similar characteristics (architecture, subsidence rate,  
685 stratigraphic partitioning, alternating episodes of intraplate extension and short duration  
686 compressions with periods of tectonic quiescence, etc.) have been documented in North  
687 America (e.g. Allen and Armitage, 2011; Beaumont et al., 1988; Burgess, 2008; Burgess et  
688 al., 1997; Eaton and Darbyshire, 2010; Pinet et al., 2013; Potter, 2006; Sloss, 1963; Xie and  
689 Heller, 2006), South America (Allen and Armitage, 2011; de Brito Neves et al., 1984; Milani  
690 and Zalan, 1999; de Oliveira and Mohriak, 2003; Soares et al., 1978; Zalan et al., 1990),  
691 Russia (Allen and Armitage, 2011; Nikishin et al., 1996) and Australia (Harris, 1994; Lindsay  
692 and Leven, 1996; Mory et al., 2017). However, the nature of the potential driving processes  
693 (lithospheric folding, far-field stresses, local increase in the geotherm, mechanical anisotropy  
694 from lithospheric rheological heterogeneity, etc.) associated with the formation of  
695 intracratonic Paleozoic basins remains highly speculative (Allen and Armitage, 2011;  
696 Armitage and Allen, 2010; Braun et al., 2014; Burgess and Gurnis, 1995; Burov and  
697 Cloetingh, 2009; Cacace and Scheck-Wenderoth, 2016; Célérier et al., 2005; Gac et al., 2013;  
698 Heine et al., 2008; Leeder, 1991; Vauchez et al., 1998).

699 The multiscale and multidisciplinary analysis performed in this study enable us to document a  
700 model of Paleozoic intracratonic Central Saharan basins coupling basin architecture and  
701 basement structures (Fig. 43–17). While we do not provide any quantitative explanations for  
702 the dynamics of these basins, our synthesis highlights that their subsidence is not the result of  
703 a single process and we attempt here to make a check-list of the properties that a generic  
704 model of formation of such basins must capture:

705 (A) The association of syncline-shaped wide basins and neighboring arches (i.e. paleo-highs).  
706 The structural framework shows a close association of syncline-shaped basins, inter-basin  
707 principal to secondary arches, and intra-basin secondary arches (see Fig. 3–2).

708 (B) By local horst and graben architecture linked to steep-dipping planar normal faults and  
709 associated with normal fault-related fold structures (i.e. forced folds; a, Fig. 43–17A). Locally,  
710 the extensional structures are disrupted by positive inversion structures (b, Fig. 43–17A) or  
711 transported normal faults (c, Fig. 43–17A).

712 (C) A low rate of subsidence ranging between 5 to 50 m/Myr (Fig. 11–14).

713 (D) Long periods of extension and tectonic quiescence are interrupted by brief periods of  
714 compression or glaciation/deglaciation events (Beuf et al., 1971; Denis et al., 2007; Le Heron  
715 et al., 2006). These periods of compression are possibly related to intraplate compression  
716 linked to distal orogenies (i.e. Late Silurian Caledonian event, Late Carboniferous Hercynian,  
717 (Frizon de Lamotte et al., 2013) or to intraplate arch uplift related to magmatism (Derder et  
718 al., 2016; Fabre, 2005; Frizon de Lamotte et al., 2013; Moreau et al., 1994).

719 (E) Synsedimentary divergent onlaps and local unconformities are identified from integrated  
720 seismic data, satellite images, and borehole data (Figs 4, 5, 6, 7–9 and 10 to 13). The periods  
721 of tectonic activity are characterized by normal to reverse reactivation of border faults,

722 emplacement of wedge-shaped units, and erosional unconformities neighboring the arches  
723 ([Figs 3, 4, 5, 6, 9, 10 and 13](#)).

724 (F) The stratigraphic architecture displays a lateral facies variation and partitioning between  
725 distal marine facies infilling the intracratonic basins (i.e. offshore deposits) and proximal  
726 amalgamated facies (i.e. fluvio-marine, shoreface) associated with prominent stratigraphic  
727 hiatus and erosional unconformities in the vicinity of the arches.

728 (G) A close connection is evidenced between the period of tectonic deformation and the  
729 presence of erosional unconformities (i.e. 2, 3, 6, 8, 10 geodynamic events in Fig. [13](#) [17B](#)).  
730 By contrast, the periods of tectonic quiescence and extension are characterized by low lateral  
731 facies variations, thin deposits, and the absence of erosional surfaces.

732 (H) The Precambrian heritage corresponds to Archean to Paleoproterozoic terranes identified  
733 in the Hoggar massif and reactivated during the Meso-Neoproterozoic Pan-African cycle (Fig.  
734 1). The Precambrian lithospheric heterogeneity illustrated by the different characteristics of  
735 Precambrian terranes (wavelength, age, nature, fault zones) spatially control the emplacement  
736 of the syncline-shaped intracratonic basins underlain by Meso–Neoproterozoic oceanic  
737 terranes and the arches underlain by Archean to Paleoproterozoic continental terranes (Figs 1,  
738 [3](#) [2](#) and [13](#) [16](#)). Many authors suggest control of the basement fabrics is inherited from the  
739 Pan-African orogeny in the Saharan basins (Beuf et al., 1968b, 1971; Boote et al., 1998;  
740 Carruba et al., 2014; Coward and Ries, 2003; Eschard et al., 2010; Guiraud et al., 2005;  
741 Sharata et al., 2015).

742 **9 Conclusion**

743 Our integrated approach using both geophysical (seismic, gravity, aeromagnetic, etc.) and  
744 geological (well, seismic, satellite images, etc.) data has enabled us to decrypt the  
745 characteristics of the intracratonic Paleozoic Saharan basins and the control of the

746 heterogeneous lithospheric heritage of the horst and graben architecture, low rate subsidence,  
747 association of long-lived broad synclines and anticlines (i.e. arches swells, domes, highs or  
748 ridges) with very different wavelengths ( $\lambda$ ) (tens to hundreds of kilometers). A coupled basin  
749 architecture and basement structures model is proposed (Fig. 17).

750 This study highlights a tight control of the heterogeneous lithosphere zonation over the  
751 structuring of the intracratonic Central Saharan basin. This particular type of basin is  
752 characterized by a low rate of subsidence and fault activation controlling the homogeneity of  
753 sedimentary facies and the distribution of the main unconformities. The low rate activation of  
754 vertical mega-shear zones bounding the intracratonic basin during Paleozoic times contrasts  
755 markedly with classic rift kinematics and architecture. Three different periods of tectonic  
756 compressional pulses (i.e. Caledonian, Middle to Late Devonian, Pre-Hercynian), extension  
757 and quiescence are identified and controlled the sedimentary distribution (Fig. 17). An  
758 understanding of tectono-sedimentary interaction is key to understanding the distribution of  
759 the Paleozoic petroleum reservoirs of this first-order oil province.

## 760 Acknowledgements

761 We are most grateful to ENGIE/NEPTUNE who provided the database used in this paper and  
762 who funded the work. Special thanks to the data management service of ENGIE/NEPTUNE  
763 (especially Aurelie Galvani) for their help with the database. Specific appreciations for  
764 detailed reviews/comments from Jobst Wendt, Réda Samy Zazoun and Fabio Lottaroli, along  
765 with a short comment from Alexander Peace, which have considerably enriched and  
766 improved this paper.

## 767 References

- 768 Abdelsalam, M. G., Liégeois, J.-P. and Stern, R. J.: The saharan metacraton, J. Afr. Earth Sci.,  
769 34(3), 119–136, 2002.

- 770 Abdesselam-Rouighi, F.: Etude palynologique du sondage Sebkhet El Melah (unpublished),  
771 Entreprise nationale Sonatrach division hydrocarbures direction Laboratoire central des  
772 hydrocarbures, Boumerdès., 1977.
- 773 Abdesselam-Rouighi, F.: Résultats de l'étude palynologiques des sondage Garet El Guefoul  
774 Bassin de l'Ahnet-Mouydir (unpublished), Entreprise nationale Sonatrach division  
775 hydrocarbures direction Laboratoire central des hydrocarbures, Boumerdès., 1991.
- 776 Ahmed, A. A.-K. and Moussine-Pouchkine, A.: Lithostratigraphie, sédimentologie et  
777 évolution de deux bassins molassiques intramontagneux de la chaîne Pan-Africaine: la Série  
778 pourprée de l'Ahnet, Nord-Ouest du Hoggar, Algérie, *J. Afr. Earth Sci.* 1983, 6(4), 525–535,  
779 1987.
- 780 Aigner, T.: Storm depositional systems: dynamic stratigraphy in modern and ancient shallow-  
781 marine sequences, *Lect. Notes Earth Sci. Berl. Springer Verl.*, 3, 1–158, 1985.
- 782 Allen, J. R. L.: Studies in fluvial sedimentation: bars, bar-complexes and sandstone sheets  
783 (low-sinuosity braided streams) in the Brownstones (L. Devonian), Welsh Borders, *Sediment.*  
784 *Geol.*, 33(4), 237–293, 1983.
- 785 Allen, P. A. and Allen, J. R.: Subsidence and thermal history, in *Basin analysis: Principles*  
786 and applications, pp. 349–401, Wiley-Blackwell, Oxford., 2005.
- 787 Allen, P. A. and Armitage, J. J.: Cratonic Basins, in *Tectonics of Sedimentary Basins*, edited  
788 by C. Busby and A. Azor, pp. 602–620, John Wiley & Sons, Ltd., 2011.
- 789 Angevine, C. L., Heller, P. L. and Paola, C.: Quantitative sedimentary basin modeling,  
790 American Association of Petroleum Geologists., 1990.

- 791 Armitage, J. J. and Allen, P. A.: Cratonic basins and the long-term subsidence history of  
792 continental interiors, *J. Geol. Soc.*, 167(1), 61–70, doi:10.1144/0016-76492009-108, 2010.
- 793 Askri, H., Belmecheri, A., Benrabah, B., Boudjema, A., Boumendjel, K., Daoudi, M., Drid,  
794 M., Ghalem, T., Docca, A. M., Ghandriche, H. and others: Geology of Algeria, in Well  
795 Evaluation Conference Algeria, pp. 1–93, Schlumberger-Sonatrach., 1995.
- 796 Azzoune, N.: Analyse palynologique de trois (03) échantillons de carottes du sondages W7,  
797 Sonatrach (unpublished), Entreprise nationale Sonatrach division hydrocarbures direction  
798 Laboratoire central des hydrocarbures, Boumerdès., 1999.
- 799 Badalini, G., Redfern, J. and Carr, I. D.: A synthesis of current understanding of the structural  
800 evolution of North Africa, *J. Pet. Geol.*, 25(3), 249–258, 2002.
- 801 Beaumont, C., Quinlan, G. and Hamilton, J.: Orogeny and stratigraphy: Numerical models of  
802 the Paleozoic in the eastern interior of North America, *Tectonics*, 7(3), 389–416, 1988.
- 803 Bellahsen, N. and Daniel, J. M.: Fault reactivation control on normal fault growth: an  
804 experimental study, *J. Struct. Geol.*, 27(4), 769–780, doi:10.1016/j.jsg.2004.12.003, 2005.
- 805 Bennacef, A., Beuf, S., Biju-Duval, B., Charpal, O. de, Gariel, O. and Rognon, P.: Example  
806 of Cratonic Sedimentation: Lower Paleozoic of Algerian Sahara, *AAPG Bull.*, 55(12), 2225–  
807 2245, 1971.
- 808 Bennacef, A., Attar, A., Froukhi, R., Beuf, S., Philippe, G., Schmerber, G. and Vermeire, J.  
809 C.: Cartes Géologiques d'Iherir-Dider (NG-32-IX), Iherir (NG-32-X), Illizi (NG-32-XV),  
810 Aharhar (NG-32-VIII), Oued Samène (NG-32-XIV), Erg Tihodaine (NG-32-VII), Tin  
811 Alkoum (NG-32-V), Djanet (NG-32-IV), Ta-N-Mellet (NG-32-XIII), Ta-N-Elak (NG-32-  
812 XIX), Fort Tarat (NG-32-XVI), Tilmas El Mra (NG-31-XXIV), Ers Oum El Lil (NG-31-

- 813 XXII), Amguid (NG-31-XVIII), 1/200000 Sonatrach-Ministère de l'Industrie et des Mines,  
814 Algérie, 1974.
- 815 Bensalah, A., Beuf, S., Gabriel, O., Philippe, G., Lacot, R., Paris, A., Basseto, D., Conrad, J.  
816 and Moussine-Pouchkine, A.: Cartes Géologiques de Khanguet El Hadid (NG-31-XVII), Aïn  
817 Tidjoubar (NG-31-XVI), Oued Djaret (NG-31-XV), Aoulef El Arab (NG-31-XIV), Reggane  
818 (NG-31-XIII), Ifetessene (NG-31-IX), Arak (NG-31-X et NG-31-IV), Meredoua (NG-31-  
819 XIII), Tanezrouft (NG-31-VII et NG-31-I), In Heguis (NG-31-IX), Tin Senasset (NG-31-III),  
820 Ouallene (NG-31-II) 1/200000 Sonatrach-Ministère de l'Industrie et des Mines, Algérie, 1971.
- 821 Berger, J., Ouzegane, K., Bendaoud, A., Liégeois, J.-P., Kiénast, J.-R., Bruguier, O. and  
822 Caby, R.: Continental subduction recorded by Neoproterozoic eclogite and garnet  
823 amphibolites from Western Hoggar (Tassendjanet terrane, Tuareg Shield, Algeria),  
824 Precambrian Res., 247, 139–158, doi:10.1016/j.precamres.2014.04.002, 2014.
- 825 Bertrand, J. M. L. and Caby, R.: Geodynamic evolution of the Pan-African orogenic belt: A  
826 new interpretation of the Hoggar shield (Algerian Sahara), Geol. Rundsch., 67(2), 357–388,  
827 doi:10.1007/BF01802795, 1978.
- 828 Beuf, S. and Montadert, L.: Géologie-sur une discordance angulaire entre les unites II et III  
829 du Cambro-Ordovicien au sud-est de la plaine de Dider (Tassili des Ajers), Compte Rendus  
830 Hebd. Séances L'Académie Sci., 254(6), 1108, 1962.
- 831 Beuf, S., Biju-Duval, B., Mauvier, A. and Legrand, P.: Nouvelles observations sur le  
832 ‘Cambro-Ordovicien’ du Bled El Mass (Sahara central), Publ. Serv. Géologique Algér. Bull.,  
833 38, 39–51, 1968a.
- 834 Beuf, S., Biju-Duval, B., De Charpal, O., Gariel, O., Bennacef, A., Black, R., Arene, J.,  
835 Boissonnas, J., Chachau, F., Guérangé, B. and others: Une conséquence directe de la structure

- 836 du bouclier Africain: L'ébauche des bassins de l'Ahnet et du Mouydir au Paléozoïque  
837 inférieur, Publ. Serv. Géologique L'Algérie Nouv. Sér. Bull., 38, 105–34, 1968b.
- 838 Beuf, S., Biju-Duval, B., De Charpal, O. and Gariel, O.: Homogénéité des directions des  
839 paléocourants du Dévonien inférieur au Sahara central, Comptes Rendus L'Académie Sci.  
840 Sér. D, 268, 2026–9, 1969.
- 841 Beuf, S., Biju-Duval, B., de Charpal, O., Rognon, P., Gabriel, O. and Bennacef, A.: Les grès  
842 du Paléozoïque inférieur au Sahara: Sédimentation et discontinuités évolution structurale d'un  
843 craton, Technip., Paris., 1971.
- 844 Biju-Duval, B., de Charpal, O., Beuf, S. and Bennacef, A.: Lithostratigraphie du Dévonien  
845 inférieur dans l'Ahnet et le Mouydir (Sahara Central), Bull Serv Géologique Algérie, (38),  
846 83–104, 1968.
- 847 Black, R., Latouche, L., Liégeois, J. P., Caby, R. and Bertrand, J. M.: Pan-African displaced  
848 terranes in the Tuareg shield (central Sahara), Geology, 22(7), 641–644, 1994.
- 849 Bonini, M., Sani, F. and Antonielli, B.: Basin inversion and contractional reactivation of  
850 inherited normal faults: A review based on previous and new experimental models,  
851 Tectonophysics, 522–523, 55–88, doi:10.1016/j.tecto.2011.11.014, 2012.
- 852 Boote, D. R. D., Clark-Lowes, D. D. and Traut, M. W.: Palaeozoic petroleum systems of  
853 North Africa, Geol. Soc. Lond. Spec. Publ., 132(1), 7–68,  
854 doi:10.1144/GSL.SP.1998.132.01.02, 1998.
- 855 Borocco, J. and Nyssen, R.: Nouvelles observations sur les “gres inférieurs” cambro-  
856 ordoviciens du Tassili interne (Nord-Hoggar), Bull. Société Géologique Fr., S7-I(2), 197–206,  
857 doi:10.2113/gssgbull.S7-I.2.197, 1959.

- 858 Boudjema, A.: Evolution structurale du bassin pétrolier" triasique" du Sahara nord oriental  
859 (Algérie), Doctoral dissertation, Paris 11, France., 1987.
- 860 Boumendjel, K.: Les chitinozoaires du silurien supérieur et du devonien du sahara algérien  
861 (cadre géologique, systématique, biostratigraphie), Doctoral dissertation, Rennes 1, France.,  
862 1987.
- 863 Boumendjel, K., Loboziak, S., Paris, F., Steemans, P. and Streel, M.: Biostratigraphie des  
864 Miospores et des Chitinozoaires du Silurien supérieur et du Dévonien dans le bassin d'Illizi  
865 (S.E. du Sahara algérien), *Geobios*, 21(3), 329–357, doi:10.1016/S0016-6995(88)80057-3,  
866 1988.
- 867 Bournas, N., Galdeano, A., Hamoudi, M. and Baker, H.: Interpretation of the aeromagnetic  
868 map of Eastern Hoggar (Algeria) using the Euler deconvolution, analytic signal and local  
869 wavenumber methods, *J. Afr. Earth Sci.*, 37(3–4), 191–205,  
870 doi:10.1016/j.jafrearsci.2002.12.001, 2003.
- 871 Brahimi, S., Liégeois, J.-P., Ghienne, J.-F., Munschy, M. and Bourmatte, A.: The Tuareg  
872 shield terranes revisited and extended towards the northern Gondwana margin: Magnetic and  
873 gravimetric constraints, *Earth-Sci. Rev.*, 185, 572–599, doi:10.1016/j.earscirev.2018.07.002,  
874 2018.
- 875 Braun, J., Simon-Labré, T., Murray, K. E. and Reiners, P. W.: Topographic relief driven by  
876 variations in surface rock density, *Nat. Geosci.*, 7(7), 534–540, doi:10.1038/ngeo2171, 2014.
- 877 de Brito Neves, B. B., Fuck, R. A., Cordani, U. G. and Thomaz Fº, A.: Influence of basement  
878 structures on the evolution of the major sedimentary basins of Brazil: A case of tectonic  
879 heritage, *J. Geodyn.*, 1(3), 495–510, doi:10.1016/0264-3707(84)90021-8, 1984.

- 880 Buchanan, P. G. and McClay, K. R.: Sandbox experiments of inverted listric and planar fault  
881 systems, *Tectonophysics*, 188(1), 97–115, doi:10.1016/0040-1951(91)90317-L, 1991.
- 882 Burgess, P. M.: Phanerozoic evolution of the sedimentary cover of the North American  
883 craton, in *Sedimentary Basins of the World*, vol. 5, pp. 31–63, Elsevier., 2008.
- 884 Burgess, P. M. and Gurnis, M.: Mechanisms for the formation of cratonic stratigraphic  
885 sequences, *Earth Planet. Sci. Lett.*, 136(3), 647–663, doi:10.1016/0012-821X(95)00204-P,  
886 1995.
- 887 Burgess, P. M., Gurnis, M. and Moresi, L.: Formation of sequences in the cratonic interior of  
888 North America by interaction between mantle, eustatic, and stratigraphic processes, *Geol.*  
889 *Soc. Am. Bull.*, 109(12), 1515–1535, 1997.
- 890 Burke, K., MacGregor, D. S. and Cameron, N. R.: Africa's petroleum systems: four tectonic  
891 'Aces' in the past 600 million years, *Geol. Soc. Lond. Spec. Publ.*, 207(1), 21–60, 2003.
- 892 Burov, E. and Cloetingh, S.: Controls of mantle plumes and lithospheric folding on modes of  
893 intraplate continental tectonics: differences and similarities, *Geophys. J. Int.*, 178(3), 1691–  
894 1722, doi:10.1111/j.1365-246X.2009.04238.x, 2009.
- 895 Butler, R. W. H.: The influence of pre-existing basin structure on thrust system evolution in  
896 the Western Alps, *Geol. Soc. Lond. Spec. Publ.*, 44(1), 105–122,  
897 doi:10.1144/GSL.SP.1989.044.01.07, 1989.
- 898 Caby, R.: Terrane assembly and geodynamic evolution of central-western Hoggar: a  
899 synthesis, *J. Afr. Earth Sci.*, 37(3–4), 133–159, doi:10.1016/j.jafrearsci.2003.05.003, 2003.
- 900 Cacace, M. and Scheck-Wenderoth, M.: Why intracontinental basins subside longer: 3-D  
901 feedback effects of lithospheric cooling and sedimentation on the flexural strength of the

- 902 lithosphere: Subsidence at Intracontinental Basins, *J. Geophys. Res. Solid Earth*, 121(5),  
903 3742–3761, doi:10.1002/2015JB012682, 2016.
- 904 Cagnard, F., Barbey, P. and Gapais, D.: Transition between “Archaean-type” and “modern-  
905 type” tectonics: Insights from the Finnish Lapland Granulite Belt, *Precambrian Res.*, 187(1–  
906 2), 127–142, doi:10.1016/j.precamres.2011.02.007, 2011.
- 907 Carr, I. D.: Second-Order Sequence Stratigraphy of the Palaeozoic of North Africa, *J. Pet.*  
908 *Geol.*, 25(3), 259–280, doi:10.1111/j.1747-5457.2002.tb00009.x, 2002.
- 909 Carruba, S., Perotti, C., Rinaldi, M., Bresciani, I. and Bertozzi, G.: Intraplate deformation of  
910 the Al Qarqaf Arch and the southern sector of the Ghadames Basin (SW Libya), *J. Afr. Earth*  
911 *Sci.*, 97, 19–39, doi:10.1016/j.jafrearsci.2014.05.001, 2014.
- 912 Catuneanu, O., Abreu, V., Bhattacharya, J. P., Blum, M. D., Dalrymple, R. W., Eriksson, P.  
913 G., Fielding, C. R., Fisher, W. L., Galloway, W. E., Gibling, M. R., Giles, K. A., Holbrook, J.  
914 M., Jordan, R., Kendall, C. G. S. C., Macurda, B., Martinsen, O. J., Miall, A. D., Neal, J. E.,  
915 Nummedal, D., Pomar, L., Posamentier, H. W., Pratt, B. R., Sarg, J. F., Shanley, K. W., Steel,  
916 R. J., Strasser, A., Tucker, M. E. and Winker, C.: Towards the standardization of sequence  
917 stratigraphy, *Earth-Sci. Rev.*, 92(1–2), 1–33, doi:10.1016/j.earscirev.2008.10.003, 2009.
- 918 Célérier, J., Sandiford, M., Hansen, D. L. and Quigley, M.: Modes of active intraplate  
919 deformation, Flinders Ranges, Australia, *Tectonics*, 24(6), 1–17, doi:10.1029/2004TC001679,  
920 2005.
- 921 Chardon, D., Gapais, D. and Cagnard, F.: Flow of ultra-hot orogens: A view from the  
922 Precambrian, clues for the Phanerozoic, *Tectonophysics*, 477(3–4), 105–118,  
923 doi:10.1016/j.tecto.2009.03.008, 2009.

- 924 Chaumeau, J., Legrand, P. and Renaud, A.: Contribution a l'étude du Couvinien dans le  
925 bassin de Fort-de-Polignac (Sahara), Bull. Société Géologique Fr., S7-III(5), 449–456,  
926 doi:10.2113/gssgbull.S7-III.5.449, 1961.
- 927 Chavand, J. C. and Claracq, P.: La disparition du Tassili externe à l'E de Fort-Polignac  
928 (Sahara central), CR Soc Géol Fr, 1959, 172–174, 1960.
- 929 Choukroune, P., Gapais, D. and Merle, O.: Shear criteria and structural symmetry, J. Struct.  
930 Geol., 9(5–6), 525–530, doi:10.1016/0191-8141(87)90137-4, 1987.
- 931 Claracq, P., Fabre, C., Freulon, J. M. and Nougarède, F.: Une discordance angulaire dans les  
932 “Grès inférieurs” de l'Adrar Tan Elak (Sahara central), C. r. Somm. Séances Soc. Géologique  
933 Fr., 309–310, 1958.
- 934 Collomb, G. R.: Étudé géologique du Jebel Fezzan et de sa bordure paléozoïque, Compagnie  
935 française des pétroles., 1962.
- 936 Conrad, J.: Les grandes lignes stratigraphiques et sédimentologiques du Carbonifère de  
937 l'Ahnet-Mouydir (Sahara central algérien), Rev. Inst. Fr. Pétrole, 28, 3–18, 1973.
- 938 Conrad, J.: Les séries carbonifères du Sahara central algérien: stratigraphie, sédimentation,  
939 évolution structurale, Doctoral dissertation, Université Aix-Marseille III, France., 1984.
- 940 Coward, M. P. and Ries, A. C.: Tectonic development of North African basins, Geol. Soc.  
941 Lond. Spec. Publ., 207(1), 61–83, doi:10.1144/GSL.SP.2003.207.4, 2003.
- 942 Cózar, P., Somerville, I. D., Vachard, D., Coronado, I., García-Frank, A., Medina-Varea, P.,  
943 Said, I., Del Moral, B. and Rodríguez, S.: Upper Mississippian to lower Pennsylvanian  
944 biostratigraphic correlation of the Sahara Platform successions on the northern margin of

945 Gondwana (Morocco, Algeria, Libya), Gondwana Res., 36, 459–472,  
946 doi:10.1016/j.gr.2015.07.019, 2016.

947 Craig, J., Rizzi, C., Said, F., Thusu, B., Luning, S., Asbali, A. I., Keeley, M. L., Bell, J. F.,  
948 Durham, M. J. and Eales, M. H.: Structural styles and prospectivity in the Precambrian and  
949 Palaeozoic hydrocarbon systems of North Africa, Geol. East Libya, 4, 51–122, 2008.

950 Dalrymple, R. W. and Choi, K.: Morphologic and facies trends through the fluvial-marine  
951 transition in tide-dominated depositional systems: A schematic framework for environmental  
952 and sequence-stratigraphic interpretation, Earth-Sci. Rev., 81(3–4), 135–174,  
953 doi:10.1016/j.earscirev.2006.10.002, 2007.

954 Dalrymple, R. W., Zaitlin, B. A. and Boyd, R.: A conceptual model of estuarine  
955 sedimentation, J. Sediment. Petrol., 62(1130–1146), 116, 1992.

956 Dalrymple, R. W., Mackay, D. A., Ichaso, A. A. and Choi, K. S.: Processes,  
957 Morphodynamics, and Facies of Tide-Dominated Estuaries, in Principles of Tidal  
958 Sedimentology, pp. 79–107, Springer, Dordrecht., 2012.

959 Denis, M., Buoncristiani, J.-F., Konaté, M., Ghienne, J.-F. and Guiraud, M.: Hirnantian  
960 glacial and deglacial record in SW Djado Basin (NE Niger)., Geodin. Acta, 20(3), 177–195,  
961 doi:10.3166/ga.20.177-195, 2007.

962 Derder, M. E. M., Maouche, S., Liégeois, J. P., Henry, B., Amenna, M., Ouabadi, A., Bellon,  
963 H., Bruguier, O., Bayou, B., Bestandji, R., Nouar, O., Bouabdallah, H., Ayache, M. and  
964 Beddiasf, M.: Discovery of a Devonian mafic magmatism on the western border of the Murzuq  
965 basin (Saharan metacraton): Paleomagnetic dating and geodynamical implications, J. Afr.  
966 Earth Sci., 115, 159–176, doi:10.1016/j.jafrearsci.2015.11.019, 2016.

- 967 Djouder, H., Lüning, S., Da Silva, A.-C., Abdallah, H. and Boulvain, F.: Silurian deltaic  
968 progradation, Tassili n’Ajjer plateau, south-eastern Algeria: Sedimentology, ichnology and  
969 sequence stratigraphy, *J. Afr. Earth Sci.*, 142, 170–192, 2018.
- 970 Dokka, A. M.: Sedimentological core description WELL: W7, Block - 340, (District - 3)  
971 (unpublished), Core description, Sonatrach division exploration direction des operations  
972 département assistance aux opérations service géologique, Algérie., 1999.
- 973 Dott, R. H. and Bourgeois, J.: Hummocky stratification: Significance of its variable bedding  
974 sequences, *Geol. Soc. Am. Bull.*, 93(8), 663, doi:10.1130/0016-  
975 7606(1982)93<663:HSSOIV>2.0.CO;2, 1982.
- 976 Dubois, P.: Stratigraphie du Cambro-Ordovicien du Tassili n’Ajjer (Sahara central), *Bull.*  
977 *Société Géologique Fr.*, S7-III(2), 206–209, doi:10.2113/gssgbull.S7-III.2.206, 1961.
- 978 Dubois, P. and Mazelet, P.: Stratigraphie du Silurien du Tassili N’Ajjer, *Bull. Société*
- 979 *Géologique Fr.*, S7-VI(4), 586–591, doi:10.2113/gssgbull.S7-VI.4.586, 1964.
- 980 Dubois, P., Beuf, S. and Biju-Duval, B.: Lithostratigraphie du Dévonien inférieur gréseux du  
981 Tassili n ‘Ajjer, in *Symposium on the Lower Devonian and its limits: Bur. Recherche Geol. et*  
982 *Minieres Mem*, pp. 227–235., 1967.
- 983 Dumas, S. and Arnott, R. W. C.: Origin of hummocky and swaley cross-stratification—the  
984 controlling influence of unidirectional current strength and aggradation rate, *Geology*, 34(12),  
985 1073–1076, 2006.
- 986 Eaton, D. W. and Darbyshire, F.: Lithospheric architecture and tectonic evolution of the  
987 Hudson Bay region, *Tectonophysics*, 480(1–4), 1–22, doi:10.1016/j.tecto.2009.09.006, 2010.

- 988 Echikh, K.: Geology and hydrocarbon occurrences in the Ghadames basin, Algeria, Tunisia,  
989 Libya, Geol. Soc. Lond. Spec. Publ., 132(1), 109–129, 1998.
- 990 Eschard, R., Desaubliaux, G., Deschamps, R., Montadert, L., Ravenne, C., Bekkouche, D.,  
991 Abdallah, H., Belhaouas, S., Benkouider, M., Braïk, F., Henniche, M., Maache, N. and  
992 Mouaici, R.: Illizi-Berkine Devonian Reservoir Consortium (unpublished), Institut Française  
993 du Pétrole - Sonatrach, unpublished, Algérie., 1999.
- 994 Eschard, R., Abdallah, H., Braik, F. and Desaubliaux, G.: The Lower Paleozoic succession in  
995 the Tassili outcrops, Algeria: sedimentology and sequence stratigraphy, First Break, 23(10),  
996 2005.
- 997 Eschard, R., Braik, F., Bekkouche, D., Rahuma, M. B., Desaubliaux, G., Deschamps, R. and  
998 Proust, J. N.: Palaeohighs: their influence on the North African Palaeozoic petroleum systems,  
999 Pet. Geol. Mature Basins New Front. 7th Pet. Geol. Conf., 707–724, 2010.
- 1000 Fabre, J.: Les séries paléozoïques d’Afrique: une approche, J. Afr. Earth Sci. Middle East,  
1001 7(1), 1–40, doi:10.1016/0899-5362(88)90051-6, 1988.
- 1002 Fabre, J.: Géologie du Sahara occidental et central, Musée royal de l’Afrique centrale., 2005.
- 1003 Fabre, J., Kaci, A. A., Bouima, T. and Moussine-Pouchkine, A.: Le cycle molassique dans le  
1004 Rameau trans-saharien de la chaîne panafricaine, J. Afr. Earth Sci., 7, 41–55,  
1005 doi:10.1016/0899-5362(88)90052-8, 1988.
- 1006 Fekirine, B. and Abdallah, H.: Palaeozoic lithofacies correlatives and sequence stratigraphy of  
1007 the Saharan Platform, Algeria, Geol. Soc. Lond. Spec. Publ., 132(1), 97–108,  
1008 doi:10.1144/GSL.SP.1998.132.01.05, 1998.

- 1009 Fezaa, N., Liégeois, J.-P., Abdallah, N., Cherfouh, E. H., De Waele, B., Bruguier, O. and  
1010 Ouabadi, A.: Late Ediacaran geological evolution (575–555Ma) of the Djanet Terrane,  
1011 Eastern Hoggar, Algeria, evidence for a Murzukian intracontinental episode, Precambrian  
1012 Res., 180(3–4), 299–327, doi:10.1016/j.precamres.2010.05.011, 2010.
- 1013 Follot, J.: Sur l'existence de mouvements calédoniens au Mouydir (Sahara Central), Compte  
1014 Rendus Hebd. Séances L'Académie Sci., 230(25), 2217–2218, 1950.
- 1015 Frey, R. W., Pemberton, S. G. and Saunders, T. D.: Ichnofacies and bathymetry: a passive  
1016 relationship, J. Paleontol., 64(1), 155–158, 1990.
- 1017 Frizon de Lamotte, D., Tavakoli-Shirazi, S., Leturmy, P., Averbuch, O., Mouchot, N., Raulin,  
1018 C., Leparmentier, F., Blanpied, C. and Ringenbach, J.-C.: Evidence for Late Devonian  
1019 vertical movements and extensional deformation in northern Africa and Arabia: Integration in  
1020 the geodynamics of the Devonian world: Devonian evolution Northern Gondwana, Tectonics,  
1021 32(2), 107–122, doi:10.1002/tect.20007, 2013.
- 1022 Fröhlich, S., Petitpierre, L., Redfern, J., Grech, P., Bodin, S. and Lang, S.: Sedimentological  
1023 and sequence stratigraphic analysis of Carboniferous deposits in western Libya: Recording  
1024 the sedimentary response of the northern Gondwana margin to climate and sea-level changes,  
1025 J. Afr. Earth Sci., 57(4), 279–296, doi:10.1016/j.jafrearsci.2009.09.007, 2010.
- 1026 Gac, S., Huismans, R. S., Simon, N. S. C., Podladchikov, Y. Y. and Faleide, J. I.: Formation  
1027 of intracratonic basins by lithospheric shortening and phase changes: a case study from the  
1028 ultra-deep East Barents Sea basin, Terra Nova, 25(6), 459–464, doi:10.1111/ter.12057, 2013.
- 1029 Galeazzi, S., Point, O., Haddadi, N., Mather, J. and Druesne, D.: Regional geology and  
1030 petroleum systems of the Illizi–Berkine area of the Algerian Saharan Platform: An overview,  
1031 Mar. Pet. Geol., 27(1), 143–178, doi:10.1016/j.marpetgeo.2008.10.002, 2010.

- 1032 Galloway, W. E.: Genetic Stratigraphic Sequences in Basin Analysis I: Architecture and  
1033 Genesis of Flooding-Surface Bounded Depositional Units, AAPG Bull., 73(2), 125–142,  
1034 1989.
- 1035 Galushkin, Y. I. and Eloghbi, S.: Thermal history of the Murzuq Basin, Libya, and generation  
1036 of hydrocarbons in its source rocks, Geochem. Int., 52(6), 486–499,  
1037 doi:10.1134/S0016702914060032, 2014.
- 1038 Gariel, O., de Charpal, O. and Bennacef, A.: Sur la sedimentation des gres du Cambro-  
1039 Ordovicien (Unite II) dans l’Ahnet et le Mouydir (Sahara central): Algerie, Serv. Geol, Bull N  
1040 Ser, (38), 7–37, 1968.
- 1041 Ghienne, J.-F., Deynoux, M., Manatschal, G. and Rubino, J.-L.: Palaeovalleys and fault-  
1042 controlled depocentres in the Late-Ordovician glacial record of the Murzuq Basin (central  
1043 Libya), Comptes Rendus Geosci., 335(15), 1091–1100, doi:10.1016/j.crte.2003.09.010, 2003.
- 1044 Ghienne, J.-F., Moreau, J., Degermann, L. and Rubino, J.-L.: Lower Palaeozoic  
1045 unconformities in an intracratonic platform setting: glacial erosion versus tectonics in the  
1046 eastern Murzuq Basin (southern Libya), Int. J. Earth Sci., 102(2), 455–482,  
1047 doi:10.1007/s00531-012-0815-y, 2013.
- 1048 Gindre, L., Le Heron, D. and Bjørnseth, H. M.: High resolution facies analysis and sequence  
1049 stratigraphy of the Siluro-Devonian succession of Al Kufrah basin (SE Libya), J. Afr. Earth  
1050 Sci., 76, 8–26, doi:10.1016/j.jafrearsci.2012.08.002, 2012.
- 1051 Girard, F., Ghienne, J.-F. and Rubino, J.-L.: Channelized sandstone bodies ('cordons') in the  
1052 Tassili N'Ajjer (Algeria & Libya): snapshots of a Late Ordovician proglacial outwash  
1053 plain, Geol. Soc. Lond. Spec. Publ., 368(1), 355–379, doi:10.1144/SP368.3, 2012.

- 1054 Grasemann, B., Martel, S. and Passchier, C.: Reverse and normal drag along a fault, *J. Struct.*  
1055 *Geol.*, 27(6), 999–1010, doi:10.1016/j.jsg.2005.04.006, 2005.
- 1056 Greigertt, J. and Pougnet, R.: Carte Géologique du Niger, 1/2000000, BRGM, République du  
1057 Niger, 1965.
- 1058 Guiraud, R., Bosworth, W., Thierry, J. and Delplanque, A.: Phanerozoic geological evolution  
1059 of Northern and Central Africa: An overview, *J. Afr. Earth Sci.*, 43(1–3), 83–143,  
1060 doi:10.1016/j.jafrearsci.2005.07.017, 2005.
- 1061 Haddoum, H., Guiraud, R. and Moussine-Pouchkine, A.: Hercynian compressional  
1062 deformations of the Ahnet-Mouydir Basin, Algerian Saharan Platform: far-field stress effects  
1063 of the Late Palaeozoic orogeny, *Terra Nova*, 13(3), 220–226, 2001.
- 1064 Haddoum, H., Mokri, M., Ouzegane, K., Ait-Djaffer, S. and Djemai, S.: Extrusion de l'In  
1065 Ouzzal vers le Nord (Hoggar occidental, Algérie): une conséquence d'un poinçonnement  
1066 panafricain, *J. Hydrocarb. Mines Environ. Res.* Vol. 4(1), 6–16, 2013.
- 1067 Haq, B. U. and Schutter, S. R.: A Chronology of Paleozoic Sea-Level Changes, *Science*,  
1068 322(5898), 64–68, doi:10.1126/science.1161648, 2008.
- 1069 Harris, L. B.: Structural and tectonic synthesis for the Perth basin, Western Australia, *J. Pet.*  
1070 *Geol.*, 17(2), 129–156, 1994.
- 1071 Hartley, R. W. and Allen, P. A.: Interior cratonic basins of Africa: relation to continental  
1072 break-up and role of mantle convection, *Basin Res.*, 6(2–3), 95–113, 1994.
- 1073 Hassan, A.: Etude palynologique Paléozoïque du sondage Razzal-Allah-Nord (unpublished),  
1074 Entreprise nationale Sonatrach division hydrocarbures direction Laboratoire central des  
1075 hydrocarbures, Boumerdès., 1984.

- 1076 Heine, C., Dietmar Müller, R., Steinberger, B. and Torsvik, T. H.: Subsidence in  
1077 intracontinental basins due to dynamic topography, *Phys. Earth Planet. Inter.*, 171(1–4), 252–  
1078 264, doi:10.1016/j.pepi.2008.05.008, 2008.
- 1079 Henniche, M.: *Architecture et modèle de dépôts d'une série sédimentaire paléozoïque en*  
1080 *contexte cratonique*, Rennes 1, France., 2002.
- 1081 Holbrook, J. and Schumm, S. A.: Geomorphic and sedimentary response of rivers to tectonic  
1082 deformation: a brief review and critique of a tool for recognizing subtle epeirogenic  
1083 deformation in modern and ancient settings, *Tectonophysics*, 305(1), 287–306, 1999.
- 1084 Hollard, H., Choubert, G., Bronner, G., Marchand, J. and Sougy, J.: Carte géologique du  
1085 Maroc, scale 1: 1,000,000, Serv Carte Géol Maroc, 260(2), 1985.
- 1086 Holt, P. J., Allen, M. B., van Hunen, J. and Bjørnseth, H. M.: Lithospheric cooling and  
1087 thickening as a basin forming mechanism, *Tectonophysics*, 495(3–4), 184–194,  
1088 doi:10.1016/j.tecto.2010.09.014, 2010.
- 1089 Jacquemont, P., Jutard, G., Plauchut, B., Grégoire, J. and Mouflard, R.: Etude du bassin du  
1090 Djado, Bur. Rech. Pétroles Rapp., 1215, 1959.
- 1091 Jäger, H., Lewandowski, E. and Lampart, V.: Palynology of the upper Silurian to middle  
1092 Devonian in the Reggane Basin, southern Algeria, Ext. Abstr. DGMK-Tagungsbericht 2009-1  
1093 DGMKÖGEW Spring Meet. Celle, 47–51, 2009.
- 1094 Jardiné, S. and Yapaudjian, L.: Lithostratigraphie et palynologie du Dévonien-Gothlandien  
1095 gréseux du Bassin de Polignac (Sahara), *Rev. L'Institut Fr. Pétrole*, 23(4), 439–469, 1968.
- 1096 Joulia, F.: Carte géologique de reconnaissance de la bordure sédimentaire occidentale de l'Aïr  
1097 au 1/500 000, Éditions BRGM Orléans Fr., 1963.

- 1098 Kermadjji, A. M.: Silurian–Devonian miospores from the western and central Algeria, Rev.
- 1099 Micropaléontologie, 50(1), 109–128, doi:10.1016/j.revmic.2007.01.003, 2007.
- 1100 Kermadjji, A. M. H., Kowalski, M. W. and Pharisat, A.: Palynologie et séquences de
- 1101 l’Emsien de la région d’In Salah, Sahara central Algérien, Bull. Société D’Histoire Nat. Pays
- 1102 Montbél., 301–306, 2003.
- 1103 Kermadjji, A. M. H., Kowalski, W. M. and Touhami, F. K.: Miospore stratigraphy of Lower
- 1104 and early Middle Devonian deposits from Tidikelt, Central Sahara, Algeria, Geobios, 41(2),
- 1105 227–251, doi:10.1016/j.geobios.2007.05.002, 2008.
- 1106 Kermadjji, A. M. H., Touhami, F. K., Kowalski, W. M., Abbés, S. B., Boularak, M.,
- 1107 Chabour, N., Laifa, E. L. and Hannachi, H. B.: Stratigraphie du Dévonien Inférieur du Plateau
- 1108 du Tidikelt d’In Salah (Sahara Central Algérie), Comun. Geológicas, (t. 96), 67–82, 2009.
- 1109 Khalil, S. M. and McClay, K. R.: Extensional fault-related folding, northwestern Red Sea,
- 1110 Egypt, J. Struct. Geol., 24(4), 743–762, 2002.
- 1111 Khiar, S.: Résultats palynologiques du sondage Garet El Guefoul (unpublished), Entreprise
- 1112 nationale Sonatrach division hydrocarbures direction Laboratoire central des hydrocarbures,
- 1113 Alger., 1974.
- 1114 Kracha, N.: Relation entre sédimentologie, fracturation naturelle et diagénèse d’un réservoir à
- 1115 faible perméabilité application aux réservoirs de l’Ordovicien bassin de l’Ahnet, Sahara
- 1116 central, Algérie, Doctoral dissertation, Université des sciences et technologies de Lille,
- 1117 France., 2011.

1118 Le Heron, D. P.: Interpretation of Late Ordovician glaciogenic reservoirs from 3-D seismic  
1119 data: an example from the Murzuq Basin, Libya, *Geol. Mag.*, 147(01), 28,  
1120 doi:10.1017/S0016756809990586, 2010.

1121 Le Heron, D. P., Craig, J., Sutcliffe, O. E. and Whittington, R.: Late Ordovician glaciogenic  
1122 reservoir heterogeneity: An example from the Murzuq Basin, Libya, *Mar. Pet. Geol.*, 23(6),  
1123 655–677, doi:10.1016/j.marpetgeo.2006.05.006, 2006.

1124 Le Heron, D. P., Craig, J. and Etienne, J. L.: Ancient glaciations and hydrocarbon  
1125 accumulations in North Africa and the Middle East, *Earth-Sci. Rev.*, 93(3–4), 47–76,  
1126 doi:10.1016/j.earscirev.2009.02.001, 2009.

1127 Leeder, M. R.: Denudation, vertical crustal movements and sedimentary basin infill, *Geol.*  
1128 *Rundsch.*, 80(2), 441–458, doi:10.1007/BF01829376, 1991.

1129 Legrand, P.: Le Devonien du Sahara Algérien, *Can. Soc. Pet. Geol.*, 1, 245–284, 1967a.

1130 Legrand, P.: Nouvelles connaissances acquises sur la limite des systèmes Silurien et Dévonien  
1131 au Sahara algérien, *Bull. Bur. Rech. Géologiques Minières*, 33, 119–37, 1967b.

1132 Legrand, P.: The lower Silurian graptolites of Oued In Djerane: a study of populations at the  
1133 Ordovician-Silurian boundary, *Geol. Soc. Lond. Spec. Publ.*, 20(1), 145–153,  
1134 doi:10.1144/GSL.SP.1986.020.01.15, 1986.

1135 Legrand, P.: Late Ordovician-early Silurian paleogeography of the Algerian Sahara, *Bull.*  
1136 *Société Géologique Fr.*, 174(1), 19–32, 2003a.

1137 Legrand, P.: Silurian stratigraphy and paleogeography of the northern African margin of  
1138 Gondwana, in *Silurian Lands and Seas: Paleogeography Outside of Laurentia*, edited by E.  
1139 Landing and M. E. Johnson, pp. 59–104, New York., 2003b.

- 1140 Legrand-Blain, M.: Dynamique des Brachiopodes carbonifères sur la plate-forme carbonatée  
1141 du Sahara algérien: paléoenvironnements, paléobiogéographie, évolution, Doctoral  
1142 dissertation, Université de Bordeaux 1, France., 1985.
- 1143 Lessa, G. and Masselink, G.: Morphodynamic evolution of a macrotidal barrier estuary, Mar.  
1144 Geol., 129(1–2), 25–46, 1995.
- 1145 Leuven, J. R. F. W., Kleinhans, M. G., Weisscher, S. A. H. and van der Vegt, M.: Tidal sand  
1146 bar dimensions and shapes in estuaries, Earth-Sci. Rev., 161, 204–223,  
1147 doi:10.1016/j.earscirev.2016.08.004, 2016.
- 1148 Lewis, M. M., Jackson, C. A.-L., Gawthorpe, R. L. and Whipp, P. S.: Early synrift reservoir  
1149 development on the flanks of extensional forced folds: A seismic-scale outcrop analog from  
1150 the Hadahid fault system, Suez rift, Egypt, AAPG Bull., 99(06), 985–1012,  
1151 doi:10.1306/12011414036, 2015.
- 1152 Liégeois, J. P., Latouche, L., Boughrara, M., Navez, J. and Guiraud, M.: The LATEA  
1153 metacraton (Central Hoggar, Tuareg shield, Algeria): behaviour of an old passive margin  
1154 during the Pan-African orogeny, J. Afr. Earth Sci., 37(3–4), 161–190,  
1155 doi:10.1016/j.jafrearsci.2003.05.004, 2003.
- 1156 Liégeois, J.-P., Black, R., Navez, J. and Latouche, L.: Early and late Pan-African orogenies in  
1157 the Air assembly of terranes (Tuareg Shield, Niger), Precambrian Res., 67(1), 59–88, 1994.
- 1158 Liégeois, J.-P., Benhallou, A., Azzouni-Sekkal, A., Yahiaoui, R. and Bonin, B.: The Hoggar  
1159 swell and volcanism: Reactivation of the Precambrian Tuareg shield during Alpine  
1160 convergence and West African Cenozoic volcanism, Geol. Soc. Am. Spec. Pap., 388, 379–  
1161 400, doi:10.1130/0-8137-2388-4.379, 2005.

- 1162 Liégeois, J.-P., Abdelsalam, M. G., Ennih, N. and Ouabadi, A.: Metacraton: Nature, genesis  
1163 and behavior, *Gondwana Res.*, 23(1), 220–237, doi:10.1016/j.gr.2012.02.016, 2013.
- 1164 Lindsay, J. F. and Leven, J. H.: Evolution of a Neoproterozoic to Palaeozoic intracratonic  
1165 setting, Officer Basin, South Australia, *Basin Res.*, 8(4), 403–424, doi:10.1046/j.1365-  
1166 2117.1996.00223.x, 1996.
- 1167 Logan, P. and Duddy, I.: An investigation of the thermal history of the Ahnet and Reggane  
1168 Basins, Central Algeria, and the consequences for hydrocarbon generation and accumulation,  
1169 *Geol. Soc. Lond. Spec. Publ.*, 132(1), 131–155, 1998.
- 1170 Loi, A., Ghienne, J.-F., Dabard, M. P., Paris, F., Botquelen, A., Christ, N., Elaouad-Debbaj,  
1171 Z., Gorini, A., Vidal, M., Videt, B. and Destombes, J.: The Late Ordovician glacio-eustatic  
1172 record from a high-latitude storm-dominated shelf succession: The Bou Ingarf section (Anti-  
1173 Atlas, Southern Morocco), *Palaeogeogr. Palaeoclimatol. Palaeoecol.*, 296(3–4), 332–358,  
1174 doi:10.1016/j.palaeo.2010.01.018, 2010.
- 1175 Lubeseder, S.: Silurian and Devonian sequence stratigraphy of North Africa; Regional  
1176 correlation and sedimentology (Morocco, Algeria, Libya), Doctoral dissertation, University of  
1177 Manchester, UK., 2005.
- 1178 Lubeseder, S., Redfern, J., Petitpierre, L. and Fröhlich, S.: Stratigraphic trapping potential in  
1179 the Carboniferous of North Africa: developing new play concepts based on integrated outcrop  
1180 sedimentology and regional sequence stratigraphy (Morocco, Algeria, Libya), in Geological  
1181 Society, London, Petroleum Geology Conference series, vol. 7, pp. 725–734, Geological  
1182 Society of London., 2010.
- 1183 Lüning, S.: North African Phanerozoic, in *Phanerozoic in the Northern african basins*,  
1184 Encyclopedia of Geology, pp. 152–172, Elsevier., 2005.

- 1185 Lüning, S., Craig, J., Loydell, D. K., Štorch, P. and Fitches, B.: Lower Silurian 'hot shales' in  
1186 North Africa and Arabia: regional distribution and depositional model, *Earth-Sci. Rev.*, 49(1–  
1187 4), 121–200, doi:10.1016/S0012-8252(99)00060-4, 2000.
- 1188 Lüning, S., Adamson, K. and Craig, J.: Frasnian organic-rich shales in North Africa: regional  
1189 distribution and depositional model, *Geol. Soc. Lond. Spec. Publ.*, 207(1), 165–184,  
1190 doi:10.1144/GSL.SP.2003.207.9, 2003.
- 1191 Lüning, S., Wendt, J., Belka, Z. and Kaufmann, B.: Temporal–spatial reconstruction of the  
1192 early Frasnian (Late Devonian) anoxia in NW Africa: new field data from the Ahnet Basin  
1193 (Algeria), *Sediment. Geol.*, 163(3–4), 237–264, doi:10.1016/S0037-0738(03)00210-0, 2004.
- 1194 Madritsch, H., Schmid, S. M. and Fabbri, O.: Interactions between thin-and thick-skinned  
1195 tectonics at the northwestern front of the Jura fold-and-thrust belt (eastern France), *Tectonics*,  
1196 27(5), 1–31, doi:10.1029/2008TC002282, 2008.
- 1197 Magloire, L.: Étude stratigraphique, par la Palynologie, des dépôts argilo-gréseux du Silurien  
1198 et du Dévonien inférieur dans la Région du Grand Erg Occidental (Sahara Algérien), *Can.  
1199 Soc. Pet. Geol.*, 2, 473–491, 1967.
- 1200 Makhous, M. and Galushkin, Y. I.: Burial history and thermal evolution of the northern and  
1201 eastern Saharan basins, *AAPG Bull.*, 87(10), 1623–1651, doi:10.1306/04300301122, 2003a.
- 1202 Makhous, M. and Galushkin, Y. I.: Burial history and thermal evolution of the southern and  
1203 western Saharan basins: Synthesis and comparison with the eastern and northern Saharan  
1204 basins, *AAPG Bull.*, 87(11), 1799–1822, 2003b.

- 1205 Marchal, D., Guiraud, M., Rives, T. and van den Driessche, J.: Space and time propagation  
1206 processes of normal faults, *Geol. Soc. Lond. Spec. Publ.*, 147(1), 51–70,  
1207 doi:10.1144/GSL.SP.1998.147.01.04, 1998.
- 1208 Marchal, D., Guiraud, M. and Rives, T.: Geometric and morphologic evolution of normal  
1209 fault planes and traces from 2D to 4D data, *J. Struct. Geol.*, 25(1), 135–158,  
1210 doi:10.1016/S0191-8141(02)00011-1, 2003.
- 1211 Massa, D.: Paléozoïque de Libye occidentale: stratigraphie et paléogéographie, Doctoral  
1212 dissertation, Université de Nice, France., 1988.
- 1213 Mélou, M., Oulebsir, L. and Paris, F.: Brachiopodes et chitinozoaires ordoviciens dans le NE  
1214 du Sahara algérien: Implications stratigraphiques et paléogéographiques, *Geobios*, 32(6),  
1215 822–839, doi:10.1016/S0016-6995(99)80865-1, 1999.
- 1216 Milani, E. J. and Zalan, P. V.: An outline of the geology and petroleum systems of the  
1217 Paleozoic interior basins of South America, *Episodes*, 22, 199–205, 1999.
- 1218 Milton, N. J., Bertram, G. T. and Vann, I. R.: Early Palaeogene tectonics and sedimentation in  
1219 the Central North Sea, *Geol. Soc. Lond. Spec. Publ.*, 55(1), 339–351, 1990.
- 1220 Moreau, C., Demaiffe, D., Bellion, Y. and Boullier, A.-M.: A tectonic model for the location  
1221 of Palaeozoic ring complexes in Air (Niger, West Africa), *Tectonophysics*, 234(1), 129–146,  
1222 1994.
- 1223 Mory, A. J., Zhan, Y., Haines, P. W., Hocking, R. M., Thomas, C. M. and Copp, I. A.: A  
1224 paleozoic perspective of Western Australia, Geological Survey of Western Australia., 2017.

- 1225 Najem, A., El-Arnauti, A. and Bosnina, S.: Delineation of Paleozoic Tecto-stratigraphic  
1226 Complexities in the Northern Part of Murzuq Basin-Southwest Libya, in SPE North Africa  
1227 Technical Conference and Exhibition, Society of Petroleum Engineers., 2015.
- 1228 Nikishin, A. M., Ziegler, P. A., Stephenson, R. A., Cloetingh, S., Furne, A. V., Fokin, P. A.,  
1229 Ershov, A. V., Bolotov, S. N., Korotaev, M. V. and Alekseev, A. S.: Late Precambrian to  
1230 Triassic history of the East European Craton: dynamics of sedimentary basin evolution,  
1231 Tectonophysics, 268(1–4), 23–63, 1996.
- 1232 Ogg, J. G., Ogg, G. and Gradstein, F. M.: Introduction, in A Concise Geologic Time Scale:  
1233 2016, p. 3, Elsevier., 2016.
- 1234 de Oliveira, D. C. and Mohriak, W. U.: Jaíbaras trough: an important element in the early  
1235 tectonic evolution of the Parnaíba interior sag basin, Northern Brazil, Mar. Pet. Geol., 20(3),  
1236 351–383, doi:[https://doi.org/10.1016/S0264-8172\(03\)00044-8](https://doi.org/10.1016/S0264-8172(03)00044-8), 2003.
- 1237 Oudra, M., Beraaouz, H., Ikenne, M., Gasquet, D. and Soulaimani, A.: La Tectonique  
1238 Panafricaine du Secteur d'Igherm: Implication des dômes extensifs tardis à post-orogéniques  
1239 (Anti-Atlas occidental, Maroc), Estud. Geológicos, 61(3–6), 177–189, 2005.
- 1240 Oulebsir, L. and Paris, F.: Chitinozoaires ordoviciens du Sahara algérien: biostratigraphie et  
1241 affinités paléogéographiques, Rev. Palaeobot. Palynol., 86(1), 49–68, doi:10.1016/0034-  
1242 6667(94)00098-5, 1995.
- 1243 Owen, G.: Senni Beds of the Devonian Old Red Sandstone, Dyfed, Wales: anatomy of a  
1244 semi-arid floodplain, Sediment. Geol., 95(3–4), 221–235, 1995.
- 1245 Paris, F.: The Ordovician chitinozoan biozones of the Northern Gondwana domain, Rev.  
1246 Palaeobot. Palynol., 66(3–4), 181–209, doi:10.1016/0034-6667(90)90038-K, 1990.

- 1247 Paris, F., Bourahrouh, A. and Hérissé, A. L.: The effects of the final stages of the Late  
1248 Ordovician glaciation on marine palynomorphs (chitinozoans, acritarchs, leiospheres) in well  
1249 NI-2 (NE Algerian Sahara), *Rev. Palaeobot. Palynol.*, 113(1–3), 87–104, doi:10.1016/S0034-  
1250 6667(00)00054-3, 2000.
- 1251 Peace, A., McCaffrey, K., Imber, J., van Hunen, J., Hobbs, R. and Wilson, R.: The role of  
1252 pre-existing structures during rifting, continental breakup and transform system development,  
1253 offshore West Greenland, *Basin Res.*, 30(3), 373–394, 2018.
- 1254 Pemberton, S. G. and Frey, R. W.: Trace fossil nomenclature and the *Planolites*-*Palaeophycus*  
1255 dilemma, *J. Paleontol.*, 56(4), 843–881, 1982.
- 1256 Peucat, J. J., Drareni, A., Latouche, L., Deloule, E. and Vidal, P.: U–Pb zircon (TIMS and  
1257 SIMS) and Sm–Nd whole-rock geochronology of the Gour Oumelalen granulitic basement,  
1258 Hoggar massif, Tuareg shield, Algeria, *J. Afr. Earth Sci.*, 37(3–4), 229–239,  
1259 doi:10.1016/j.jafrearsci.2003.03.001, 2003.
- 1260 Peucat, J.-J., Capdevila, R., Drareni, A., Mahdjoub, Y. and Kahoui, M.: The Eglab massif in  
1261 the West African Craton (Algeria), an original segment of the Eburnean orogenic belt:  
1262 petrology, geochemistry and geochronology, *Precambrian Res.*, 136(3–4), 309–352,  
1263 doi:10.1016/j.precamres.2004.12.002, 2005.
- 1264 Phillips, T. B., Jackson, C. A.-L., Bell, R. E. and Duffy, O. B.: Oblique reactivation of  
1265 lithosphere-scale lineaments controls rift physiography – the upper-crustal expression of the  
1266 Sorgenfrei–Tornquist Zone, offshore southern Norway, *Solid Earth*, 9(2), 403–429,  
1267 doi:10.5194/se-9-403-2018, 2018.

- 1268 Pinet, N., Lavoie, D., Dietrich, J., Hu, K. and Keating, P.: Architecture and subsidence history  
1269 of the intracratonic Hudson Bay Basin, northern Canada, *Earth-Sci. Rev.*, 125, 1–23,  
1270 doi:10.1016/j.earscirev.2013.05.010, 2013.
- 1271 Potter, D.: Relationships of Cambro-Ordovician Stratigraphy to Paleotopography on the  
1272 Precambrian Basement, Williston Basin, *Sask. Geol. Soc.*, 63–73, 2006.
- 1273 Reading, H. G. and Collinson, J. D.: Clastic coasts, in *Sedimentary environments: processes,*  
1274 facies, and stratigraphy, pp. 154–231, John Wiley & Sons, Oxford ; Cambridge, Mass., 2009.
- 1275 Rider, M. H.: Facies, Sequences and Depositional Environments from Logs, in *The geological*  
1276 *interpretation of well logs*, pp. 226–238, Whittles Publishing, Caithness, Scotland., 1996.
- 1277 Rougier, S., Missenard, Y., Gautheron, C., Barbarand, J., Zeyen, H., Pinna, R., Liégeois, J.-P.,  
1278 Bonin, B., Ouabadi, A., Derder, M. E.-M. and Lamotte, D. F. de: Eocene exhumation of the  
1279 Tuareg Shield (Sahara Desert, Africa), *Geology*, 41(5), 615–618, doi:10.1130/G33731.1,  
1280 2013.
- 1281 Sabaou, N., Ait-Salem, H. and Zazoun, R. S.: Chemostratigraphy, tectonic setting and  
1282 provenance of the Cambro-Ordovician clastic deposits of the subsurface Algerian Sahara, *J.*  
1283 *Afr. Earth Sci.*, 55(3–4), 158–174, doi:10.1016/j.jafrearsci.2009.04.006, 2009.
- 1284 Schlische, R. W.: Geometry and origin of fault-related folds in extensional settings, *AAPG*  
1285 *Bull.*, 79(11), 1661–1678, 1995.
- 1286 Sclater, J. G. and Christie, P. A. F.: Continental stretching: An explanation of the Post-Mid-  
1287 Cretaceous subsidence of the central North Sea Basin, *J. Geophys. Res. Solid Earth*, 85(B7),  
1288 3711–3739, doi:10.1029/JB085iB07p03711, 1980.

- 1289   Scotese, C. R., Boucot, A. J. and McKerrow, W. S.: Gondwanan palaeogeography and  
1290   paleoclimatology, *J. Afr. Earth Sci.*, 28(1), 99–114, doi:10.1016/S0899-5362(98)00084-0,  
1291   1999.
- 1292   Serra, O. and Serra, L.: Well logging, facies, sequence and environment, in *Well logging and*  
1293   *geology*, pp. 197–238, Technip Editions, France., 2003.
- 1294   Sharata, S., Röth, J. and Reicherter, K.: Basin evolution in the North African Platform,  
1295   *Geotecton. Res.*, 97(1), 80–81, doi:10.1127/1864-5658/2015-31, 2015.
- 1296   Shaw, J. H., Connors, C. D. and Suppe, J.: Recognizing growth strata, in *Seismic*  
1297   *interpretation of contractional fault-related folds: an AAPG seismic atlas*, vol. 53, pp. 11–14,  
1298   American Association of Petroleum Geologists, Tulsa, Okla., U.S.A., 2005.
- 1299   Sloss, L. L.: Sequences in the cratonic interior of North America, *Geol. Soc. Am. Bull.*, 74(2),  
1300   93–114, 1963.
- 1301   Smart, J.: Seismic expressions of depositional processes in the upper Ordovician succession  
1302   of the Murzuq Basin, SW Libya, in *Geological Exploration in Murzuq Basin*, edited by M. A.  
1303   Sola and D. Worsley, pp. 397–415, Elsevier Science B.V., Amsterdam., 2000.
- 1304   Soares, P. C., Landim, P. M. B. and Fulfaro, V. J.: Tectonic cycles and sedimentary sequences  
1305   in the Brazilian intracratonic basins, *GSA Bull.*, 89(2), 181–191, doi:10.1130/0016-  
1306   7606(1978)89<181:TCASSI>2.0.CO;2, 1978.
- 1307   Stearns, D. W.: Faulting and forced folding in the Rocky Mountains foreland, Laramide Fold.  
1308   *Assoc. Basement Block Faulting West. U. S. Geol. Soc. Am. Mem.*, 151, 1–37, 1978.
- 1309   Stow, D. a. V. and Piper, D. J. W.: Deep-water fine-grained sediments: facies models, *Geol.*  
1310   *Soc. Lond. Spec. Publ.*, 15(1), 611–646, doi:10.1144/GSL.SP.1984.015.01.38, 1984.

- 1311 Stow, D. A. V., Huc, A.-Y. and Bertrand, P.: Depositional processes of black shales in deep  
1312 water, *Mar. Pet. Geol.*, 18(4), 491–498, doi:10.1016/S0264-8172(01)00012-5, 2001.
- 1313 Suter, J. R.: Facies models revisited: clastic shelves, *Spec. Publ.-SEPM*, 84, 339, 2006.
- 1314 Tournier, F.: Mécanismes et contrôle des phénomènes diagénétiques en milieu acide dans les  
1315 grès de l'Ordovicien glaciaire du bassin de Sbaa, Algérie, Doctoral dissertation, Université de  
1316 Paris 11, France., 2010.
- 1317 Trompette, R.: Gondwana evolution; its assembly at around 600 Ma, *Comptes Rendus  
1318 Académie Sci.-Ser. IIA-Earth Planet. Sci.*, 330(5), 305–315, 2000.
- 1319 Turner, G. M., Rasson, J. L. and Reeves, C. V.: Observation and Measurement Techniques, in  
1320 Treatise on Geophysics, vol. 5, edited by G. Schubert, pp. 33–75, Blackwell Pub, Malden,  
1321 MA., 2007.
- 1322 Ustaszewski, K., Schumacher, M., Schmid, S. and Nieuwland, D.: Fault reactivation in  
1323 brittle–viscous wrench systems—dynamically scaled analogue models and application to the  
1324 Rhine–Bresse transfer zone, *Quat. Sci. Rev.*, 24(3–4), 363–380,  
1325 doi:10.1016/j.quascirev.2004.03.015, 2005.
- 1326 Van Hinte, J. E.: Geohistory analysis—application of micropaleontology in exploration  
1327 geology, *AAPG Bull.*, 62(2), 201–222, 1978.
- 1328 Vauchez, A., Tommasi, A. and Barruol, G.: Rheological heterogeneity, mechanical anisotropy  
1329 and deformation of the continental lithosphere, *Tectonophysics*, 296(1–2), 61–86,  
1330 doi:10.1016/S0040-1951(98)00137-1, 1998.

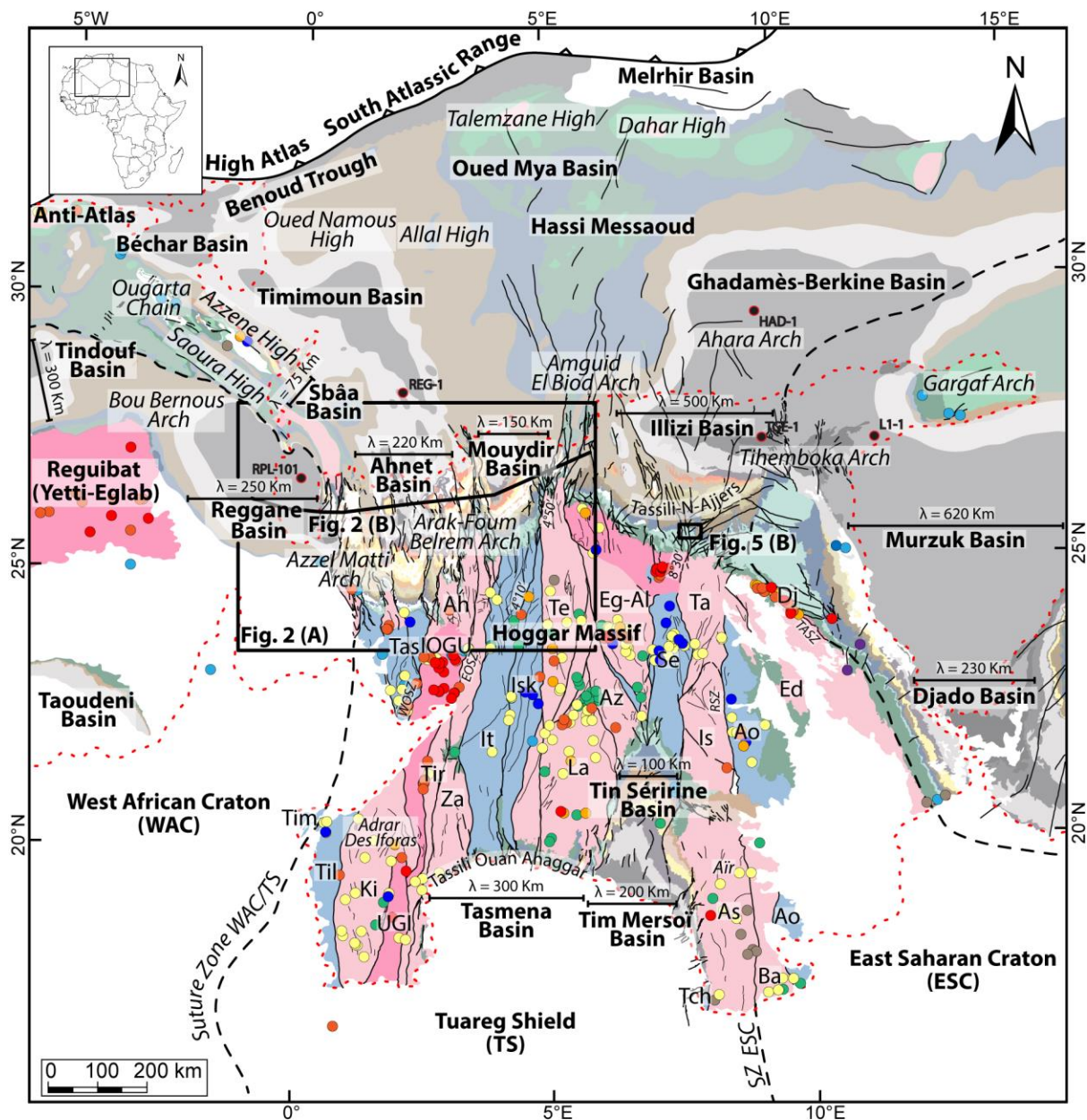
- 1331 Vecoli, M.: Palaeoenvironmental interpretation of microphytoplankton diversity trends in the  
1332 Cambrian–Ordovician of the northern Sahara Platform, *Palaeogeogr. Palaeoclimatol.*  
1333 *Palaeoecol.*, 160(3–4), 329–346, doi:10.1016/S0031-0182(00)00080-8, 2000.
- 1334 Vecoli, M. and Playford, G.: Stratigraphically significant acritarchs in uppermost Cambrian to  
1335 basal Ordovician strata of Northwestern Algeria, *Grana*, 36(1), 17–28,  
1336 doi:10.1080/00173139709362585, 1997.
- 1337 Vecoli, M., Albani, R., Ghomari, A., Massa, D. and Tongiorgi, M.: Précisions sur la limite  
1338 Cambrien-Ordovicien au Sahara Algérien (Secteur de Hassi-Rmel), *Comptes Rendus*  
1339 Académie Sci. Sér. 2 Sci. Terre Planètes, 320(6), 515–522, 1995.
- 1340 Vecoli, M., Tongiorgi, M., Abdesselam-Roughi, F. F., Benzarti, R. and Massa, D.:  
1341 Palynostratigraphy of upper Cambrian-upper Ordovician intracratonic clastic sequences,  
1342 North Africa, *Boll.-Soc. Paleontol. Ital.*, 38(2/3), 331–342, 1999.
- 1343 Vecoli, M., Videt, B. and Paris, F.: First biostratigraphic (palynological) dating of Middle and  
1344 Late Cambrian strata in the subsurface of northwestern Algeria, North Africa: Implications  
1345 for regional stratigraphy, *Rev. Palaeobot. Palynol.*, 149(1–2), 57–62,  
1346 doi:10.1016/j.revpalbo.2007.10.004, 2008.
- 1347 Videt, B., Paris, F., Rubino, J.-L., Boumendjel, K., Dabard, M.-P., Loi, A., Ghienne, J.-F.,  
1348 Marante, A. and Gorini, A.: Biostratigraphical calibration of third order Ordovician sequences  
1349 on the northern Gondwana platform, *Palaeogeogr. Palaeoclimatol. Palaeoecol.*, 296(3–4),  
1350 359–375, doi:10.1016/j.palaeo.2010.03.050, 2010.
- 1351 Wagoner, J. C. V., Mitchum, R. M., Campion, K. M. and Rahmanian, V. D.: Siliciclastic  
1352 Sequence Stratigraphy in Well Logs, Cores, and Outcrops: Concepts for High-Resolution  
1353 Correlation of Time and Facies, *AAPG Methods Explor. Ser. No 7*, 174, III–55, 1990.

- 1354 Watts, A. B.: Isostasy and Flexure of the Lithosphere, Cambridge University Press, Oxford  
1355 University., 2001.
- 1356 Wendt, J.: Disintegration of the continental margin of northwestern Gondwana: Late  
1357 Devonian of the eastern Anti-Atlas (Morocco), *Geology*, 13(11), 815–818, 1985.
- 1358 Wendt, J.: Facies Pattern and Paleogeography of the Middle and Late Devonian in the Eastern  
1359 Anti-Atlas (Morocco), *Can. Soc. Pet. Geol.*, 1(14), 467–480, 1988.
- 1360 Wendt, J.: Shell directions as a tool in palaeocurrent analysis, *Sediment. Geol.*, 95(3), 161–  
1361 186, doi:10.1016/0037-0738(94)00104-3, 1995.
- 1362 Wendt, J. and Kaufmann, B.: Mud buildups on a Middle Devonian carbonate ramp (Algerian  
1363 Sahara), *Geol. Soc. Lond. Spec. Publ.*, 149(1), 397–415,  
1364 doi:10.1144/GSL.SP.1999.149.01.18, 1998.
- 1365 Wendt, J., Belka, Z. and Moussine-Pouchkine, A.: New architectures of deep-water carbonate  
1366 buildups: Evolution of mud mounds into mud ridges (Middle Devonian, Algerian Sahara),  
1367 *Geology*, 21(8), 723–726, 1993.
- 1368 Wendt, J., Belka, Z., Kaufmann, B., Kostrewa, R. and Hayer, J.: The world's most spectacular  
1369 carbonate mud mounds (Middle Devonian, Algerian Sahara), *J. Sediment. Res.*, 67(3), 424–  
1370 436, doi:10.1306/D426858B-2B26-11D7-8648000102C1865D, 1997.
- 1371 Wendt, J., Kaufmann, B., Belka, Z., Klug, C. and Lubeseder, S.: Sedimentary evolution of a  
1372 Palaeozoic basin and ridge system: the Middle and Upper Devonian of the Ahnet and  
1373 Mouydir (Algerian Sahara), *Geol. Mag.*, 143(3), 269–299, doi:10.1017/S0016756806001737,  
1374 2006.

- 1375 Wendt, J., Kaufmann, B., Belka, Z. and Korn, D.: Carboniferous stratigraphy and depositional  
1376 environments in the Ahnet Mouydir area (Algerian Sahara), *Facies*, 55(3), 443–472,  
1377 doi:10.1007/s10347-008-0176-y, 2009a.
- 1378 Wendt, J., Kaufmann, B. and Belka, Z.: Devonian stratigraphy and depositional environments  
1379 in the southern Illizi Basin (Algerian Sahara), *J. Afr. Earth Sci.*, 54(3–4), 85–96,  
1380 doi:10.1016/j.jafrearsci.2009.03.006, 2009b.
- 1381 Withjack, M. O. and Callaway, S.: Active normal faulting beneath a salt layer: an  
1382 experimental study of deformation patterns in the cover sequence, *AAPG Bull.*, 84(5), 627–  
1383 651, 2000.
- 1384 Withjack, M. O., Olson, J. and Peterson, E.: Experimental models of extensional forced folds,  
1385 *AAPG Bull.*, 74(7), 1038–1054, 1990.
- 1386 Withjack, M. O., Schlische, R. W. and Olsen, P. E.: Rift-basin structure and its influence on  
1387 sedimentary systems, *Soc. Sediment. Geol. Spec. Publ.*, (73), 57–81, 2002.
- 1388 Xie, X. and Heller, P.: Plate tectonics and basin subsidence history, *Geol. Soc. Am. Bull.*,  
1389 121(1–2), 55–64, doi:10.1130/B26398.1, 2009.
- 1390 Yahi, N.: Petroleum generation and migration in the Berkine (Ghadames) Basin, Eastern  
1391 Algeria: an organic geochemical and basin modelling study, Doctoral dissertation,  
1392 Forschungszentrum, Zentralbibliothek, Jülich., 1999.
- 1393 Zalan, P. V., Wolff, S., Astolfi, M. A. M., Vieira, I. S., Conceicao, J. C. J., Appi, V. T., Neto,  
1394 E. V. S., Cerqueira, J. R. and Marques, A.: The Parana Basin, Brazil: Chapter 33: Part II.  
1395 Selected Analog Interior Cratonic Basins: *Analog Basins*, , 134, 681–708, 1990.

- 1396 Zazoun, R. S.: Hercynian deformation in the western Ahnet Basin and Bled El-Mass area,
- 1397 Algerian Sahara: a continuous strain, *J. Afr. Earth Sci.*, 32(4), 869–887, 2001.
- 1398 Zazoun, R. S.: The Fadnoun area, Tassili-n-Azjer, Algeria: Fracture network geometry
- 1399 analysis, *J. Afr. Earth Sci.*, 50(5), 273–285, doi:10.1016/j.jafrearsci.2007.10.001, 2008.
- 1400 Zazoun, R. S. and Mahdjoub, Y.: Strain analysis of Late Ordovician tectonic events in the In-
- 1401 Tahouite and Tamadjert Formations (Tassili-n-Ajers area, Algeria), *J. Afr. Earth Sci.*, 60(3),
- 1402 63–78, doi:10.1016/j.jafrearsci.2011.02.003, 2011.
- 1403
- 1404





#### Paleozoic series

##### Silurian

Silurian - Lower Devonian (?)

##### Cambro-Ordovician

- Cambro-Ordovician undifferentiated
- Upper Ordovician
- Lower Ordovician
- Cambrian undifferentiated
- Middle - Upper Cambrian
- Lower Cambrian

##### Devonian

- Devonian undifferentiated
- Upper Devonian undifferentiated
- Famennian
- Frasnian
- Eifelian - Givetian
- Lower Devonian undifferentiated
- Emsian
- Pragian
- Lochkovian

##### Carboniferous

- Upper Carboniferous
- Bashkirian - Kasimovian (?)
- Serpukhovian
- Lower Carboniferous
- Visean
- Upper Tournaisian
- Lower Tournaisian

#### Precambrian series (Hoggar terranes)

- Meso-Neoproterozoic terrane
- Paleoproterozoic terrane
- Archean terrane

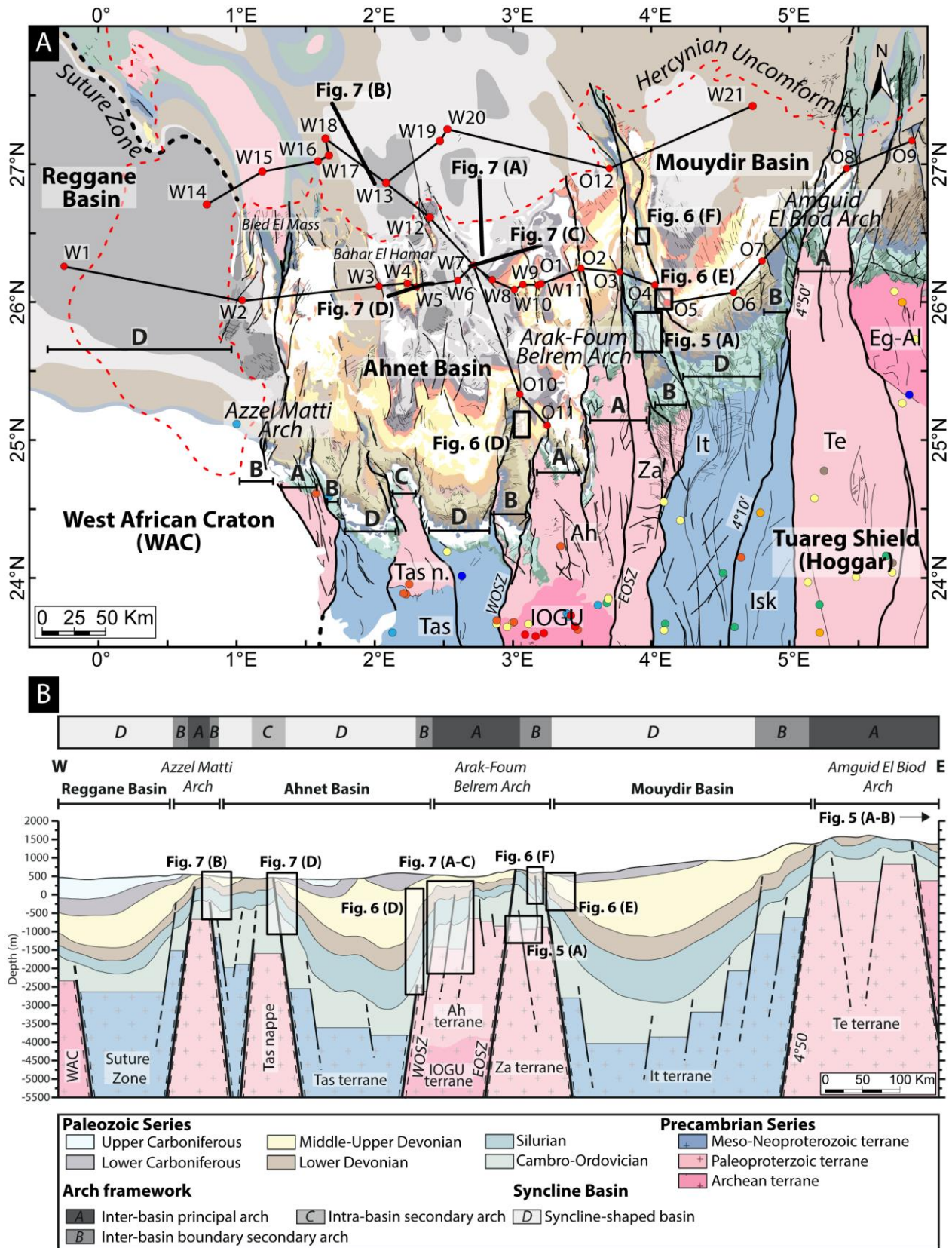
#### Structures & symbols

- Minor fault
- Major fault & shear zone
- - - Suture zone
- - - Hercynian unconformity
- $\lambda = 230 \text{ Km}$  Basin wavelength
- REG-1 Backstripped well

#### Geochronological data (Main thermo-orogenic events)

- |   |  |  |  |
|---|--|--|--|
| ● 1600 - 2500 Ma (Paleoproterozoic)<br>Eburnean event | ● 1100 - 750 Ma (Neoproterozoic)<br>Oceanization-rifting | ● 541 - 443 Ma<br>Post-Pan-African                 | ● 358 - 252 Ma (Carbo-Permian)<br>Hercynian event    |
| ● >2500 Ma (Archean)<br>Liberian, Ouzzalian event     | ● 1600 - 1100 Ma (Mesoproterozoic)<br>Kibarian event     | ● 750 - 541 Ma (Neoproterozoic)<br>Syn-Pan-African | ● 443 - 358 Ma (Siluro-Devonian)<br>Caledonian event |

1407 Figure 1: Geological map of the Paleozoic North Saharan Platform (North Gondwana)  
1408 georeferenced, compiled and modified from (1) Paleozoic subcrop distribution below the  
1409 Hercynian unconformity geology of the Saharan Platform (Boote et al., 1998; Galeazzi et al.,  
1410 2010); (2) Geological map (1/500,000) of the Djado basin (Jacquemont et al., 1959); (3)  
1411 Geological map (1/200,000) of Algeria (Bennacef et al., 1974; Bensalah et al., 1971), (4)  
1412 Geological map (1/50,000) of Aïr (Joulia, 1963), (5) Geological map (1/2,000,000) of Niger  
1413 (Greigertt and Pougnat, 1965), (6) Geological map (1/5,000,000 ) of the Lower Paleozoic of  
1414 the Central Sahara (Beuf et al., 1971), (7) Geological map (1/1,000,000) of Morocco (Holland  
1415 et al., 1985), (8) Geological map of the Djebel Fezzan (Massa, 1988); Basement  
1416 characterization of the different terranes from geochronological data compilation (see  
1417 supplementary data) and geological maps (Berger et al., 2014; Bertrand and Caby, 1978;  
1418 Black et al., 1994; Caby, 2003; Fezaa et al., 2010; Liégeois et al., 1994, 2003, 2005, 2013);  
1419 Terrane names: Tassendjanet (Tas), Tassendjanet nappe (Tas n.), Ahnet (Ah), In Ouzzal  
1420 Granulitic Unit (IOGU), Iforas Granulitic Unit (UGI), Kidal (Ki), Timétrine (Tim), Tilemsi  
1421 (Til), Tirek (Tir), In Zaouatene (Za), In Teidini (It), Iskel (Isk), Tefedest (Te), Laouni (La),  
1422 Azrou-n-Fad (Az), Egéré-Aleskod (Eg-Al), Serouenout (Se), Tazat (Ta), Issalane (Is), Assodé  
1423 (As), Barghot (Ba), Tchilit (Tch), Aouzegueur (Ao), Edembo (Ed), Djanet (Dj); Shear zone  
1424 and lineament names: Suture Zone East Saharan Craton (SZ ESC), West Ouzzal Shear Zone  
1425 (WOSZ), East Ouzzal Shear Zone (EOSZ), Raghane Shear Zone (RSZ), Tin Amali Shear  
1426 Zone (TASZ), 4°10' Shear Zone, 4°50' Shear Zone, 8°30' Shear Zone.  
1427



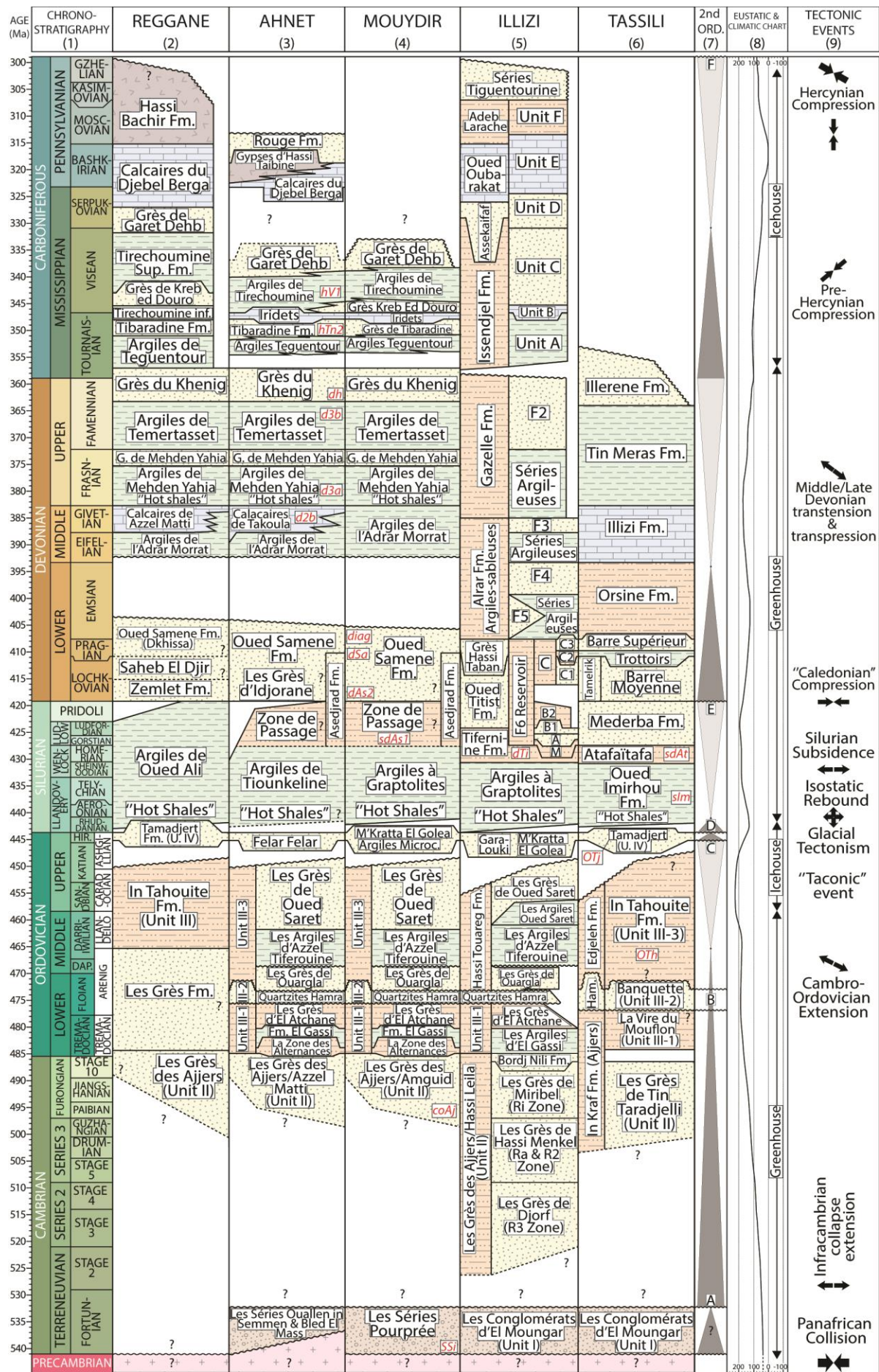
1428

1429 Figure 2 3: (A) Geological map of the Paleozoic of the Reggane, Ahnet, and Mouydir basins.

1430 Legend and references see Fig. 1. **A: Inter-basin principal arch, B: Inter-basin boundary**

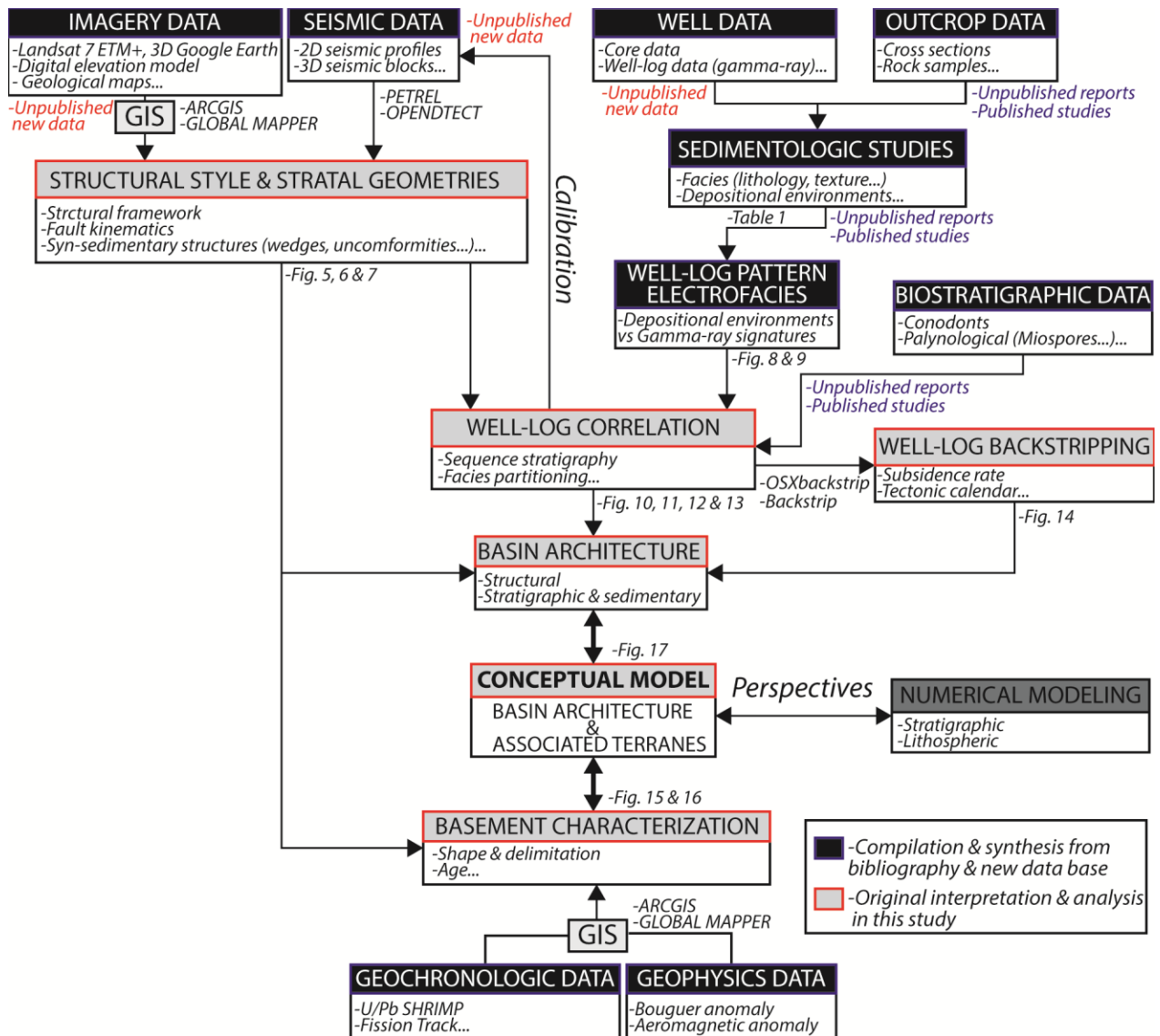
1431 ~~secondary arch, C: Intra basin secondary arch, D: Syncline shaped basin.~~ (B) E-W cross-  
1432 section of the Reggane, Ahnet, and Mouydir basins associated with the different terranes and  
1433 highlighting the classification of the different structural units (~~A: Inter basin principal arch, B:~~  
1434 ~~Inter basin boundary secondary arch, C: Intra basin arch, D: Syncline shaped basin~~).  
1435 Localization of the interpreted sections (seismic profiles and satellite images). W=Well and  
1436 O=Outcrop. See figure 1 for location of the geological map A and cross section B.

1437



1439 Figure 3 2: Paleozoic litho-stratigraphic, sequence stratigraphy and tectonic framework of the  
1440 North Peri-Hoggar basins (North African Saharan Platform) compiled from (1)  
1441 Chronostratigraphic chart (Ogg et al., 2016), (2) The Cambrian–Silurian (Askri et al., 1995)  
1442 and the Devonian–Carboniferous stratigraphy of the Reggane basin (Cózar et al., 2016;  
1443 Lubeseder, 2005; Lubeseder et al., 2010; Magloire, 1967; Wendt et al., 2006), (3) The  
1444 Cambrian–Silurian (Paris, 1990; Wendt et al., 2006) and the Devonian–Carboniferous  
1445 stratigraphy of the Ahnet basin (Beuf et al., 1971; Conrad, 1973, 1984; Legrand-Blain, 1985;  
1446 Wendt et al., 2006, 2009a), (4) The Cambrian–Silurian (Askri et al., 1995; Paris, 1990; Videt  
1447 et al., 2010) and the Devonian–Carboniferous stratigraphy of the Mouydir basin (Askri et al.,  
1448 1995; Beuf et al., 1971; Conrad, 1973, 1984; Wendt et al., 2006, 2009a), (5) The Cambrian–  
1449 Silurian (Eschard et al., 2005; Fekirine and Abdallah, 1998; Jardiné and Yapaudjian, 1968;  
1450 Videt et al., 2010) and the Devonian–Carboniferous stratigraphy of the Illizi basin (Eschard et  
1451 al., 2005; Fekirine and Abdallah, 1998; Jardiné and Yapaudjian, 1968), (6) The Cambrian–  
1452 Silurian (Dubois, 1961; Dubois and Mazelet, 1964; Eschard et al., 2005; Henniche, 2002;  
1453 Videt et al., 2010) and the Devonian–Carboniferous stratigraphy of the Tassili-N-Ajers  
1454 (Dubois et al., 1967; Eschard et al., 2005; Henniche, 2002; Wendt et al., 2009a), (7) Sequence  
1455 stratigraphy of the Saharan Platform (Carr, 2002; Eschard et al., 2005; Fekirine and Abdallah,  
1456 1998), (8) Eustatic and climatic chart (Haq and Schutter, 2008; Scotese et al., 1999), (9)  
1457 Tectonic events (Boudjema, 1987; Coward and Ries, 2003; Craig et al., 2008; Guiraud et al.,  
1458 2005; Lüning, 2005); (A) Infra-Tassilian (Pan-African) unconformity, (B) Intra-Arenig  
1459 unconformity, (C) Taconic and glacial unconformity, (D) Isostatic rebound unconformity, (E)  
1460 Caledonian unconformity, (F) Hercynian unconformity.

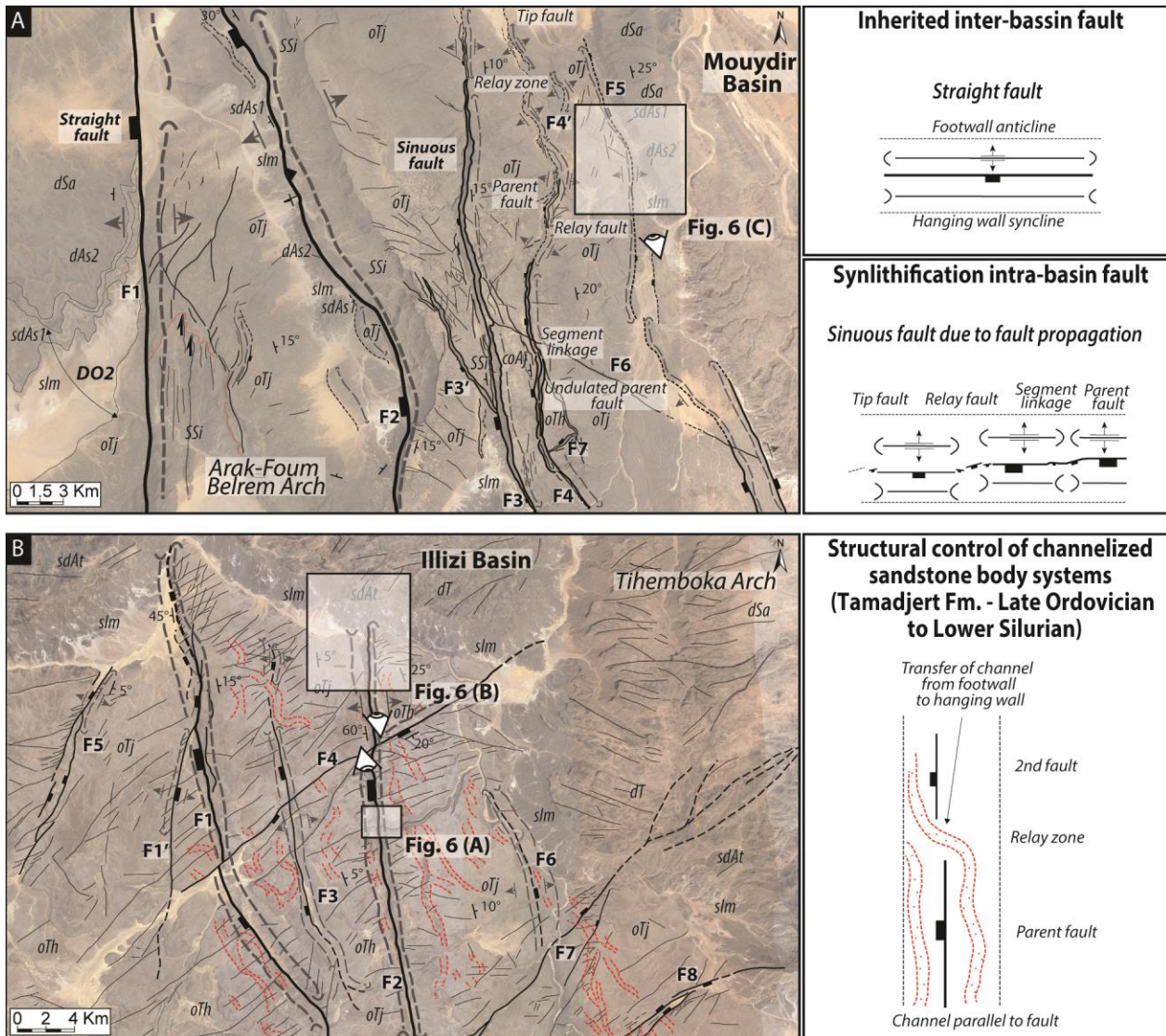
1461



1462  
1463

Figure 4: Schematic synthesis of the integrated method of basin analysis in this study.

1464

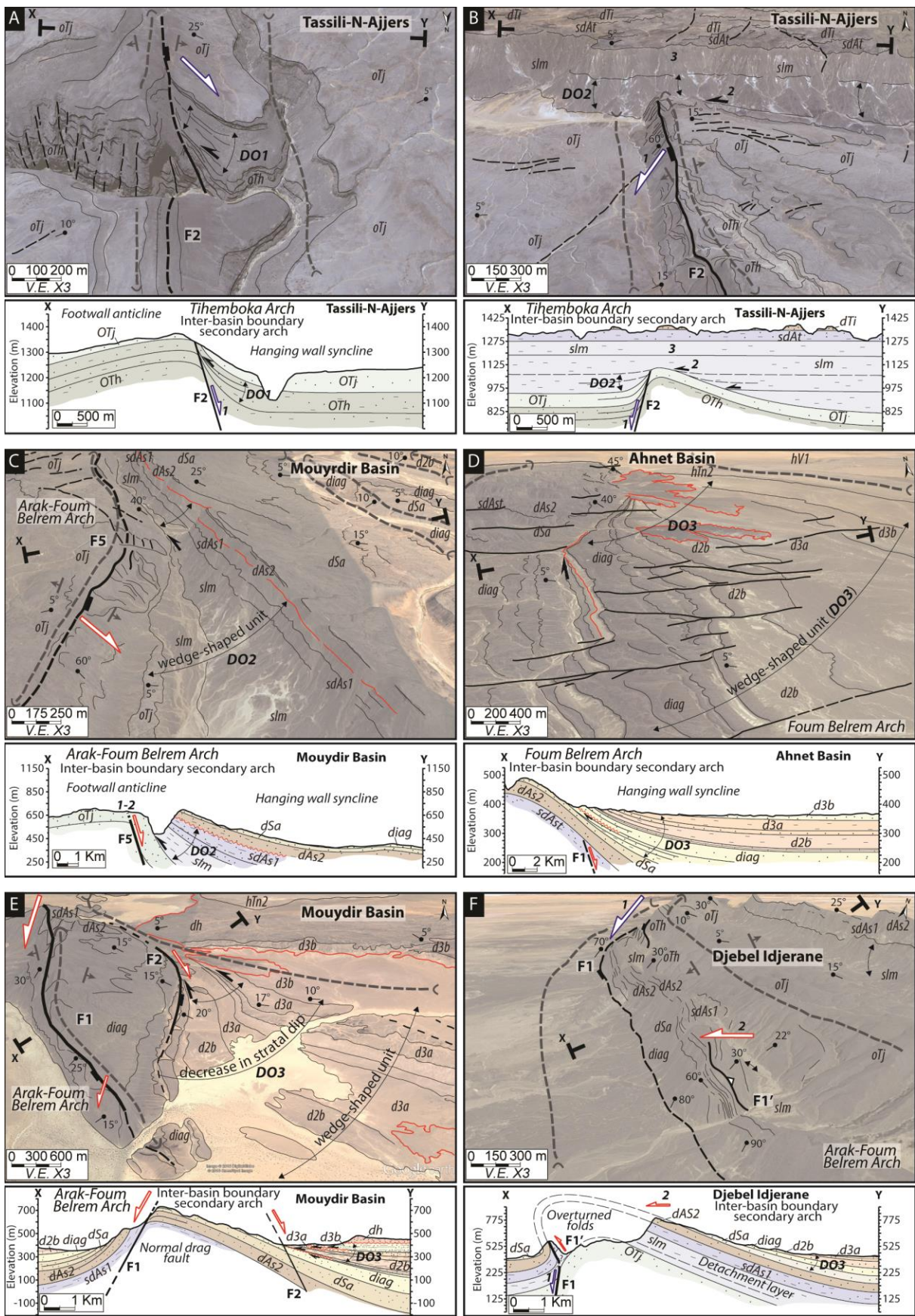


1465

1466 Figure 5 4: (A) Google Earth satellite images Structural interpretation of the Djebel Settaf  
 1467 (Arak Foum Belrem arch; inter basin boundary secondary arch between the Ahnet and  
 1468 Mouydir basins) of the Cambrian Ordovician series showing straight and sinuous normal  
 1469 faults; (A') Typology of different types of faults (inherited straight faults vs sinuous short  
 1470 synlithification propagation faults) in the Cambrian Ordovician series of the Djebel Settaf  
 1471 (Arak Foum Belrem arch; inter-basin boundary secondary arch between the Ahnet and  
 1472 Mouydir basins). (B) Google Earth satellite images Structural interpretation normal fault  
 1473 propagation in Cambrian Ordovician series of South Adrar Assaouatene, Tassili N Ajers  
 1474 (Tihemboka inter basin boundary secondary arch between the Illizi and Murzueq basins); (B')

1475 ~~Schematic model of~~ Structural control of channelized sandstone bodies in Late Ordovician  
1476 series of South Adrar Assaouatene, Tassili-N-Ajers (Tihemboka inter-basin boundary  
1477 secondary arch between the Illizi and Murzuq basins). Dotted red line: Tamadjert Fm.  
1478 channelized sandstone bodies. *OTh*: In Tahouite Fm. (Early to Late Ordovician, Floian to  
1479 Katian), *OTj*: Tamadjert Fm. (Late Ordovician, Hirnantian), *sIm*: Imirhou Fm. (Early  
1480 Silurian), *sdAs1*: Asedjrad Fm. 1 (Late Silurian to Early Devonian), *dAs2*: Asedjrad Fm. 2  
1481 (Early Devonian, Lochkovian), *dSa*: Oued Samene Fm. (Lower Devonian, Pragian). See Fig.  
1482 3 2 for map and cross-section location.

1483



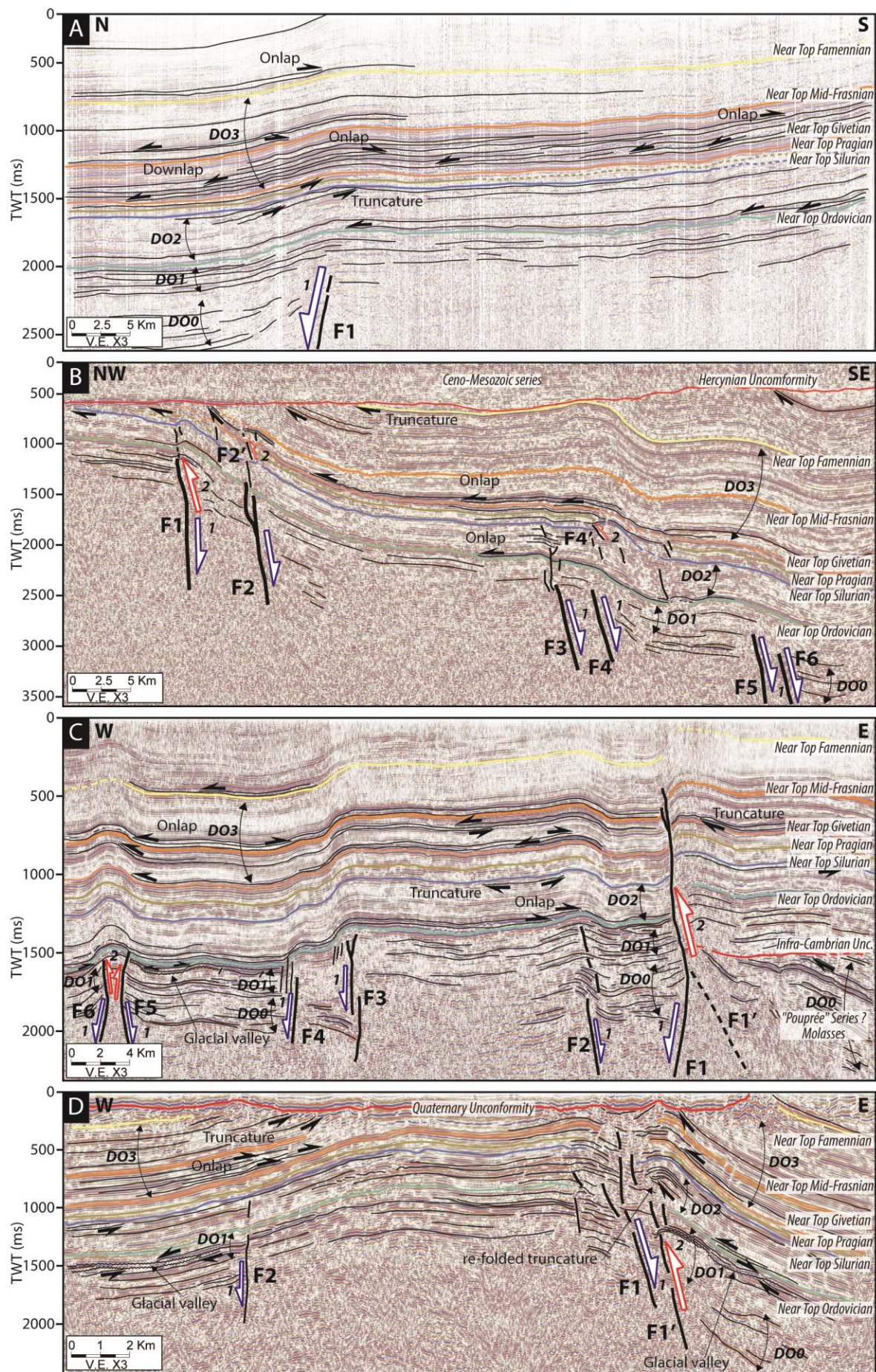
1485 Figure 6 5: (A) Google Earth satellite images structural interpretation of South Adrar  
1486 Assaouatene, Tassili N Ajers (Tihemboka inter basin boundary secondary arch between the  
1487 Illizi and Murzuq basins) showing a Normal fault (F2) associated with a footwall anticline  
1488 and a hanging wall syncline with divergent onlaps (i.e. wedge-shaped unit DO1) in the Early  
1489 to Late Ordovician In Tahouite series (Tassili-N-Ajers, Tihemboka inter-basin boundary  
1490 secondary arch between the Illizi and Murzuq basins); (A') Cross section between XY. 1:  
1491 Cambrian Ordovician extension during the deposition of In Tahouite series (Early to Late  
1492 Ordovician). See fig. 4B for location. (B) Google Earth satellite images structural  
1493 interpretation of North Adrar Assaouatene, Tassili N Ajers (Tihemboka inter basin boundary  
1494 secondary arch between the Illizi and Murzuq basins) showing an Ancient normal fault F2  
1495 escarpment reactivated and sealed during Silurian deposition (poly-historic paleo-reliefs)  
1496 linked to thickness variation, divergent onlaps (DO2) in the hanging wall synclines, and  
1497 onlaps on the fold hinge anticline (Tassili-N-Ajers, Tihemboka inter-basin boundary  
1498 secondary arch between the Illizi and Murzuq basins); (B') Cross section between X'Y'. 1:  
1499 Early to Late Ordovician extension, 2: Late Ordovician to Early Silurian extension, 3: Middle  
1500 to Late Silurian sealing (horizontal drape). See fig. 4B for location. (C) Google Earth satellite  
1501 images structural interpretation of Dejbel Settaf (Arak Foum Belrem arch; inter basin  
1502 boundary secondary arch between the Mouydir and Ahnet basins) showing a Normal fault  
1503 (F5) associated with forced fold with divergent strata (syncline-shaped hanging wall syncline  
1504 and associated wedge-shaped unit DO2) and truncation in Silurian-Devonian series of Dejbel  
1505 Settaf (Arak-Foum Belrem arch; inter-basin boundary secondary arch between the Mouydir  
1506 and Ahnet basins); (C') Cross section between XY. 1: Cambrian-Ordovician extension, 2:  
1507 Silurian-Devonian extensional reactivation (Caledonian extension). Red line: Unconformity.  
1508 See fig. 4A for location. (D) Google Earth satellite images structural interpretation in the  
1509 Ahnet basin (Arak Foum Belrem arch; inter basin boundary secondary arch between the

1510 Mouydir and Ahnet basins) showing Blind basement normal fault (F1) associated with forced  
1511 fold with in the hanging wall syncline divergent onlaps of Lower to Upper Devonian series  
1512 (wedge-shaped unit DO3) and intra-Emsian truncation (Arak-Foum Belrem arch; inter-basin  
1513 boundary secondary arch between the Mouydir and Ahnet basins); (D') Cross-section  
1514 between X'Y'. (E) Google Earth satellite images structural interpretation in the Mouydir  
1515 basin (near Arak Foum Belrem arch, eastward inter basin boundary secondary arch) showing  
1516 N170° normal blind faults F1 and F2 forming a horst-graben system associated with forced  
1517 fold with Lower to Upper Devonian series divergent onlaps (wedge-shaped unit DO3) and  
1518 intra-Emsian truncation in the hanging-wall syncline (in the Mouydir basin near Arak-Foum  
1519 Belrem arch, eastward inter-basin boundary secondary arch); (E') Cross-section between XY.  
1520 (F) Google Earth satellite images structural interpretation of Djebel Idjerane in the Mouydir  
1521 basin (Arak Foum Belrem arch, eastwards inter basin boundary secondary arch) showing an  
1522 Inherited normal fault F1 transported from footwall to hanging wall associated with inverse  
1523 fault F1' and accommodated by a detachment layer in Silurian shales series (thickness  
1524 variation of Imirhou Fm. between footwall and hanging wall) and spilled dip strata markers of  
1525 overturned folding (Djebel Idjerane, Arak-Foum Belrem arch, eastwards inter-basin boundary  
1526 secondary arch); (F') Cross-section between X'Y'. 1: Cambrian–Ordovician extension, 2:  
1527 Middle to Late Devonian compression. *OTh*: In Tahouite Fm. (Early to Late Ordovician,  
1528 Floian to Katian), *OTj*: Tamadjert Fm (Late Ordovician, Hirnantian), *sIm*: Imirhou Fm. (Early  
1529 to Mid Silurian), *sdAt*: Atafaïtafa Fm. (Middle Silurian), *dTi*: Tifernine Fm. (Middle Silurian),  
1530 *sdAsI*: Asedjrad Fm. 1 (Late Silurian to Early Devonian), *dAs2*: Asedjrad Fm. 2 (Early  
1531 Devonian, Lochkovian), *dSa*: Oued Samene Fm. (Early Devonian, Pragian), *diag*: Oued  
1532 Samene shaly-sandstones Fm. (Early Devonian, Emsian?), *d2b*: Givetian, *d3a*: Mehden Yahia  
1533 Fm. (Late Devonian, Frasnian), *d3b*: Mehden Yahia Fm. (Late Devonian, Famennian), *dh*:

1534 Khenig sandstones (late Famennian to early Tournaisian), *hTn2*: late Tournaisian, *hV1*: early

1535 Visean. Red line: Unconformity. See Figs. 1,2 and 3 5 for map and cross-section location.

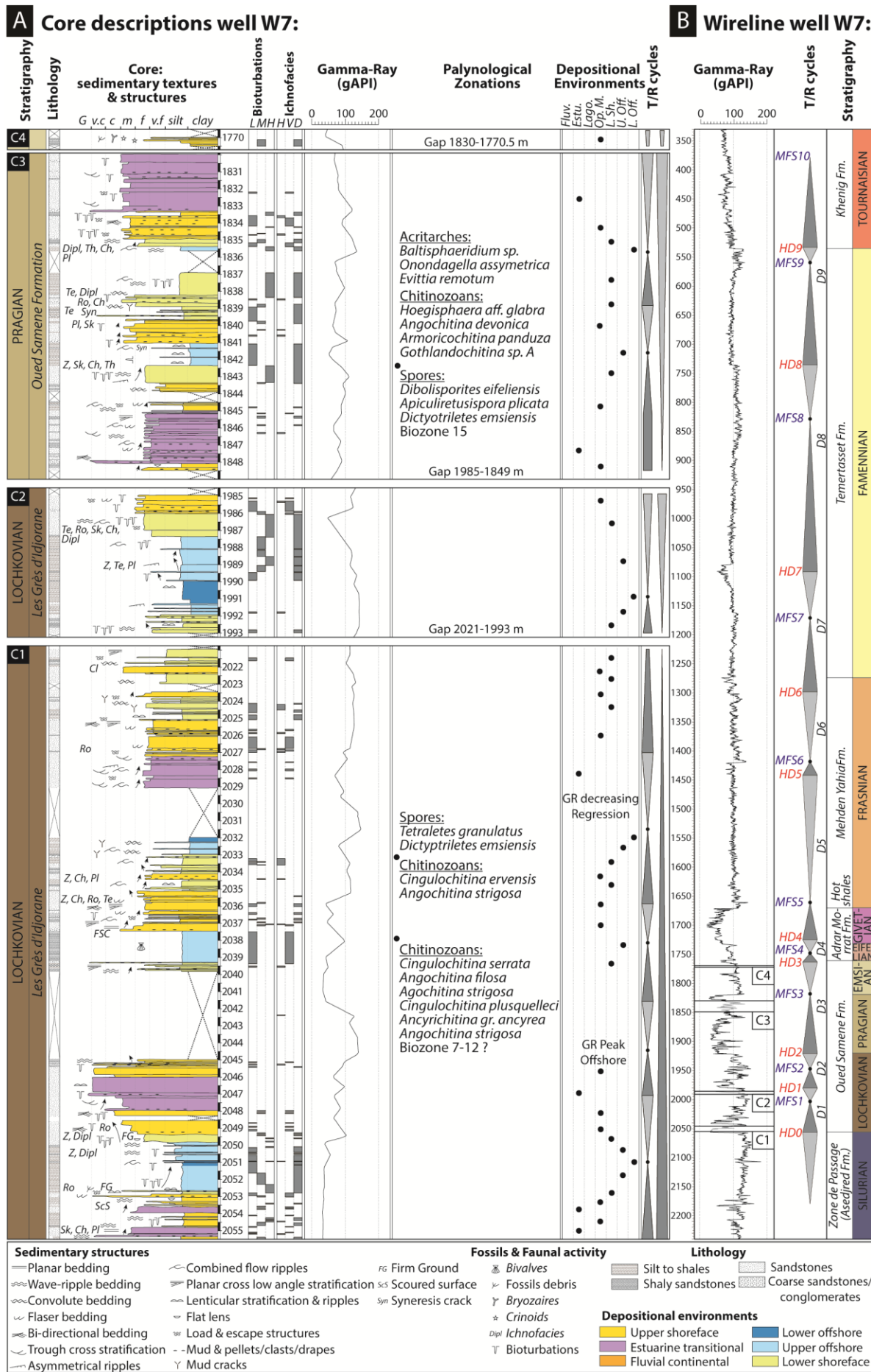
1536



1538 Figure 7 6: (A) N–S interpreted seismic profile in the Ahnet basin near Erg Teguentour (near  
1539 Arak-Foum Belrem arch, westward inter-basin boundary secondary arch) showing steeply-  
1540 dipping northward basement normal blind faults associated with forced folding. ~~Strata lapout~~  
1541 ~~geometries shows Lower Silurian onlaps on the top Ordovician, Upper Silurian and Lower~~  
1542 ~~Devonian truncations, onlaps and downlaps of Frasnian series on top Givetian unit and onlap~~  
1543 ~~near top Famennian.~~ (B) NW–SE interpreted seismic profile of near Azzel Matti arch (inter-  
1544 basin principal arch) showing steeply-dipping south-eastwards basement normal blind faults  
1545 associated with forced folds. The westernmost structures are featured by reverse fault related  
1546 propagation fold. ~~Strata lapout geometries show Silurian onlaps on top Ordovician, Frasnian~~  
1547 ~~onlaps, thinning of Frasnian and Silurian series near the arch; truncation of Paleozoic series~~  
1548 ~~by Mesozoic unit on Hercynian unconformity.~~ (C) W–E interpreted profile of the Ahnet basin  
1549 (Arak-Foum Belrem arch, westward inter-basin boundary secondary arch) showing horst and  
1550 graben structures influencing Paleozoic tectonics associated with forced folds. ~~Strata lapout~~  
1551 ~~geometries show Precambrian basement tilted structure overlain by Cambrian Ordovician~~  
1552 ~~angular unconformity, incised valley in the Ordovician series, Silurian onlaps on top~~  
1553 ~~Ordovician, Silurian onlaps on top Ordovician, Silurian Devonian truncation, Frasnian onlaps~~  
1554 ~~on top Givetian and near top Famennian onlaps.~~ (D) W–E interpreted seismic profile of Bahar  
1555 el Hammar in the Ahnet basin (Ahnet intra-basin secondary arch) showing steeply-dipping  
1556 normal faults F1 and F2 forming a horst positively inverted associated with folding. ~~Strata~~  
1557 ~~lapout geometries show glacial valley in the Ordovician series, Silurian onlaps on top~~  
1558 ~~Ordovician, Silurian onlaps on top Ordovician; Silurian Devonian truncation re-folded,~~  
1559 ~~Frasnian onlaps on top Givetian.~~ Multiple activation and inversion of normal faults are  
1560 correlated to divergent onlaps (wedge-shaped units): DO0 Infra-Cambrian extension, DO1  
1561 Cambrian–Ordovician extension, DO2 Silurian extension with local Silurian–Devonian  
1562 positive inversion, and DO3 Frasnian–Famennian extension-local compression (~~transported~~

1563 ~~fault with a tectonic transport from footwall to hanging wall~~). See figure 3 2 for map and  
1564 cross-section location.

1565

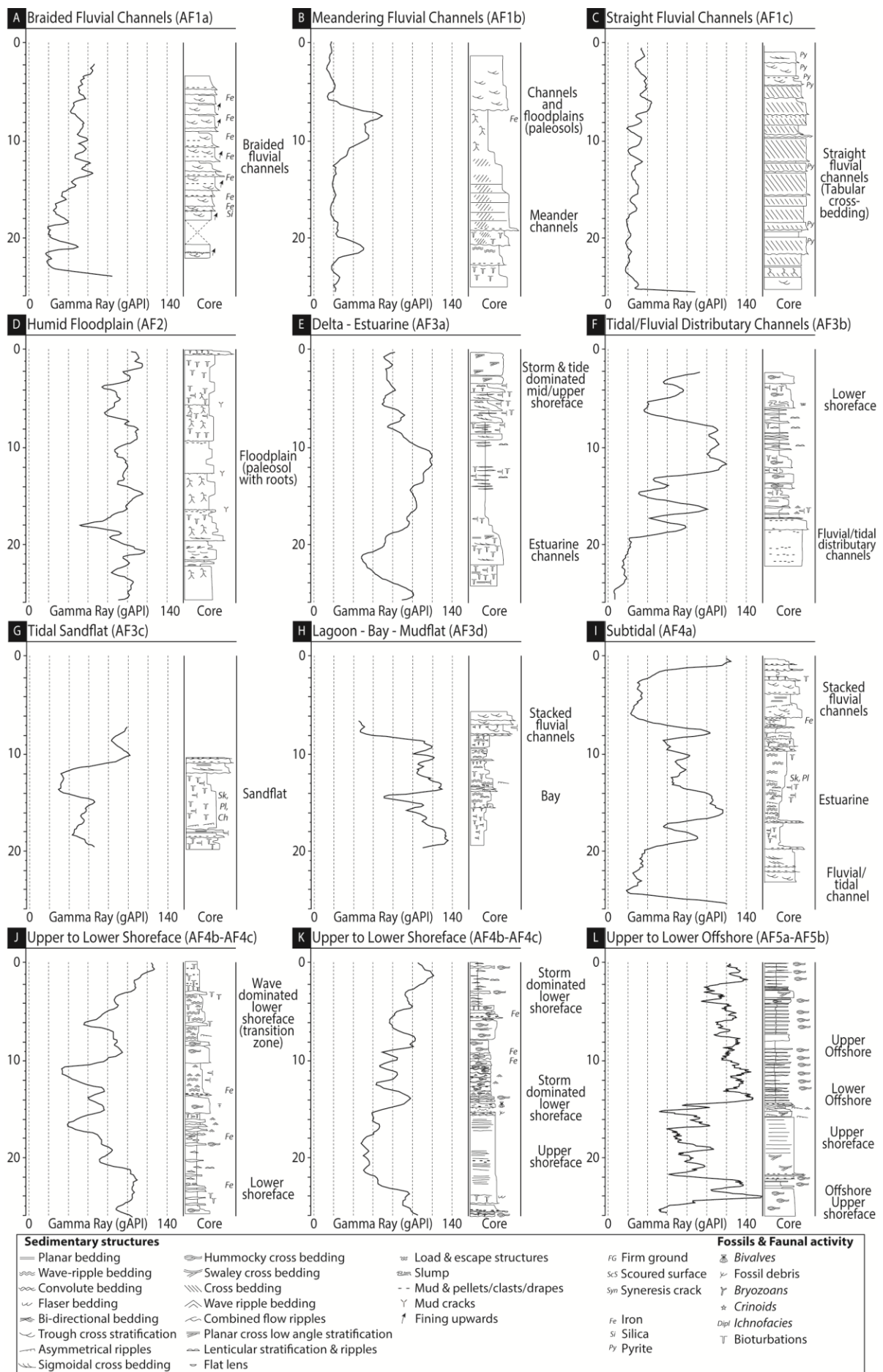


1567 Figure 8 7: **(A)** Core description, palynological calibration and gamma-ray signatures of well  
1568 W7 modified from internal core description report (Dokka, 1999) and internal palynological  
1569 report (Azzoune, 1999). **(B) Devonian sequential stratigraphy of well-log W7.** For location of  
1570 well W7 see figure 3A 2A. ~~Lithological and sedimentological studies were synthetized from~~  
1571 ~~internal Sonatrach (Dokka, 1999), IFP reports (Eschard et al., 1999), and published articles~~  
1572 ~~(Beuf et al., 1971; Biju-Duval et al., 1968; Wendt et al., 2006).~~ Biozonations from (Magloire,  
1573 ~~1967~~) and (~~Boumendjel et al., 1988~~) are based on palynological data from internal  
1574 ~~unpublished data (Abdesselam Rouighi, 1991; Azzoune, 1999; Khiar, 1974).~~ Well W18 is  
1575 ~~supported by palynological data and biozonations from (Kermandji et al., 2008).~~

Criteria & characteristics					<u>Formations</u>	Depositional environments	
Facies associations	Textures/Lithology	Sedimentary structures	Biotic/non biotic grains	Ichnofacies		Fluvial	Continental (Fluvial)
AF1	Conglomerates, mid to coarse sandstones, siltstones, shales	Trough cross-bedding, mud clasts, lag deposits, fluidal and overturn structures, imbricated grains, lenticular laminations, oblique stratification	Rare oolitic intercalations, imbricated pebbles, sandstones, ironstones, phosphorites, corroded quartz grains, calcareous matrix, brachiopod coquinas, phosphatized pebbles, hematite, azurite, quartz	Rare bioturbation	<u>Oued Samene Fm., Barre Supérieur, Barre Moyenne</u>		
AF2	Silt to argillaceous fine sandstone	Current ripples, climbing ripples, crevasse splay, root traces, paleosols, plant debris	Nodules, ferruginous horizon		<u>Oued Samene Fm., Barre Supérieur, Barre Moyenne</u>	Flood plain	
AF3a	Fine to coarse sandstones, argillaceous siltstones, shales (heterolithic)	Trough cross-bedding, some planar bedding, flaser bedding, mud clasts, mud drapes, root trace, desiccation cracks, water escape, wavy bedding, shale pebble, sigmoidal cross-bedding	Brachiopods, trilobites, tentaculites graptolites	Bioturbations, <i>Skolithos</i> (Sk), <i>Planolites</i> , (Pl)	<u>Oued Samene Fm., Grès du Khenig, Barre Supérieur, Barre Moyenne</u>	Delta/Estuarine channels	
AF3b	Very coarse-grained poorly sorted sandstone	Trough cross-bedding, sigmoidal cross-bedding, abundant mud clasts and mud drapes		Increasing upward bioturbation <i>Skolithos</i> (Sk)	<u>Oued Samene Fm., Grès du Khenig, Barre Supérieur, Barre Moyenne</u>	Fluvial/Tidal distributary channels	
AF3c	Fine-grained to very coarse-grained heterolithic sandstone	Sigmoidal cross-bedding with multidirectional tidal bundles, wavy, lenticular, flaser bedding, occasional current and oscillation ripples, occasional mud cracks		Intense bioturbation, <i>Skolithos</i> (Sk), <i>Planolites</i> , (Pl), <i>Thalassinoides</i> (Th)	<u>Talus à Tigillites</u>	Tidal sand flat	
AF3d	Mudstones, varicolored shales, thin sandstone layers	Occasional wave ripples, mud cracks, horizontal lamination, rare multidirectional ripples	Absence of ammonoids, goniatites, calymenids, pelecypod molds, brachiopods coquinas	Intense bioturbation, <i>Skolithos</i> (Sk), <i>Planolites</i> , (Pl), <i>Thalassinoides</i> (Th)	<u>Oued Samene Fm., Grès du Khenig, Atafaitafa Fm.</u>	Lagoon/Mudflat	
AF4a	Silty mudstone associated with coarse to very coarse argillaceous sandstone, poorly sorted, heterolithic silty mudstone	Sigmoidal cross-bedding, abundant mud clasts, wavy, lenticular cross-bedding and flaser bedding, abundant current and oscillation ripples, mud drapes	Shell debris (crinoids, brachiopods)	Strongly bioturbated <i>Skolithos</i> (Sk), <i>Planolites</i> , (Pl)	<u>Oued Samene Fm., Talus à Tigillites</u>	Subtidal	
AF4b	Fine to mid grained sandstones interbedded with argillaceous siltstone and mudstone, bioclastic carbonates sandstones, brownish sandstones and clays, silts	Oscillation ripples, swaley cross-bedding, bidirectional bedding, flaser bedding, rare hummocky cross-bedding, mud cracks (syneresis), convolute bedding, wavy bedding, combined flow ripples, planar cross low angle stratification, cross-bedding, ripple marks, centimetric bedding, shale pebbles	Ooids, crinoids, bryozoans, coral clasts, fossil debris, <u>stromatoporoids, tabulates, colonial rugose corals</u> , myriad pelagic styliolinids, neritic tentaculitids, brachiopods, iron ooliths, abundant micas	<i>Skolithos</i> (Sk), <i>Cruziana</i> , <i>Planolites</i> , (Pl) <i>Chondrites</i> (Ch), <i>Teichichnus</i> (Te), <i>Spirophyton</i> (Sp)	<u>Atafaitafa Fm., Zone de passage, Grès de Mehden Yahia, Calcaires d'Azzel Matti</u>	Open marine-upper shoreface	Shoreface
AF4c	Silty shales to fine sandstones (heterolithic)	Hummocky cross-bedding, planar bedding, combined flow ripples, convolute bedding, dish structures, mud drapes, remnant ripples, flat lenses, slumping	Intense bioturbation, <i>Cruziana</i>	<i>Thalassinoides</i> (Th), <i>Planolites</i> (Pl), <i>Skolithos</i> (Sk), <i>Diplocraterion</i> (Dipl), <i>Teichichnus</i> (Te), <i>Chondrites</i> (Ch), <i>Rogerella</i> (Ro), <i>Climactichnites</i> (Cl)	<u>Atafaitafa Fm., Zone de passage, Grès de Mehden Yahia, Calcaires d'Azzel Matti</u>	Lower shoreface	
AF5a	Grey silty-shales, bundles of skeletal wackestones, silty greenish shale interlayers fine grained sandstones, calcareous mudstones, black shales, polychrome clays (black, brown, grey, green, red, pink), grey and reddish shales	Lenticular sandstones, rare hummocky cross-bedding, mud mounds, mud buildups, low-angle cross-bedding, tempestite bedding, slumping, deep groove marks	Intensive burrowing, bivalve debris, horizontal burrows, skeletal remains (goniatites, orthoconic, nautiloids, styliolinids, trilobites, crinoids, solitary rugose, corals, limestone nodules, ironstone nodules and layers	<i>Zoophycos</i> (Z), <i>Teichichnus</i> (Te), <i>Planolites</i> (Pl)	<u>Argiles à Graptolites, Orsine Fm., Argiles de Mehden Yahia, Argiles de Temertasset</u>	Upper offshore	
AF5b	Black silty-shales (mudstones), bituminous mudstones-wackestones, packstones	Rare structures	parallel-aligned styliolinids, goniatites, orthoconic nautiloids, pelagic pelecypod <i>Buchiola</i> , anoxic conditions, limestone nodules, goniatites, <i>Buchiola, tentaculitids</i> , ostracods and rare fish remains, <i>Tornoceras</i> , <i>Aulatornoceras</i> , <i>Lobotornoceras</i> , <i>Manticoceras</i> , <i>Costamanticoceras</i> and <i>Virginoceras</i> , graptolites	<i>Zoophycos</i> (Z)	<u>Argiles à Graptolites, Orsine Fm., Argiles de Mehden Yahia, Argiles de Temertasset</u>	Lower offshore	Offshore

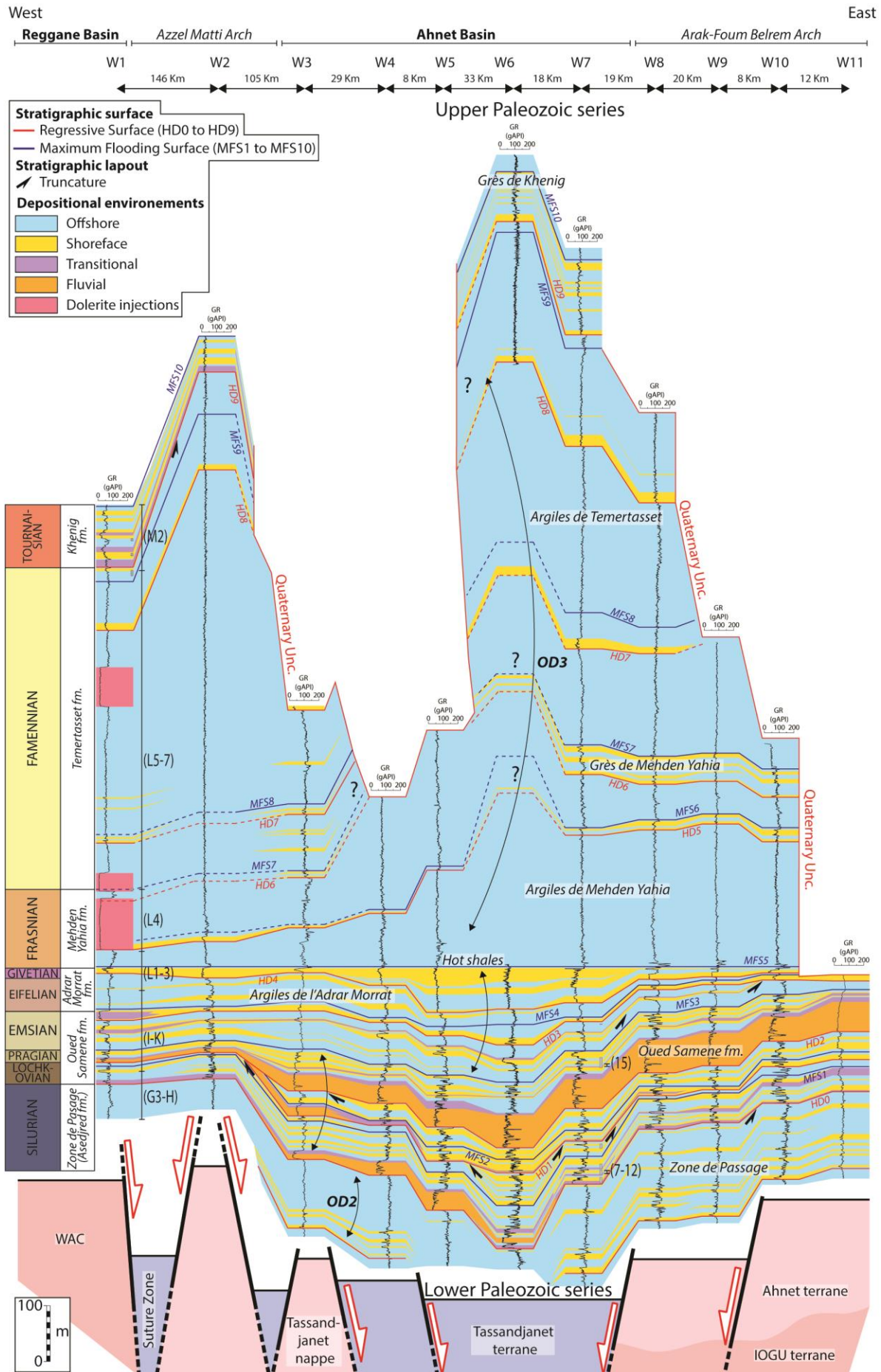
1576 Table 1: Synthesis of facies associations (AF1 to AF5), depositional environments, and  
1577 electrofacies in the Devonian series compiled from internal (Eschard et al., 1999) and  
1578 published studies (Beuf et al., 1971; Biju-Duval et al., 1968; Wendt et al., 2006).

1579



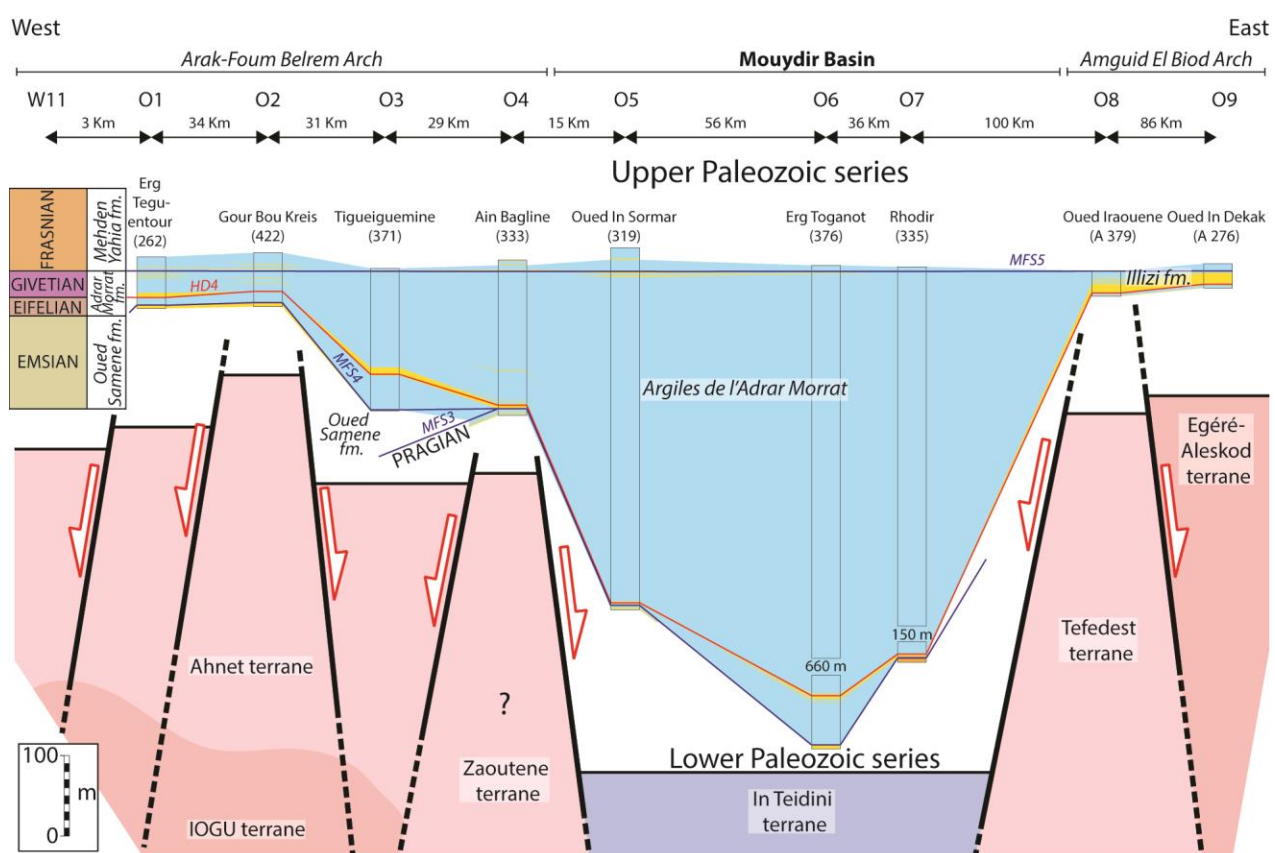
1581 Figure 9 8: The main depositional environments (A to L) and their associated electrofacies  
1582 (i.e. gamma-ray patterns) modified and compiled from (Eschard et al., 1999).

1583



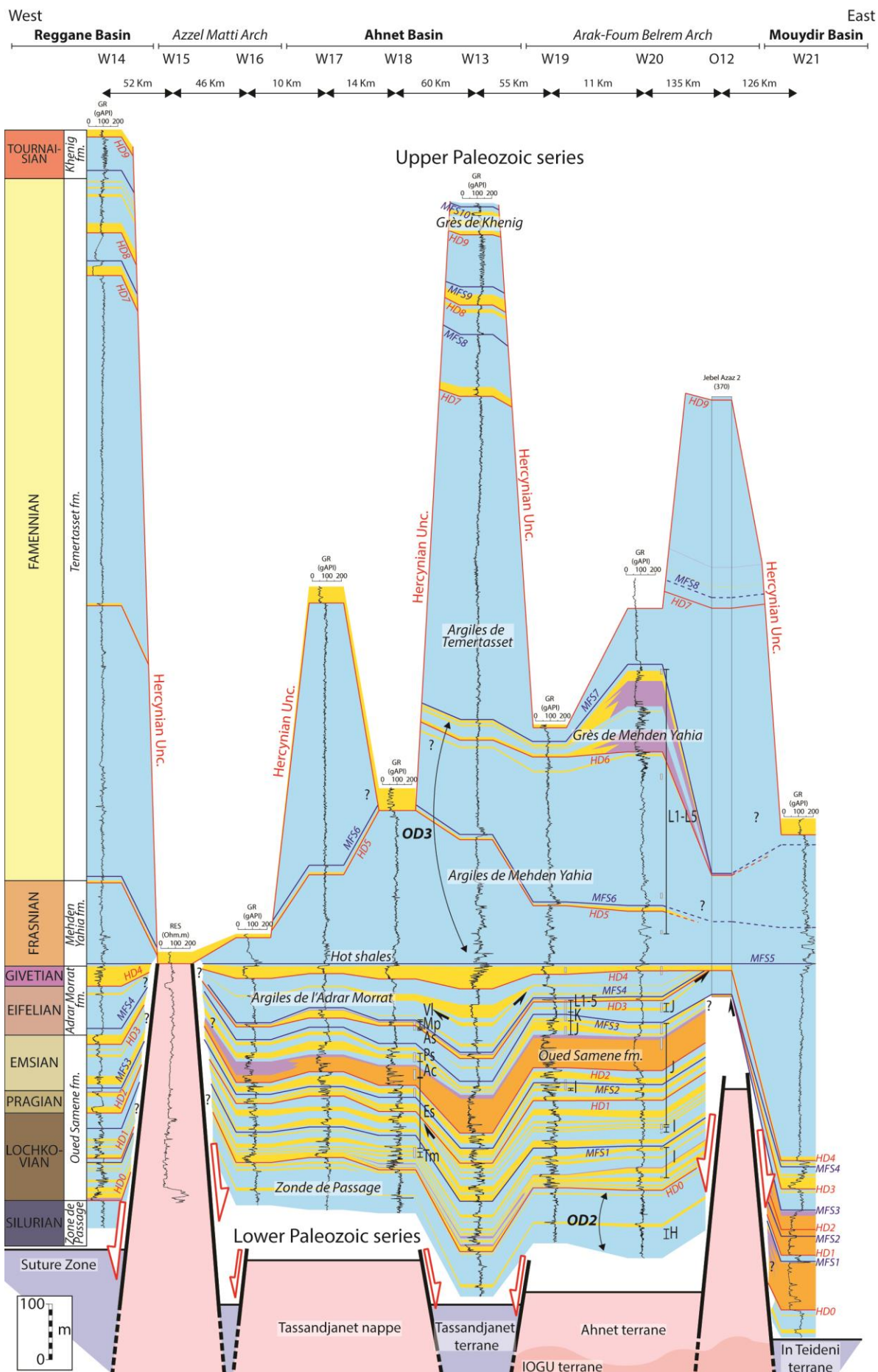
1585 Figure 10 9: SE–W cross-section between the Reggane basin, Azzel Matti arch, Ahnet basin,  
 1586 Arak-Foum Belrem arch, Mouydir basin, and Amguid El Biod arch (well locations in fig. 3).  
 1587 Well W1 biozone calibration from Hassan, (1984) internal report is based on Magloire,  
 1588 (1967) classification: biozone G3-H (Wenlock–Ludlow, Upper Silurian), biozone I-K  
 1589 (Lochkovian–Emsian, Lower Devonian), biozone L1-3 (Eifelian–Givetian, Middle  
 1590 Devonian), biozone L4 (Frasnian, Upper Devonian), biozone L5-7 (Famennian, Upper  
 1591 Devonian), biozone M2 (Tournaisian–Lower Carboniferous). Well W7 biozone calibration  
 1592 from Azzoune, (1999) internal report is based on Boumendjel, (1987) classification: biozone  
 1593 7-12 (Lochkovian, Lower Devonian), biozone 15 (Emsian, Lower Devonian). Interpretation  
 1594 of the basement is based on Figs. 1, ~~3 and supplementary data 4 2 and 15~~. Outerop Well  
 1595 location is in Fig. 3 2.

1596



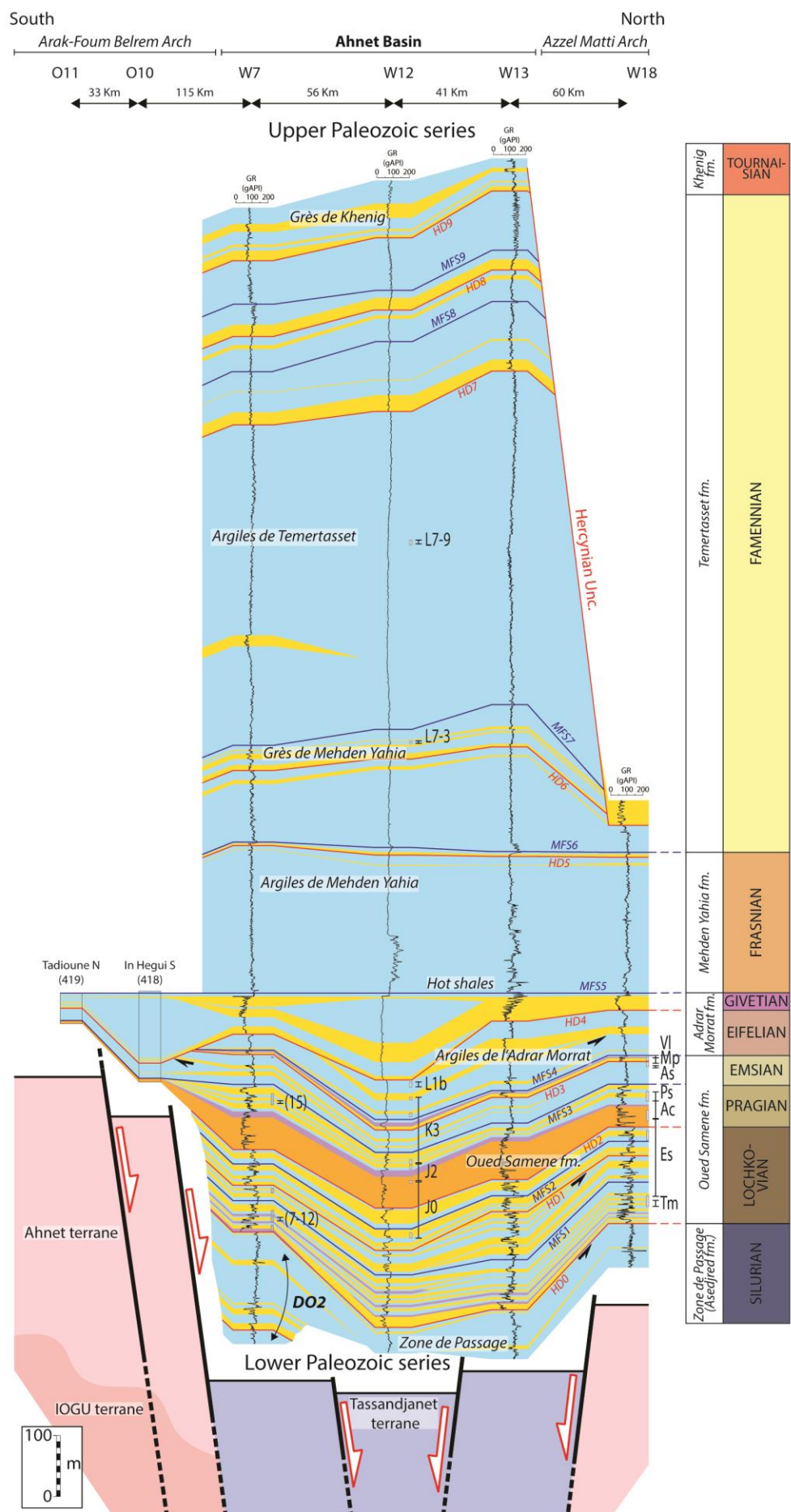
1597

1598 Figure 11: SE–W cross-section between the Arak-Foum Belrem arch, the Mouydir basin and  
1599 the Amguid El Biod arch. Outcrop cross-section correlations and biostratigraphic calibrations  
1600 are based on the compilation of published papers (Wendt et al., 2006, 2009b). Interpretation  
1601 of the basement is based on Figs. 1, 2 and 15. Outcrop location is in Fig. 2.



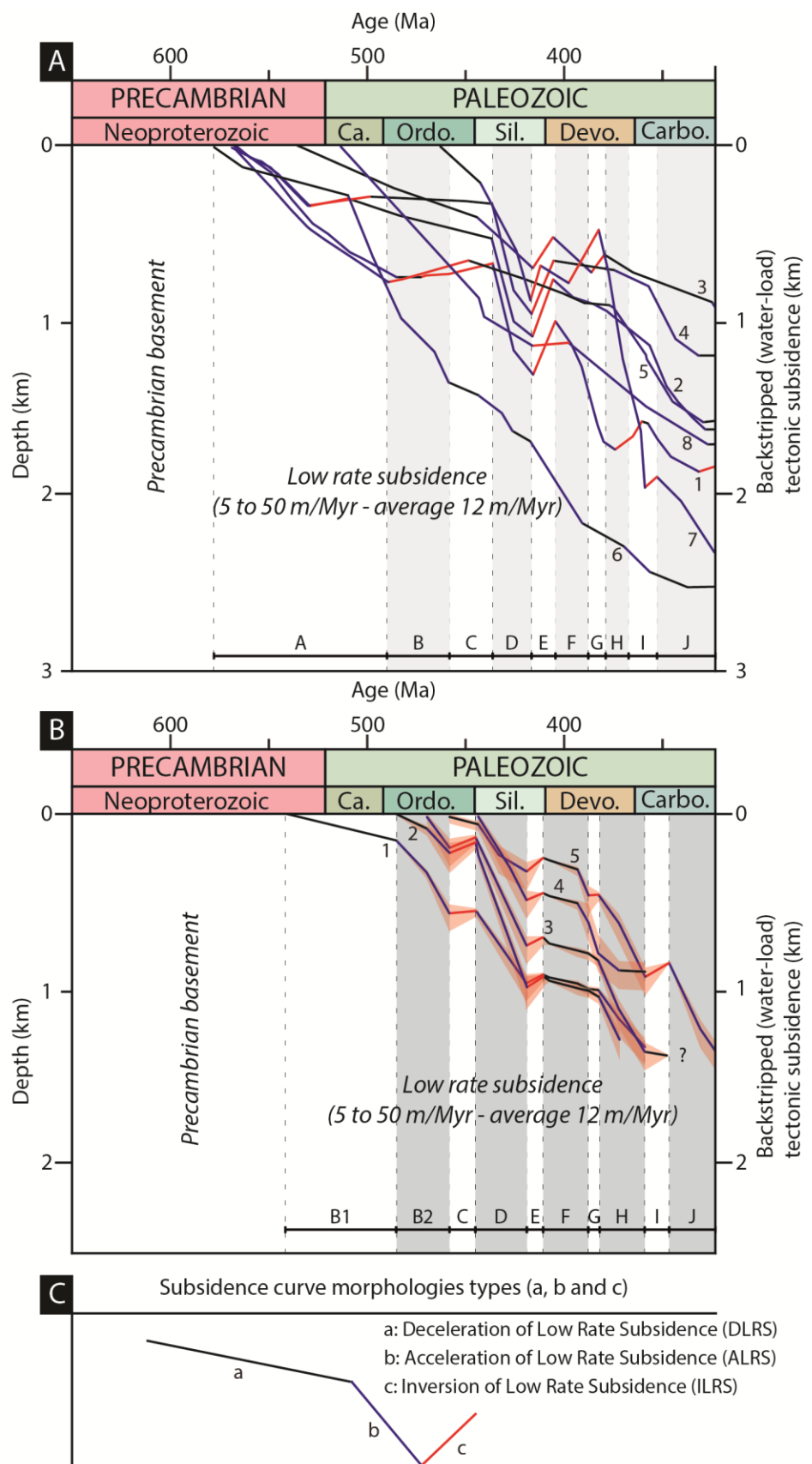
1603 Figure [12](#) [10](#): NE–W cross-section between the Reggane basin, Azzel Matti arch, Ahnet  
1604 basin, Arak-Foum Belrem arch, Mouydir basin, and Amguid El Biod arch (well locations in  
1605 fig. 3). Well W18 biozone calibration is based on Kermadji et al., (2009): biozone (Tm)  
1606 *tidikeltense microbaculatus* (Lochkovian, Lower Devonian), biozone (Es) *emsiensis*  
1607 *spinaeformis* (Lochkovian-Pragian, Lower Devonian), biozone (Ac) *arenorugosa caperatus*  
1608 (Pragian, Lower Devonian), biozone (Ps) *poligonalis subgranifer* (Pragian–Emsian, Lower  
1609 Devonian), biozone (As) *annulatus svalbardiae* (Emsian, Lower Devonian), biozone (Mp)  
1610 *microancyreus protea* (Emsian–Eifelian, Lower to Middle Devonian), biozone (Vl) *velatus*  
1611 *langii* (Eifelian, Middle Devonian). Well W19 and W20 biozones calibration from internal  
1612 reports (Abdesselam-Rouighi, 1991; Khiar, 1974) is based on Magloire, (1967) classification:  
1613 biozone H (Pridoli, Upper Silurian), biozone I (Lochkovian, Lower Devonian), biozone J  
1614 (Pragian, Lower Devonian), biozone K (Emsian, Lower Devonian), biozone L1-5 (Middle  
1615 Devonian to Upper Devonian). Interpretation of the basement is based on Figs. 1, [3](#) and  
1616 [supplementary data 4](#) [2](#) and [15](#). Outcrop [and well](#) location is in Fig. [3](#) [2](#).

1617



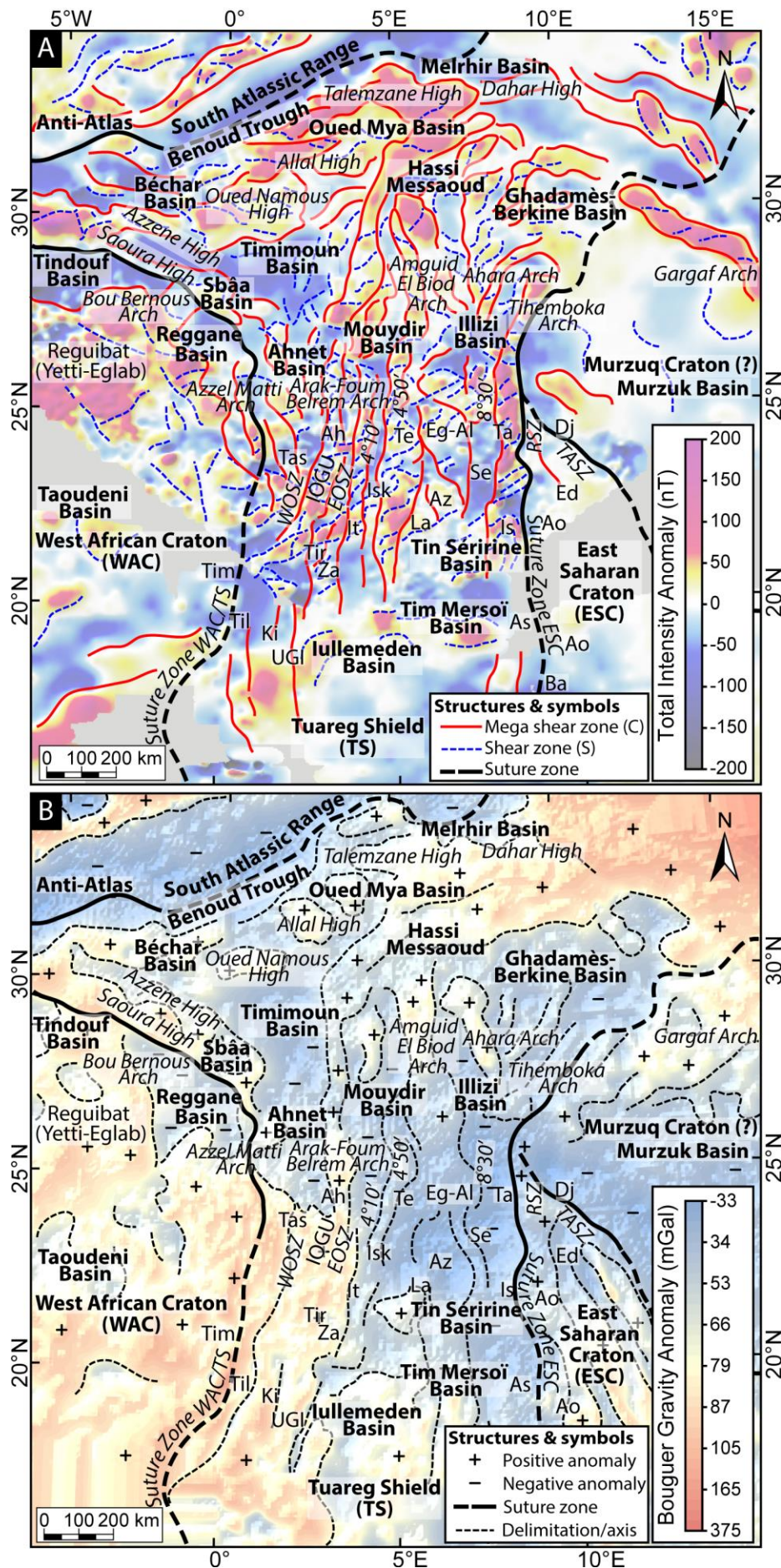
1619 Figure 13: N-S cross-section in the Ahnet basin between Azzel Matti arch and Arak-Foum  
1620 Belrem arch; Well W7 biozone calibration from Azzoune, (1999) internal report based on  
1621 Boumendjel, (1987) classification: biozones 7–12 (Lochkovian, Lower Devonian), biozone 15  
1622 (Emsian, Lower Devonian). Well W18 biozone calibration is based on Kermadjji et al.,  
1623 (2009): biozone (Tm) *tidikeltense microbaculatus* (Lochkovian, Lower Devonian), biozone  
1624 (Es) *emsiensis spinaeformis* (Lochkovian-Pragian, Lower Devonian), biozone (Ac)  
1625 *arenorugosa caperatus* (Pragian, Lower Devonian), biozone (Ps) *poligonalis subgranifer*  
1626 (Pragian-Emsian, Lower Devonian), biozone (As) *annulatus svalbardiae* (Emsian, Lower  
1627 Devonian), biozone (Mp) *microancyreus protea* (Emsian-Eifelian, Lower to Middle  
1628 Devonian), biozone (Vi) *velatus langii* (Eifelian, Middle Devonian). Well W12 biozone  
1629 calibration from Abdesselam-Rouighi, (1977) internal report is based on (Boumendjel, (1987)  
1630 classification: biozone J (Pragian, Lower Devonian), biozone K (Emsian, Lower Devonian),  
1631 biozone L1 (Eifelian, Middle Devonian), biozone L7-3, L7-9 (Frasnian-Famennian, Upper  
1632 Devonian). Interpretation of the basement is based on Figs. 1, 2 and 15. Outcrop and well  
1633 location is in Fig. 2.

1634

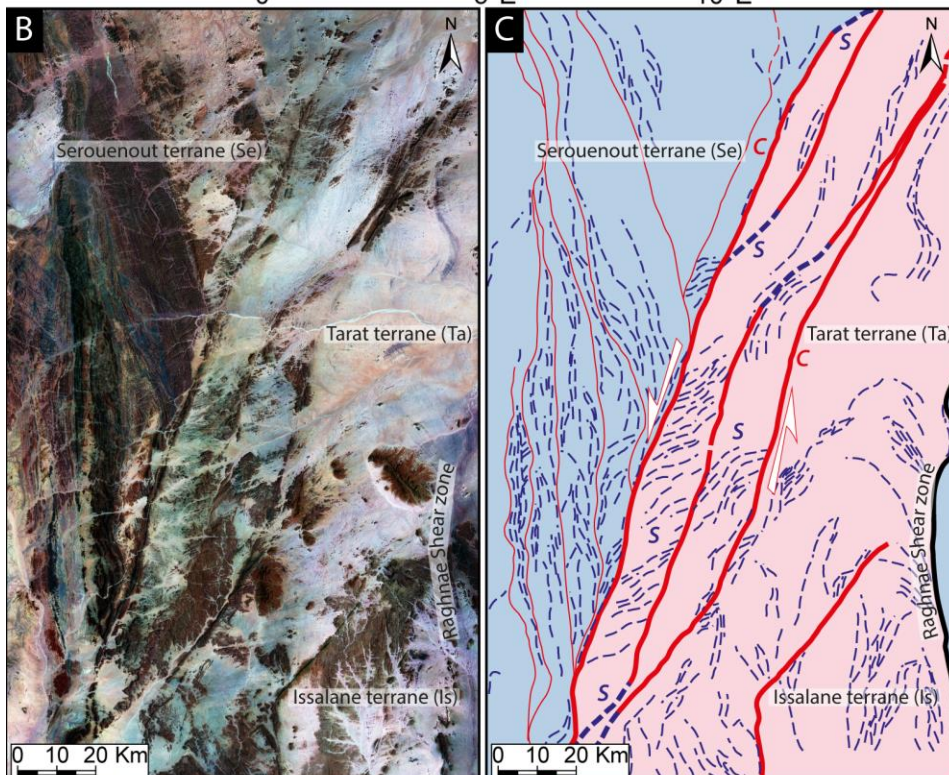
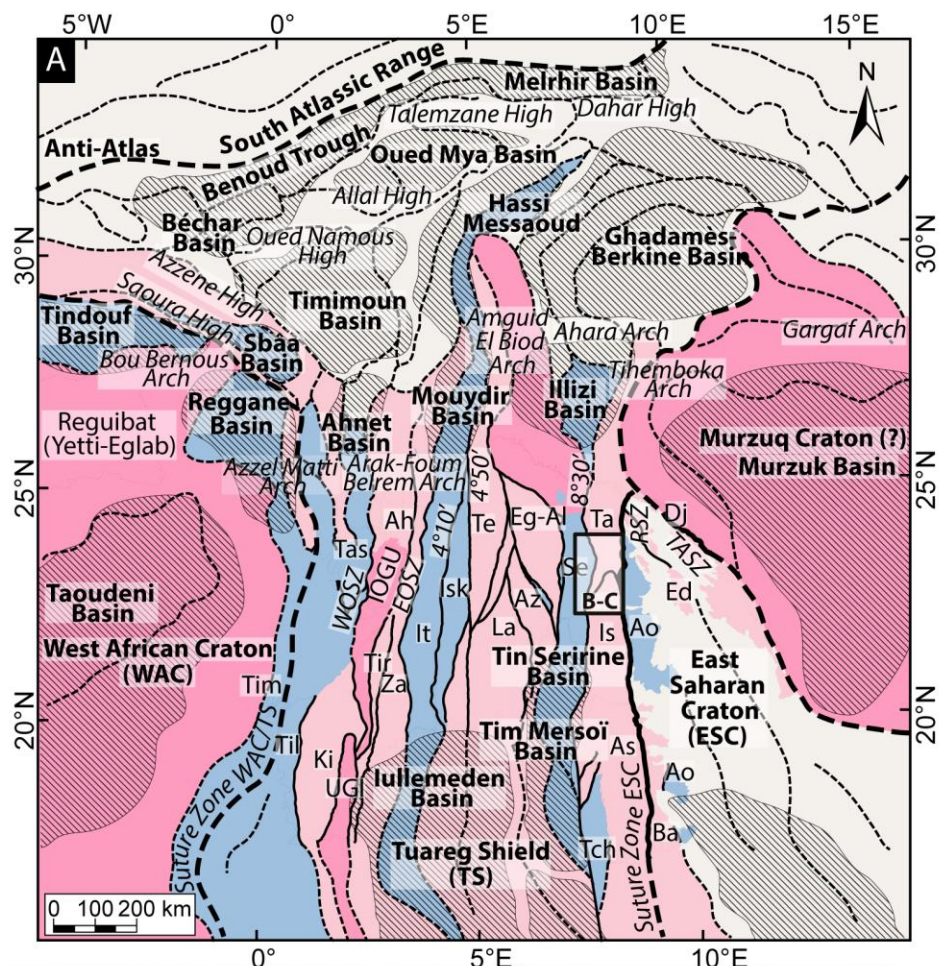


1636 Figure 14 14: (A) Tectonic backstripped curves of the Paleozoic North Saharan Platform  
1637 (peri-Hoggar basins) compiled from literature. 1: HAD-1 well in Ghadamès basin (Makhous  
1638 and Galushkin, 2003b); 2: Well RPL-101 in Reggane basin (Makhous and Galushkin, 2003b);  
1639 3: L1-1 well in Murzuq basin (Galushkin and Eloghbi, 2014); 4: TGE-1 in Illizi basin  
1640 (Makhous and Galushkin, 2003a); 5: REG-1 in Timimoun basin (Makhous and Galushkin,  
1641 2003b); 6: Ghadamès-Berkine basin (Allen and Armitage, 2011; Yahi, 1999); 7: well in Sbâa  
1642 basin (Tournier, 2010); 8: well B1NC43 in Al Kufrah basin (Holt et al., 2010). (B) Tectonic  
1643 backstripped curves of wells in the study area (1: well W17 in Ahnet basin; 2: well W5 in  
1644 Ahnet basin; 3: well W7 in Ahnet basin; 4: well W21 in Mouydir basin; 5: well W1 in  
1645 Reggane basin; (C) Typologies of subsidence curves morphologies. ~~The data show low rate~~  
1646 ~~subsidence with periods of deceleration (Deceleration of Low Rate Subsidence: DLRS),~~  
1647 ~~acceleration (Acceleration of Low Rate Subsidence: ALRS), or inversion (Inversion of Low~~  
1648 ~~Rate Subsidence: ILRS) synchronous and correlated with regional tectonic pulses (i.e. major~~  
1649 ~~geodynamic events)~~. A: Late Pan-African compression and collapse (type a, b, and c  
1650 subsidence), B: Undifferentiated Cambrian–Ordovician (type a, b, and c subsidence), B1:  
1651 Cambrian–Ordovician tectonic quiescence (type a subsidence), B2: Cambrian–Ordovician  
1652 extension (type b subsidence), C: Late Ordovician glacial and isostatic rebound (type c  
1653 subsidence), D: Silurian extension (type b subsidence), E: Late Silurian Caledonian  
1654 compression (type c subsidence), F: Early Devonian tectonic quiescence (type a subsidence),  
1655 G-H: Middle to late Devonian extension with local compression (i.e. inversion structures,  
1656 type b and c subsidence), I: Early Carboniferous extension with local tectonic pre-Hercynian  
1657 compression (type c and b subsidence), J: Middle Carboniferous tectonic extension (type b  
1658 subsidence). ~~K: Late Carboniferous Early Permian Hercynian compression (type c~~  
1659 ~~subsidence)~~.

1660



1662 Figure [15](#) [12](#): (A) Interpreted aeromagnetic anomaly map (<https://www.geomag.us/>) of the  
1663 Paleozoic North Saharan Platform (peri-Hoggar basins) showing the different terranes  
1664 delimited by NS, NW–SE and NE–SW lineaments and mega-sigmoid structures (SC shear  
1665 fabrics); (B) Bouguer anomaly map (from International Gravimetric Bureau:  
1666 <http://bgi.omp.obs-mip.fr/>) of North Saharan Platform (peri-Hoggar basins) presenting  
1667 evidence of positive anomalies under arches and negative anomalies under basins.



**Precambrian Series (Hoggar terranes)**

Meso-Neoproterozoic terrane

Paleoproterozoic terrane

Archean terrane

**Structures & symbols**

Mega shear zone (C)

Shear zone (S)

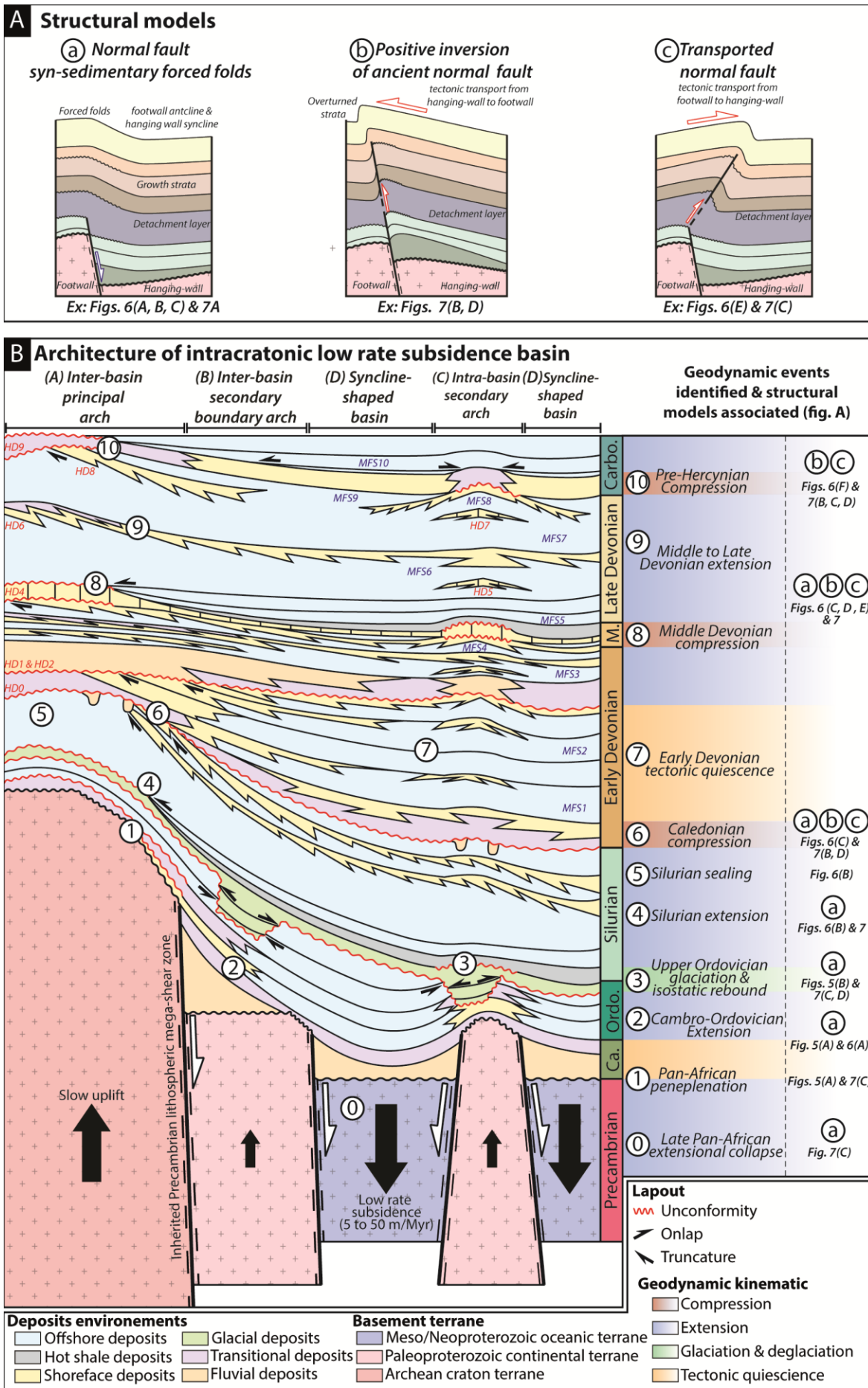
Suture zone

Delimitation/axis

Basin/depocenter

1669 Figure [16 42](#): (**C A**) Interpreted map of basement terranes according to their age (compilation  
1670 of data sets in Fig. 1 and supplementary data [4 1](#)); (**D B**) Satellite images (7ETM+ from  
1671 USGS: <https://earthexplorer.usgs.gov/>) of Paleoproterozoic Issalane-Tarat terrane, Central  
1672 Hoggar (see [fig 12 C](#) for location); (**E C**) Interpreted satellite images of Paleoproterozoic  
1673 Issalane-Tarat terrane showing sinistral sigmoid mega-structures associated with transcurrent  
1674 lithospheric shear fabrics SC.

1675



1677 Figure 17 13: (A) Different structural model styles identified from the analysis of seismic  
1678 profiles and from interpretation of the satellite images; (B) Conceptual model of the  
1679 architecture of intracratonic low rate subsidence basin and synthesis of the tectonic kinematics  
1680 during the Paleozoic. Note that the differential subsidence between arches and basins is  
1681 controlled by terrane heterogeneity (i.e. thermo-chronologic age, rheology, etc.).

1682

1683 Supplementary data 1 4: Georeferenced geochronological dating data compilation of the study  
1684 area.